Novel roles of the SRP RNA in co-translational protein targeting

Thesis by

Kuang Shen

In Partial Fulfillment of the Requirements

for the Degree of

Doctor of Philosophy

California Institute of Technology

Pasadena, California 91125

2013

(Defended May 7, 2013)

Dedicated to my parents, Mr. Yi Shen and Mrs. Yukun Wu

谨以此文献给我的父母和家人

Acknowledgement

First, I would like to thank my advisor, Shu-ou Shan, for the guidance along my graduate work. Her encouragement, advice, and scientific criticism are invaluable to me. I am grateful to my thesis committee, Professor Douglas Rees, Professor Harry Gray, and Professor Judith Campbell, for the sparkling comments and suggestions about my projects we have enjoyed over the years.

I am privileged to have had opportunities to work with my brilliant labmates, who are also wonderful friends, of the Shan lab: Sowmya Chandrasekar, David Akopian, Aileen Ariosa, Un Seng Chio, Yu-Hsien Hwang Fu, Peera Jaru-Ampornpan, Vinh Lam, Camille McAvoy, Thang Nguyen, Nathan Pierce, Rumana Rashid, Michael Rome, Ishu Saraogi, Dawei Zhang, and Xin Zhang. This exciting intellectual environment was the best I could ask for.

Collaboration has been an important part of my research experience at Caltech. I thank Professor Taekjip Ha from UIUC and his students Sinan Arslan, Kyung Suk Lee, and Ruobo Zhou, for their generous help in setting up the single-molecule instrument. I thank Professor Long Cai and his student Timur Zhiyentayev for helping label RNC. I thank Professor Juli Feigon from UCLA and her students Yaqiang Wang and Qi Zhang, for setting up the NMR experiments.

I could not have finished my graduate work without the support from my friends and family. I thank all my friends for their wonderful friendship. Finally, I thank my parents for their love and support over the years.

Abstract

The signal recognition particle (SRP) and its receptor (SR) are universally conserved protein machineries that deliver nascent peptides to their proper destination. The SRP RNA is a universally conserved and essential component of SRP, which serves as the "catalyst" of the protein targeting cycle. The SRP RNA accelerates SRP-SR complex formation at the beginning of the protein targeting reaction, and triggers GTP hydrolysis and SRP-SR complex disassembly at the end. Here we combined biochemical and biophysical approaches to investigate the molecular mechanism of the functions of the SRP RNA. We found that two functional ends in the SRP RNA mediate distinct functions. The tetraloop end facilitates initial assembly of SRP and SR by mediating an electrostatic interaction with the Lys399 receptor, which ensures efficient and accurate substrate targeting. At the later stage of the SRP cycle, the SRP-SR complex relocalizes ~ 100 Å to the 5',3'-distal end of the RNA, a conformation crucial for GTPase activation and cargo handover. These results, combined with recent structural work, elucidate the functions of the SRP RNA during the protein targeting reaction.

Table of Contents

Introduction to the SRP pathway*

* A modified version of this section was published as: ***Signal Recognition Particle: An essential protein targeting machine***, David Akopian*, Kuang Shen*, Xin Zhang* and Shu-ou Shan, *Annu Rev Biochem*, **2013**. (*: equal contribution)

1.1 Abstract

The signal recognition particle (SRP) and its receptor comprise a universally conserved cellular machinery that couples the synthesis of nascent proteins to their proper membrane localization, and is essential for the order and organization that sustain life. The past decade has witnessed an explosion in in-depth mechanistic investigations of this targeting machine at increasingly higher resolution. In this section, we will summarize recent studies that elucidate how the SRP and SRP receptor interact with the cargo protein and the target membrane, respectively, and how these interactions are coupled to a novel GTPase cycle in the SRP-receptor complex to provide the vectorial driving force and enhance the fidelity of this fundamental cellular pathway. We will also discuss emerging frontiers where important questions remain to be addressed.

1.2 Introduction

The proper localization of proteins to their correct cellular destinations is essential for sustaining the order and organization in all cells. Roughly 30% of the proteins encoded in a cell's genome are initially destined for the eukaryotic endoplasmic reticulum (ER), or the bacterial plasma membrane. Although the precise number of proteins remains to be determined, it is generally recognized that the majority of these proteins are delivered by the signal recognition particle (SRP), an essential and universally conserved protein targeting machine (Pool 2005; Driessen 2008; Cross 2009; Shao 2011). Over thirty years ago, the components and pathway for SRP-dependent protein targeting were first elucidated in mammalian cells through *in vitro* reconstitutions in cell extracts (Walter 1980; Gilmore 1982a; Gilmore 1982b; Walter 1983; Walter 1984b). The identification of a homologous SRP pathway in prokaryotes a decade later further highlighted the salient, universally conserved features of this pathway (Bernstein 1989; Römisch 1989; Bernstein 1993). The biochemical accessibility of the bacterial SRP system has allowed high-resolution biophysical techniques to be applied for investigation of this pathway in the past decade, allowing us to understand its underlying molecular mechanism at unprecedented depth and resolution.

With the exception of chloroplast SRP (see below), protein targeting by the SRP is a strictly co-translational process that begins when a nascent polypeptide destined for the ER or plasma membrane emerges from the ribosome (Figure 1.1A). The N-terminal signal sequence on the nascent polypeptide serves as the 'signal' that allows the ribosome•nascent chain complex (termed the RNC or cargo) to engage the SRP and, through interaction with the SRP receptor (SR), delivered to the vicinity of the Sec61p

(or SecYEG) translocation machinery on the target membrane (Figure 1.1A). There, the RNC is transferred to the Sec61p (or SecYEG) machinery, which integrates the nascent polypeptide into the membrane bilayer or translocates it across the membrane to enter the secretory pathway. Meanwhile, SRP and SR dissociate from one another to enter another round of targeting (Figure 1.1A).

The size and composition of SRP vary widely across species (see Figure 1.5 below). Surprisingly, the bacterial SRP and SR, though highly simplified compared to those in eukaryotes, can replace their mammalian homologues to mediate efficient targeting of mammalian proteins into ER microsomes (Bernstein 1993; Powers 1997). This demonstrates the remarkable evolutionary conservation of the SRP pathway and shows that the functional core of SRP necessary and sufficient for protein targeting can be represented by the bacterial machinery, which provides a useful starting point for mechanistic dissections.

The bacterial SRP contains the universally conserved SRP54 protein (called Ffh in bacteria) bound to the 4.5S SRP RNA. Ffh has two structurally and functionally distinct domains (Figure 1.1B, blue): a methionine-rich M-domain that recognizes the signal sequence and binds, with picomolar affinity, to the SRP RNA (Keenan 1998b; Batey 2000b; Janda 2010b); and a special GTPase, NG-domain that interacts with a highly homologous NG-domain in the SR (Egea 2004b; Focia 2004b) (Figure 1.1B). The bacterial SR, called FtsY, also contains an acidic A-domain at its N-terminus that allows this receptor to peripherally associate with the membrane (Parlitz 2007; Weiche 2008).

The co-translational SRP pathway minimizes the aggregation or misfolding of nascent proteins before they arrive at their cellular destination, and is therefore highly advantageous in the targeted delivery of membrane and secretory proteins. Nevertheless, an increasing number of pathways have been identified that deliver nascent proteins post-translationally (Figure 1.1A, left). The best characterized thus far is the bacterial SecB/A system, which delivers bacterial secretory and outer-membrane proteins to the SecYEG complex and, through the ATPase cycles of SecA, drives the translocation of preproteins across the SecYEG translocon (Driessen 2008; Cross 2009). In yeast, the Sec62/63/71/72 system is a major pathway that mediates protein secretion (Goldshmidt 2008; Muller 2010). Additional targeting pathways, including the Tat, Hsp70, and most recently the Get pathway, have been found (Figure 1.1A, left path) (Deshaies 1988; Driessen 2008; Natale 2008; Cross 2009; Hegde 2011; Frobel 2012).

Despite the divergence of targeting machineries, the SRP pathway illustrates several key features that are general to all the protein targeting processes. First, the cellular destination of a protein is dictated by its 'signal sequence', which allows it to engage specific cellular targeting machineries. Second, targeting machinery cycles between the cytosol and membrane, acting catalytically to bring cargo proteins to membrane translocation sites. Third, targeting requires the accurate coordination of multiple dynamic events including cargo loading / unloading, targeting complex assembly / disassembly, and the productive handover of cargo from the targeting to translocation machinery. Not surprisingly, such molecular choreography requires energy input, which is often provided by GTPase or ATPase modules in the targeting machinery.

Below, we discuss recent advances in our understanding of the molecular mechanisms that underlie these key events in the SRP pathway.

1.3 Molecular interactions and regulation of SRP

1.3.1 Cargo Recognition by the SRP

Co-translational protein targeting is initiated when SRP recognizes an N-terminal signal sequence on the nascent polypeptide that emerges from the ribosome. Signal sequences that effectively engage the SRP are characterized, in general, by a core of 8-12 hydrophobic amino acids that preferentially adopts an α-helical structure (von Heijne 1985; Gierasch 1989). Crosslinking and phylogenetic analysis have implicated the M-domain of Ffh/SRP54 in binding the signal sequence (Krieg 1986; Kurzchalia 1986; Zopf 1990). The unusually high methionine content of this domain further led to a 'methionine bristle' hypothesis, in which the flexible methionine side chains provide a hydrophobic environment with sufficient plasticity to accommodate a variety of signal sequences (Bernstein 1989). In support of this model, crystallographic analyses of Ffh (Keenan 1998) and of SRP54-signal peptide fusion proteins (Janda 2010; Hainzl 2011) showed that the signal sequence binds to a groove in the Ffh/SRP54 M-domain comprised almost exclusively of hydrophobic residues. Two different modes of signal peptide docking were observed in these structures (Janda 2010; Hainzl 2011); this is probably due to the different signal sequences used in the two studies, and supports the flexibility of signal sequence interaction with the M-domain. A conserved, long flexible fingerloop connects the a1 and a2 helices that lie at the 'bottom' of the signal sequence binding groove. This loop has been suggested to act as a flexible flap that closes upon the signal sequence (Keenan 1998; Rosendal 2003; Hainzl 2007), though direct evidence for this model remain to be obtained. Intriguingly, mutations in this loop disrupts the interaction between the SRP and SR GTPases (Bradshaw 2007), suggesting that it plays a role beyond that of facilitating signal sequence recognition. The precise role of the

fingerloop remains to be clarified.

Despite these interactions, SRP binds isolated signal sequence weakly, with dissociation constants (K_d) in the micromolar range (Swain 2001; Bradshaw 2009). In comparison, RNCs containing no signal sequence or even empty ribosomes bind SRP with K_d values of 80–100 nM (Flanagan 2003; Bornemann 2008; Zhang 2010). Thus, the ribosome makes a significant contribution to the recruitment of SRP. The binding site of SRP with the ribosome was identified by crosslinking studies (Pool 2002; Gu 2003) and cryo-electron microscopy (EM) reconstructions of the RNC-SRP complex in both the eukaryotic and bacterial systems (Halic 2004; Halic 2006; Schaffitzel 2006). Together, these results show that basic residues on the 'tip' of the Ffh N-domain contact ribosomal proteins L23 and, to a lesser extent, L29 (Rpl25 and Rpl35 in eukaryotes, respectively) in the vicinity of the ribosome exit site (Figure 1.2A). In the cryo-EM structure, the M-domain also forms contacts with ribosomal RNAs and perhaps ribosomal proteins L22 (Rpl17 in eukaryotes) and L24, although these contacts remain to be verified biochemically. These ribosomal contacts, together with the interaction of the Ffh/SRP54 M-domain with the signal sequence, allow the SRP to bind to its correct cargos with sub- to nano-molar affinity (Flanagan 2003; Bornemann 2008; Zhang 2010; Saraogi 2011).

1.3.2 Membrane localization of the SRP receptor

Bacterial SR is a single protein, FtsY, which lacks a bona fide transmembrane (TM) domain. The results of microscopy (Rubio 2005; Mircheva 2009), cell fractionation (Luirink 1994), and *in vitro* binding experiments using synthetic liposomes (de Leeuw 2000; Parlitz 2007; Lam 2010) indicate that the interaction of FtsY with the

bacterial inner membrane is weaker and more dynamic than that of integral membrane proteins. Although the N-terminal A-domain has been speculated to mediate its membrane association, recent studies show that FtsY(NG+1), in which only Phe196 immediately preceding the NG-domain is retained, is sufficient to sustain lipid binding of FtsY and co-translational protein targeting *in vivo* and *in vitro* (Eitan 2004; Bahari 2007; Parlitz 2007; Lam 2010). Similar observations were made with a chloroplast FtsY homologue (Marty 2009). Comparison of the crystal structure of FtsY(NG+1) with that of FtsY-NG (Montoya 1997; Parlitz 2007) showed that Phe196-induced folding of an amphiphilic α-helix rich in basic residues at the junction between the A- and N-domains, which provides FtsY's primary lipid-binding motif (Figure 1.2B, orange).

This structure, together with *in vitro* binding studies, also showed that FtsY preferentially binds anionic phospholipids, phosphatidylglycerol (PG), and cardiolipin (CL) (de Leeuw 2000; Parlitz 2007; Lam 2010). This preference is corroborated by experiments *in vivo*, in which an FtsY mutant defective in lipid binding was rescued by overexpression of genes involved in PG and CL biosynthesis (Erez 2010). Anionic phospholipids have also been found to preferentially interact with and activate the SecYEG machinery (Gold 2010) and the SecA ATPase (Lill 1990; Hendrick 1991), and stimulate the integration and export of membrane and secretory proteins (de Vruje 1988; Kusters 1991; Ridder 2001). Together, these observations suggest that sites of bacterial inner membrane enriched in anionic phospholipids could comprise active zones for protein targeting and translocation, an attractive hypothesis that remain to be tested.

In addition to lipid interactions, a direct interaction of FtsY with SecYEG would provide an attractive mechanism to more precisely localize the targeting complex to the

translocon. Evidence for this interaction was obtained only recently though crosslinking and co-purification studies (Angelini 2005; Angelini 2006). Subsequent crosslinking and mutational studies further showed that the A-domain of FtsY and the cytosolic loops of SecYEG connecting TMs 6-7 and TMs 8-9 (termed C4 and C5 loops in prokaryotes and L6/7 and L8/9 loops in eukaryotes) participate in this interaction (Angelini 2006; Weiche 2008; Kuhn 2011). Nevertheless, several puzzling observations remain unexplained. Given the low sequence conservation of FtsY A-domain and its dispensability for co-translational targeting, it is unclear to what extent this domain helps facilitate the targeting reaction. The NG-domain of FtsY was also suggested to interact with SecYEG (Kuhn 2011), but direct evidence for this interaction remains to be obtained. Most importantly, the SecYEG L6/7 and L8/9 loops that interact with FtsY are also crucial for its interaction with the ribosome (Kuhn 2011) (see section below), suggesting that the interaction of FtsY with SecYEG is transient and must be broken to allow stable docking of RNC on the SecYEG machinery. The timing, mechanism, and precise roles of the FtsY-SecYEG interaction, and its contribution relative to the FtsY-lipid interaction remain challenging questions for future studies.

Eukaryotic SR is a heterodimeric complex comprised of the α and β subunits (Tajima 1986). SRα is a soluble protein highly homologous to FtsY. Instead of the A-domain, SRα contains an N-terminal X-domain that dimerizes with SRβ, an integral membrane protein, thus localizing the SRP receptor to the ER membrane (Schwartz 2003). SRβ also contains a GTPase domain that, unlike the two GTPases in SRP and FtsY/SRα described later, shares the most homology to the Arf family of G-proteins (Miller 1995; Schwartz 2003). Crystallographic and biochemical analyses showed that

stable SRα-β association requires SRβ to be bound with GTP (Schwartz 2003). Intriguingly, the Sec61β subunit of Sec61p complex could accelerate GDP dissociation from SRβ (Helmers 2003), suggesting that the translocon potentially serves as a nucleotide exchange factor that maintains SRβ in the GTP-bound state. Direct interaction of SRβ with the yeast Sec61p homologue, Ssh1p, was demonstrated *in vivo* using a split ubiquitin assay (Wittke 2002), and disruption of this interaction leads to defects in co-translational protein targeting and cell growth (Jiang 2003). Together, these results suggest functional interactions of the eukaryotic SR with the Sec61p translocon that parallel findings with the bacterial FtsY and show that the membrane localization of SR in eukaryotes may be subject to more complex regulation.

1.3.3 Regulation of protein targeting by the SRP and SRP-receptor GTPases

At the membrane, SRP and SR meet and interact with one another through their GTPase modules. Both SRP and SR contain a central GTPase, G-domain that shares homology with the classical *Ras* fold (Freymann 1997; Montoya 1997). Unique to the SRP and SR GTPases is an additional b-a-b-a insertion box domain (IBD), in which a flexible IBD loop (red in Figure 1.3A) contains multiple catalytic residues and provides an equivalent of the switch II loop in *Ras*-type GTPases (Freymann 1997; Montoya 1997). In addition, a four-helix bundle preceding the *Ras* fold forms the N-domain, which together with the G-domain comprises a structural and functional unit termed the NG-domain (Figure 1.2). Unlike classic signaling GTPases that exert regulation by switching between a GTP-bound, active state and a GDP-bound, inactive state (Gilman 1987; Bourne 1990), both the SRP and SR represent a novel class of nucleotide

hydrolases whose activities are regulated by nucleotide-dependent homo- or hetero-dimerization cycles (Gasper 2009). Members of this family also include FlhF, MinD, MnmE, the Septins, Toc proteins, human guanylate binding protein-1, and the dynamin family of GTPases (Leipe 2002; Gasper 2009; Chappie 2010; Bange 2011). In the past decade, mechanistic studies of the bacterial SRP and SR GTPases have elucidated the biological logic and regulatory mechanism for these twin GTPases, which could provide general principles for understanding other members of this NTPase family.

Free Ffh and FtsY exhibit minor structural differences among the apo, GDP-, and GTP-bound states (Freymann 1997; Montoya 1997; Freymann 1999; Padmanabhan 2001; Gawronski-Salerno 2006; Reyes 2007). Even with GTP-bound, both GTPases by themselves are in an inactive *open* conformation, exhibiting fast nucleotide dissociation and exchange rates as their nucleotide binding pocket is wide open (Figure 1.2 and 1.3A), and low basal GTPase activity as their catalytic loops are not correctly positioned (Peluso 2001). Their GTPase cycle is driven by a series of conformational changes during their dimerization that culminate in reciprocal GTPase activation (Figure 1.3) (Shan 2009). GTPase assembly is initiated with a transient *early* intermediate, which forms rapidly but is highly unstable ($K_d \sim 4–10\ \mu M$ and $k_{off} \sim 62\ s^{-1}$; Figure 1.3, step 2) (Zhang 2008). This intermediate lacks stable contacts between the G-domains of Ffh and FtsY, and is primarily stabilized by electrostatic attractions between their N-domains (Figure 1.3A, right panel) (Estrozi 2011; Zhang 2011). Subsequent GTP-dependent rearrangements, primarily involving readjustments at the intramolecular NG-domain interface (Shan 2003; Egea 2004; Focia 2004; Shan 2004) and removal of an inhibitory N-terminal helix (Shepotinovskaya 2001; Gawronski-Salerno 2007; Neher 2008), lead to the formation of

a stable (K_d ~ 16–30 nM) *closed* complex (Figure 1.3A, step 3) in which extensive stereospecific interactions are formed between G-domains of both proteins (Figure 1.3A, lower panel). In addition, two pairs of hydrogen bonds are formed across the dimer interface through the 3'-OH of one GTP and the γ-phosphoryl oxygen of the other, which further stabilize the GTPase dimer (Egea 2004; Focia 2004). The final GTPase activation step involves local rearrangements of the IBD loops, which must be brought into close proximity to the two bound GTP molecules (Figure 1.3A, step 4). Each IBD loop provides at least three catalytic residues (Asp135, Arg138, and Gln148 in Ffh and their homologous residues in FtsY) that coordinate the nucleophilic water, the γ-phosphoryl oxygen and the active site Mg^{2+}, forming a composite active site at the dimer interface primed for hydrolyzing GTP (Figure 1.3A, left panel) (Egea 2004; Focia 2004; Shan 2004). Following hydrolysis, the GDP-bound SRP•FtsY complex is much less stable and quickly disassembles (Figure 1.3A, step 5) (Connolly 1991; Peluso 2001).

Importantly, each of the GTPase rearrangements during the dimerization and activation of SRP and FtsY provides a discrete regulatory point at which they can sense and respond to the presence of the RNC and target membrane, thus allowing the loading of cargo on the SRP to be tightly coupled to its membrane delivery. For example, with free SRP and FtsY, assembly of a stable *closed* complex is extremely slow (k_{on} ~ 10^2–10^3 $M^{-1}s^{-1}$) (Peluso 2000; Peluso 2001; Bradshaw 2009) and insufficient to sustain the protein targeting reaction. The RNC, by stabilizing the *early* intermediate over 100-fold and preventing its premature disassembly, accelerates stable SRP-FtsY GTPase assembly 10^3-fold (Zhang 2009). Analogously, phospholipid membranes, by helping to pre-organize FtsY into the *closed* conformation, accelerate their assembly 160-fold (Lam 2010; Braig

2011; Stjepanovic 2011). These allosteric regulations ensure the rapid delivery of cargo to the membrane, and minimize futile cycles of interactions between the free SRP and SR.

Intriguingly, the RNC also disfavors the rearrangement of the GTPase complex to the *closed* and *activated* states, and delays GTPase activation in the targeting complex (Zhang 2009; Zhang 2010). This generates a greatly stabilized *early* targeting intermediate in which the RNC is predicted to be bound to the SRP with picomolar affinity, while GTP hydrolysis is 'paused' (Zhang 2009). These effects are highly beneficial in preventing abortive reactions at early stages of targeting; however, they pose serious challenges for the subsequent cargo unloading and GTPase activation events at later stages. Multiple observations strongly suggest that part of the resolution to this problem is provided by the subsequent GTPase rearrangements to the *closed* and *activated* states, which helps switch the targeting complex from a cargo-binding to cargo-releasing mode. The interaction of cargo with SRP is estimated to weaken ~ 400-fold when the *early* targeting complex rearranges to the subsequent conformational states (Zhang 2009). Further, mutant GTPases that block the *closed* → *activated* rearrangement specifically block the engagement of cargo with the translocon (Shan 2007). Finally, crosslinking and cryo-EM analyses showed that in the presence of SR and GTP analogues, the NG-domain of SRP becomes mobile and detaches from L23 (Pool 2002; Halic 2006). Importantly, these late GTPase rearrangements can be induced by anionic phospholipid membranes (Figure 1.3, step 3) (Lam 2010), suggesting an attractive mechanism to spatially couple the membrane delivery of translating ribosomes to their subsequent unloading at late stages of protein targeting.

Collectively, these results provide a coherent picture for how the unusual GTPase cycle of SRP and SR is used to provide exquisite spatial and temporal coordination of protein targeting (Figure 1.3B). GTPase assembly is minimized in the absence of biological cues, but is initiated when the SRP is loaded with RNCs bearing strong signal sequences (steps 1-2). In the absence of target membrane, however, the RNC-SRP-SR complex is primarily stalled in the *early* conformational stage, where the cargo is tightly bound to SRP and GTP hydrolysis is delayed. Interaction of FtsY with phospholipid membranes helps relieve this 'pause' and induce the GTPase rearrangements into the *closed/activated* states, in which the interaction of ribosome with the SRP is weakened and the RNC could be more readily released from the targeting complex (step 3). It is still unclear what ultimately drives the completion of the cargo handover event and re-activates GTP hydrolysis (steps 4-5), although the SecYEG translocation machinery provides an attractive candidate. GTP hydrolysis then drives the disassembly and recycling of SRP and SR, allowing them to initiate new rounds of protein targeting.

1.3.4 Fidelity of SRP: binding, induced fit, and kinetic proofreading

Like other topogenic sequences that mediate protein localization, SRP signal sequences are highly divergent (von Heijne 1985; Kaiser 1987; Gierasch 1989; Zheng 1996), and the SRP must be sufficiently flexible to accommodate diverse signal sequences. Despite its flexibility, SRP must also remain highly specific to its substrates to minimize the mislocalization of proteins that would be detrimental to cells. How the SRP or any protein targeting machinery faithfully selects their correct substrates has been a challenging question. Although previous work has focused on the observation that SRP

binds weakly to the 'incorrect' cargos bearing no or weak signal sequences (Figure 1.3B, red arrow a), quantitative biophysical measurements show that SRP binds with substantial affinity to the incorrect cargos or even the empty ribosome (K_d ~ 80–100 nM) (Flanagan 2003; Bornemann 2008; Zhang 2010). Given the cellular SRP concentration (~ 400 nM in bacteria), it appears unlikely that the discrimination in the cargo-binding step is sufficient to reject all the incorrect cargos.

A quantitative dissection of the individual molecular events in the bacterial SRP pathway (Figure 1.3B) demonstrates that the multiple conformational rearrangements in the SRP-FtsY GTPase complex provide a series of additional checkpoints to further reject the incorrect cargos (Zhang 2010). These include: (i) formation of the *early* intermediate, which is stabilized over 100-fold by the correct, but not incorrect cargos (Figure 1.3B, red arrow b); (ii) rearrangement of the *early* intermediate to the *closed* complex, which is ~ tenfold faster with the correct than the incorrect cargos (Figure 1.3B, red arrow c); (iii) GTP hydrolysis by the SRP•FtsY complex, which is delayed ~ eightfold by the correct cargo to give the targeting complex a sufficient time window to identify the membrane translocation machinery. In contrast, the hydrolysis event remains rapid with the incorrect cargo ($t_{1/2}$ < 1s), which could allow the targeting of incorrect cargos to be aborted (Figure 1.3B, arrow d). A mathematical simulation based on the kinetic and thermodynamic parameters of each step strongly suggest that all these fidelity checkpoints are required to reproduce the experimentally observed pattern of substrate selection by the SRP (Zhang 2010).

These results support a novel model in which the fidelity of protein targeting by the SRP is achieved through the cumulative effect of multiple checkpoints, by using a

combination of mechanisms including cargo binding, induced SRP-SR assembly, and kinetic proofreading through GTP hydrolysis. Additional discrimination could be provided by the SecYEG machinery, which further rejects the incorrect cargos (Jungnickel 1995). Analogous principles have been demonstrated in the DNA and RNA polymerases (Uptain 1997; Kundel 2000), the spliceosome (Semlow 2012), tRNA synthetases (Fersht 1976) and tRNA selection by the ribosome (Rodnina 2001), and may represent a general principle for complex biological pathways that need to distinguish between the correct and incorrect substrates based on minor differences.

1.3.5 SRP RNA: a central regulator of SRP

Besides the SRP54 (or Ffh) protein, the SRP RNA is the only other universally conserved and essential component of SRP (Rosenblad 2003). However, its precise roles in protein targeting have remained enigmatic. In early biochemical reconstitutions of the mammalian SRP, the SRP RNA appeared nothing more than a scaffold that holds different SRP protein subunits together (Figure 1.5 below). The discovery of the bacterial SRP RNA (Poritz 1988), which binds a single protein Ffh, implied a much more active role for this RNA. Recent biochemical and structural studies strongly supported this view and show that the SRP RNA can mediate global reorganization of the SRP in response to cargo binding and provide additional interactions with the SR, thus mediating the molecular communication between the cargo and the SRP/SR GTPases during protein targeting.

The bacterial 4.5S SRP RNA contains the most conserved domain IV of the SRP RNA and forms an elongated hairpin structure capped by a highly conserved GGAA

tetraloop at one end (Figure 1.4A). Two internal loops, A and B, mediate binding of this RNA to a helix-turn-helix motif in the M-domain of Ffh with picomolar affinity (Batey 2000; Batey 2001). The orientation of the M-domain/RNA complex relative to the Ffh-NG-domain, however, exhibits a high degree of variability. Crystallographic analyses and structural mapping studies have generated at least four different structures or structural models for SRP, each exhibiting a distinct interdomain arrangement (Figure 1.4B for two examples) (Keenan 1998; Rosendal 2003; Buskiewicz 2005; Buskiewicz 2005b; Mainprize 2006; Hainzl 2007). Collectively, these observations suggest that apo-SRP could exist in a variety of global conformations, likely due to the 30-amino-acid-long flexible linker connecting the M- and NG-domains of Ffh.

Upon binding the RNC, however, the SRP undergoes a global conformational change (Figure 1.4C) (Halic 2006; Schaffitzel 2006; Buskiewicz 2009). The bi-dentate interaction of the RNC with Ffh re-oriented its M- and NG-domains, such that the SRP RNA now lies parallel to the ribosome surface, with its GGAA tetraloop positioned adjacent to the FtsY-interacting surface on the Ffh-NG-domain (Figure 1.4C). This is important, as the RNA tetraloop is required for rapid assembly of a stable SRP-FtsY complex (Peluso 2000; Jagath 2001; Peluso 2001; Siu 2006; Zhang 2008). More recent kinetic and phylogenetic analyses (Shen 2010), hydroxylradical footprinting experiments (Spanggord 2005), and cryo-EM analysis (Estrozi 2011) identified a key electrostatic interaction between the SRP RNA tetraloop and conserved basic residues surrounding Lys399 on the lateral surface of FtsY (Figure 1.4D). This interaction stabilizes the otherwise highly labile *early* intermediate, thus accelerating stable SRP-FtsY assembly 10^2–10^3 fold (Zhang 2008; Shen 2010). Importantly, the RNA tetraloop or FtsY Lys399

exerts these stimulatory effects only when the SRP is bound to RNCs bearing strong signal sequences (Shen 2010; Shen 2011) and, to a lesser extent, to signal peptide or signal peptide mimics (Bradshaw 2009). Combined with structural analyses (Halic 2006; Schaffitzel 2006; Estrozi 2011; Hainzl 2011), a coherent model emerges in which the RNC optimizes the conformation of SRP so that the SRP RNA tetraloop is pre-positioned to interact with the incoming FtsY, thus allowing rapid recruitment of the SR to be achieved specifically for the correct cargos (Figure 1.4B–D).

Intriguingly, neither the SRP RNA tetraloop nor FtsY Lys399 affect the equilibrium stability of the SRP-FtsY complex in the *closed/activated* states (Peluso 2000; Shen 2010), suggesting that their interaction is highly transient and occurs only during the *early* intermediate stage of GTPase assembly. A recent crystallographic study using full-length 4.5S RNA (Ataide 2011) revealed a completely different configuration of the SRP-FtsY complex, in which a *closed/activated* GTPase complex docks at a distinct site near the 5', 3'-end of the SRP RNA ~ 100 Å away from the tetraloop end (Figure 1.4A, distal site and Figure 1.4E). Mutations of the distal site compromised GTPase activation in the SRP-FtsY complex, supporting the importance of this alternative RNA-GTPase interaction (Ataide 2011). Although it is still at early stages, these results suggest an intriguing model in which the Ffh-FtsY-NG-domain complex, after initial assembly near the RNA tetraloop, relocalizes to the opposite end of the SRP RNA where its GTPase activity is fully activated. In the context of the protein targeting reaction, this movement is highly attractive as it removes the GTPase complex from the ribosome exit site, generating a conformation that allows the RNC to be more easily released from the targeting complex and the SecYEG complex to more readily access the

ribosome exit site (Figure 1.4E). In addition, the unloading of cargo could be tightly coupled to GTPase activation in such a mechanism. Nevertheless, direct evidence for such a large-scale GTPase movement on the SRP RNA, its underlying driving forces and molecular mechanisms, and its precise roles in the protein targeting reaction remain to be demonstrated.

1.3.6 Transition from the targeting to translocation machinery

At the end of the protein targeting reaction, the RNC must be unloaded from the SRP-FtsY complex to the heterotrimeric SecYEG (or Sec61p). The readers are referred to (Rapaport 1996; Johnson 1999; Driessen 2008; de Plessis 2011) for more comprehensive reviews of this machinery. In the context of the co-translational targeting reaction, rich structural information has been obtained in recent years to explain how this translocon interacts with the RNC and potentially interfaces with the SRP targeting machinery. A crystal structure of *M. jannaschii* SecYEβ (van der Berg 2003) showed that TMs 1–10 of SecY form an hourglass-shaped pore in this channel. Lining one side of this pore are TMs 2b and 7, which form the lateral gate where hydrophobic signal sequences and TMs in the nascent polypeptide bind and subsequently enter the lipid bilayer (Plath 1998; Heinrich 2000; Cannon 2005). Cryo-EM reconstructions of the complex of RNC with SecYEG or its eukaryotic homologues at increasing resolution (Beckmann 2001; Mitra 2005; Becker 2009; Fraunfeld 2011), combined with biochemical and genetic studies (Cheng 2005; Menetret 2007), further identified the highly conserved basic residues in the C4 and C5 (or L6/7 and L8/9) loops of SecY as the key motifs that mediate interaction with ribosomal proteins L23 and L35 at the exit site.

Remarkably, the binding sites of the SecYEG/Sec61p complex on the translating ribosome overlap extensively with those of SRP (Figure 1.2A). This raises challenging questions as to how the RNC is handed over from the targeting to translocation machinery without nonproductive loss of the translating ribosome. The most productive mechanism for the cargo transfer event is probably through a concerted pathway, in which the two contacts of SRP with the RNC, those with the L23/L35 ribosomal proteins and with the signal sequence, are sequentially dissolved and replaced by those of the SecYEG machinery. Many observations described earlier, including the loss of density for the Ffh-FtsY-NG-domain complex in cryo-EM reconstructions of the targeting complex (Halic 2006), the ability of the NG-domain complex to re-localize to the SRP RNA distal end (Ataide 2011), and the requirement of GTPase rearrangements for detachment of SRP from the ribosome (Shan 2007; Zhang 2009) provide clues that support such a mechanism. The ability of SR to directly interact with the SecYEG/Sec61p complex (Wittke 2002; Helmers 2003; Jiang 2003; Angelini 2006; Kuhn 2011) further raises the possibility that the translocon plays an active role in the cargo handover process. Nevertheless, the cargo handover event remains the least understood aspect of the co-translational targeting reaction. The fate of the ribosomal proteins and the signal sequence in this cargo handover event, their timing relative to one another and to the hydrolysis of GTP, and the molecular forces that drive this step remain challenging questions for future investigations.

1.4 Eukaryotic SRP

1.4.1 Mammalian SRP: additional layers of complexity

Compared to its bacterial homologue, the mammalian SRP is significantly larger and more complex, comprised of six proteins and a 7S SRP RNA (Figure 1.5). It can be divided into two distinct domains: the S-domain, comprised of domains II–IV of 7S RNA and the SRP 19, 54, and 68/72 protein subunits, and the Alu domain, comprised of domain I of 7S RNA and the SRP 9/14 subunits (Figure 1.5). The increased complexity adds additional layers of nuance and regulation for the mammalian SRP, many of which await to be elucidated.

For example, the mammalian SRP54 subunit binds the 7S RNA weakly by itself. Indeed, premature binding of SRP54 could cause the two RNA-binding loops for SRP19 to misfold, disrupting the native assembly of SRP (Maity 2006; Maity 2007). *In vivo*, assembly of the mammalian SRP goes through an ordered pathway in which all the SRP proteins except for SRP54 are imported to the nucleus to bind SRP RNA; the partially assembled SRP is then exported to the cytoplasm for SRP54 binding, thus completing its assembly [(Poritz 1988; Jacobson 1998; Ciufo 2000; Grosshans 2001); see (Leung 2010) for a more complete review of SRP assembly]. *In vitro* reconstitutions showed that pre-binding of SRP19 to the 7S RNA is required for loading the SRP54 subunit on the SRP RNA (Walter 1983; Siegel 1985). Crystallographic analyses showed that SRP19 bridges the two tetraloops in both domains III and IV (or helices 6 and 8) of the 7S RNA and pre-organizes the internal loops in domain IV into a conformation required for stable SRP54 binding [(Wild 2001; Hainzl 2002; Oubridge 2002; Hainzl 2005; Menichelli 2007; Egea 2008); see (Sauer-Eriksson 2003) for a more complete review]. Why the mammalian

SRP requires this additional layer of allostery during its assembly remains unclear.

In addition, although much is known about the binding sites of SRP68/72 on the 7S RNA (Iakhiaeva 2005; Iakhiaeva 2006; Yin 2007; Iakhiaeva 2008; Iakhiaeva 2009; Iakhiaeva 2010), the structure and precise function of the SRP68/72 subunits remain to be defined. Chemical probing experiments have suggested that SRP68/72 cooperates with SRP19 to pre-organize the 7S RNA into a conformation competent for SRP54 binding, by exposing the SRP54 binding sites on the 7S RNA (Menichelli 2007; Maity 2008). These subunits have also been implicated in controlling the interaction of SRP54 with the SR (Siegel 1988). Direct evidence for both of these models remains to be obtained.

The most interesting aspect of mammalian SRP, aside from the core functions, is the 'Alu' domain (Figure 1.5) that arrests translation elongation just after the signal sequence emerges from the ribosome. Early biochemical work found that SRP interacts with the ribosome during elongation factor-2 catalyzed translocation of tRNA (Ogg 1995), suggesting that it competes with the binding of elongation factors. Recent biochemical and crosslinking studies further show that SRP9/14 electrostatically interacts with ribosomal RNA via at least two stretches of basic residues and is also in close contact with ribosomal proteins at the interface between the large and small ribosomal subunits (Terzi 2004; Mary 2010). Consistent with this notion, cryo-EM analysis showed that mammalian SRP forms an elongated, kinked structure in which the Alu domain reaches into the elongation factor binding site at the ribosome subunit interface (Halic 2004) (Figure 1.5B). Although the elongation arrest activity is not a prerequisite for protein targeting *in vitro*, deletion of SRP9/14 *in vivo* results in severe defects in protein targeting and mammalian cell growth (Lakkaraju 2008). Together with the observation

that the SRP could not target proteins when the nascent polypeptide exceeds a critical length (Siegel 1988; Flanagan 2003), these results suggest that elongation arrest provides a crucial time window that allows the targeting complex to engage the translocon before the nascent chain loses translocation competence. The precise mechanism and degree of elongation arrest by the Alu domain, and how it communicates and/or collaborates with the S-domain during the targeting reaction remain to be determined.

1.4.2 Chloroplast SRP: a unique post-translational SRP

The co-translational nature of the SRP pathway is universally conserved except for the chloroplast in green plants, where a unique post-translational SRP pathway has evolved. Instead of delivering RNCs as its cargo, the chloroplast SRP (cpSRP) is dedicated to the delivery of the light-harvesting chlorophyll-binding (LHC) proteins from the chloroplast stroma to the thylakoid membrane (Schunemann 1998; Cline 2002). Analogous to the cytosolic SRP, the chloroplast SRP (cpSRP) pathway is mediated by close homologues of the SRP54 and SR GTPases, called cpSRP54 and cpFtsY, respectively (Franklin 1993; Li 1995; Schunemann 1998; Tu 1999). However, the M-domain of cpSRP54 has lost the ability to bind the otherwise universally conserved SRP RNA (Richter 2008). Instead, a unique SRP subunit in chloroplast, cpSRP43, binds a C-terminal extension in the cpSRP54 M-domain to form the cpSRP (Funke 2005; Hermkes 2006). As detailed below, these changes likely reflect adaptation of the cpSRP system to the post-translational targeting of its substrate protein, the LHCPs. In addition, another pool of cpSRP43-free cpSRP54 was found in stroma, which together with cpFtsY mediate the co-translational targeting of some of the chloroplast-encoded membrane

proteins, such as D1 (Nilsson 2002). The readers are referred to (Schunemann 2004; Aldridge 2009; Richter 2010) for comprehensive reviews of the cpSRP. Here, we will focus on valuable lessons that came from comparison of the cpSRP with the classic cytosolic SRP in recent years.

How does the cpSRP bypass the otherwise strictly conserved SRP RNA? In cytosolic systems, a major function of the SRP RNA is to accelerate the interaction between the SRP and FtsY GTPases and thus ensure rapid cargo delivery. Kinetic analysis in the cpSRP system showed that, even in the absence of an SRP RNA, the cpSRP and cpFtsY GTPases interact 400-fold faster than their bacterial homologues (Jaru-Ampornpan 2007). Subsequent crystallographic (Stengel 2007; Chandrasekar 2008) and biochemical cross-complementation (Jaru-Ampornpan 2009) analyses further revealed two key molecular mechanisms underlying this phenomenon: (i) compared to bacterial FtsY, the NG-domain conformation of cpFtsY more closely resembles that in the *closed* SRP-FtsY complex; this may allow cpFtsY to bypass some of the rearrangements required for stable GTPase assembly (Stengel 2007; Chandrasekar 2008); (ii) more importantly, the M-domain of cpSRP54 functionally mimics the SRP RNA, accelerating its interaction with cpFtsY 100-fold and allowing them to achieve an interaction rate that matches the RNA-catalyzed interaction between their bacterial homologues (Jaru-Ampornpan 2009). It is probable that analogous to the cytosolic SRP system, the interaction between the cpSRP and cpFtsY GTPases are regulated by upstream and downstream components of the pathway, such as the substrate protein or the target membrane (Marty 2009); these allosteric regulations and their roles in the cpSRP pathway remain to be uncovered.

The unique cpSRP43 subunit is responsible for substrate recognition and enables the cpSRP to adapt to the challenge of post-translational protein targeting. Unlike the co-translational pathway, cpSRP must handle fully synthesized, highly hydrophobic LHC proteins, which are prone to aggregation and misfolding in aqueous environments. Early work found that LHC proteins are effectively chaperoned in the stroma, where it forms a soluble 'transit complex' with the cpSRP (Reed 1990; Payan 1991; Li 1995; Schunemann 1998; Tu 2000), although substrate capture by the cpSRP may require additional factors, such as LTD at the chloroplast envelope (Ouyang 2011). Recent biochemical dissections showed that cpSRP43 is necessary and sufficient for binding with high affinity to LHC proteins and maintaining them in a soluble, translocation competent state (Falk 2010; Jaru-Ampornpan 2010). cpSRP43 is comprised of a unique combination of protein-interaction motifs, with three chromodomains [CDs; (Sivaraja 2005; Kathir 2008)] and four ankyrin (Ank) repeats (Ank1–4) sandwiched between CD1 and CD2 (Klimyuk 1999; Schunemann 2004). The ankyrin repeat domain specifically recognizes L18, a relatively polar 18-amino-acid motif between TM2 and TM3 of LHC proteins (Delille 2000; Tu 2000; Jonas-Straube 2001). Crystallographic analyses further showed that the CD1-Ank4 fragment of cpSRP43 folds into an elongated horseshoe structure, in which a groove across the concave surface of Ank2 to 4 binds a highly conserved DPLG turn in the L18 peptide (Stengel 2008), enabling specific recognition of LHC proteins by cpSRP43. As a molecular chaperone, cpSRP43 likely also interacts with and shields the hydrophobic TMs in LHC proteins, although the molecular basis of these interactions remains to be deciphered. Finally, recent work found that even when LHC proteins have already aggregated, cpSRP43 can resolubilize the aggregate and return them to soluble

fractions *in vitro* (Falk 2010; Jaru-Ampornpan 2010). This 'disaggregase' activity was unexpected, as cpSRP43 does not contain an ATPase domain and hence must use a mechanism distinct from that of the well-studied AAA^+ family of disaggregase systems (Doyle 2008). This finding demonstrated the capability and diversity of chaperone function during post-translational membrane protein targeting; the molecular basis underlying cpSRP43's 'disaggregase' activity, and its precise roles in LHC protein biogenesis *in vivo* remain to be determined.

At the thylakoid membrane, LHC proteins are delivered by the cpSRP and cpFtsY to Alb3, a member of the YidC/Oxa1 family of membrane proteins that facilitate membrane protein insertion and assembly. Recently, a direct interaction between cpSRP43 and the C-terminal stromal domain of Alb3 has been shown in biochemical studies (Falk 2010; Lewis 2010) and *in vivo* complementation analyses (Bals 2010; Dunschede 2011). The molecular mechanism underlying this interaction and its precise roles in the targeting and integration of LHC proteins remain to be clarified. Nevertheless, this interaction is highly attractive, as it provides a mechanism to accurately localize the targeting complex to the Alb3 translocase and to couple the membrane delivery of LHC proteins to their subsequent integration. Many of the lessons learned from this system could be leveraged to help understand the mechanism of cargo unloading in the cytosolic SRP pathway.

1.5 Future directions

1.5.1 Molecular code of the signal sequence

Early pioneering work has identified a hydrophobicity core as the major determinant of signal sequences that mediate protein secretion, facilitated by basic amino acids at the N-terminus in some cases (von Heijne 1985; Gierasch 1989). The propensity to adopt a-helical structures in apolar media has also been identified as an important determinant of the signal sequence (Jones 1990; Wang 1993). However, subsequent work revealed additional layers of complexity. First, multiple pathways mediate protein secretion in bacteria and yeast, and signal sequences also specify the targeting pathway (Figure 1.1A) (Zheng 1996). Second, although a threshold level of hydrophobicity in signal sequences was generally thought to specify the SRP pathway, more recent studies in bacteria (Huber 2005) and yeast (Alamo 2011) indicated that the correlation between hydrophobicity and SRP-dependent targeting is poor, and signal sequences with hydrophobicity above the apparent 'threshold' failed to engage the SRP (Huber 2005). Third, special N-extensions to a strong SRP signal sequence, such as those found in the bacterial autotransporter EspP, can allow nascent proteins to escape the SRP pathway (Peterson 2006; Zhang 2010). Apparently, additional molecular features of the signal sequence play important roles, including helical propensity (Jones 1990; Wang 1993), the presence of N-terminal basic residues (von Heijne 1985; Peterson 2003), and additional properties that have yet to be identified. How the information from all the different features is integrated to comprise the 'molecular code' that specify the SRP remains unclear. Crucial to the effort to 'decode' the signal sequence will be the availability of a more comprehensive catalogue of validated SRP-dependent vs. SRP-independent substrates, which would allow more systematic analyses of the molecular features of

signal sequences and evaluation of their respective contributions to recognition by the SRP.

1.5.2 The crowded ribosome exit site

Accumulating data now indicate that the ribosome exit site is a crowded environment where multiple protein biogenesis factors interact. As a newly synthesized protein emerges from the ribosomal exit tunnel, it interacts with a host of cellular factors that facilitate its folding, localization, maturation, and quality control. These include molecular chaperones such as trigger factor (TF) in bacteria, Hsp70 (DnaK/J in bacteria), and the nascent chain-associated complex (NAC) in yeast; modification and processing enzymes such as methionine aminopeptidase (or peptide deformylase in bacteria), N-acetyl transferase, and arginyl transferase; and protein targeting and translocation machineries such as the SRP and SecYEG (Cross 2009; Kramer 2009; Fedyukina 2011). Even post-translational targeting factors, such as SecA (Huber 2011) and the Bag6 complex (Mariappan 2010), were recently reported to interact with the RNC. Many of these factors, including the SRP, SecYEG, TF and SecA, contact the ribosome via the same protein, L23 (or Rpl25 in eukaryotes) (Knoops 2011), and recognize hydrophobic sequences on the nascent polypeptide. It is currently unclear whether and how these factors compete or collaborate with one another for binding the translating ribosome (Beck 2000; Lee 2002; Ullers 2003b; Buskiewicz 2004; Eisner 2006; Alamo 2011; Zhang 2012). Further, the molecular mechanisms by which a nascent protein is sorted among different cotranslational factors and committed to the correct biogenesis pathway remain key questions to be addressed in future investigations.

1.5.3 Signaling from inside the ribosome

Most Previous models assumed that binding of the SRP or other cellular machineries to RNC occurs when signal sequences become exposed outside the ribosome. This view was initially challenged by the observation that the opening and closing of the Sec61p translocon is regulated by the nascent protein from inside the ribosome (Liao 1997). More recently, multiple biochemical and crosslinking studies showed that a signal sequence within the ribosome exit tunnel enhances the binding of SRP to the RNC (Bornemann 2008; Berndt 2009) and helps recruit a regulatory protein RAMP4 to the Sec61p translocon (Pool 2009). Further, in the GET pathway that delivers tail-anchored proteins to the ER, the Bag6 complex is specifically recruited to the RNC when the C-terminal TM of the nascent protein emerges inside the ribosome (Mariappan 2010). Together, these results suggest that sequence or structural features of the nascent polypeptide inside the ribosome provide 'signals' that can be transmitted to the ribosome exit site and lead to the recruitment of different cellular factors. The nature of ribosome structural changes that underlie these signaling events, the mechanisms ensuring the specificity of these 'signals', and their precise roles in the respective cellular pathway are important questions for future studies.

1.5.4 SRP-dependent targeting to other translocons

Although SecYEG (or Sec61p) is a central protein-conducting channel where many co- and post-translational pathways converge, membrane insertion of a subset of membrane proteins requires the translocase YidC, a member of the Oxa1 family of

membrane proteins that facilitate the insertion and assembly of membrane proteins (see (Luirink 2001; Dalbey 2011; Wang 2011) for more comprehensive reviews of the YidC/Oxa1/Alb3 family of insertases). Although some of YidC's function are exerted through cooperation with the SecYEG machinery, increasing evidence show that YidC can also constitute an independent translocon for insertion of a number of proteins, including an M13 procoat protein (Chen 2005; Stiegler 2011), the mechanosensitive channel MscL (Facey 2007; Pop 2009), and subunits of the F_1F_0 ATP synthase (van der Laan 2004; Yi 2004). In many studies, the targeting of MscL and the F_1F_0 subunits to YidC appears to be dependent on the co-translational SRP/FtsY machinery (de Gier 2003; Kol 2008; Xie 2008). As noted earlier, the cpSRP targets LHC proteins to Alb3, the YidC homologue in chloroplasts. The structure and mechanism of YidC (Ravaud 2008) as an independent membrane protein insertase, how it interacts with the ribosome and the nascent polypeptide, and how it interfaces with the SRP targeting machinery remain to be determined. The decision-making process that routes a subset of SRP substrate proteins to the YidC instead of SecYEG translocon also remain to be elucidated, and will likely reveal additional layers of nuance and regulation in this pathway.

1.5.5 Translation-independent membrane protein targeting pathways

Although targeted delivery of membrane proteins based on signals embedded in the nascent polypeptide has been long established, efforts to identify cellular mechanisms to target ribosomes to membranes based on information in the mRNA never ceased. A recent study provided evidence for an alternative pathway(s) that localizes proteins to the target membrane in a translation-independent manner, based on cis-acting elements in the

TM domain-encoding sequences on the mRNA (Nevo-Dinur 2011). It was hypothesized that codons for hydrophobic amino acids in the TM domains are highly enriched in uracil content, which could provide a distinctive signature for these mRNAs to enable their recognition and targeted delivery to the membrane (Prilusky 2009). The components, pathways and mechanisms of translation-independent targeting of membrane proteins and the contribution of these pathways to proper membrane protein localization within cells remain open questions that invite more investigations.

1.6 Acknowledgements

We are indebted to Sandra Schmid, Jennifer Doudna, Peter Walter, Douglas Rees, Raymond Deshaies and Bil Clemons for support and insightful discussion over the years. S.S. was supported by NIH grant GM078024, and career awards from the Henry and Camille Dreyfus foundation, the Arnold and Mabel Beckman foundation, and the David and Lucile Packard foundation. D. A. was supported by NIH/NRSA training grant 5T32GM07616. X.Z. was supported by a fellowship from the Ulric B. and Evelyn L. Bray Endowment Fund.

1.7 Figures and figure legends

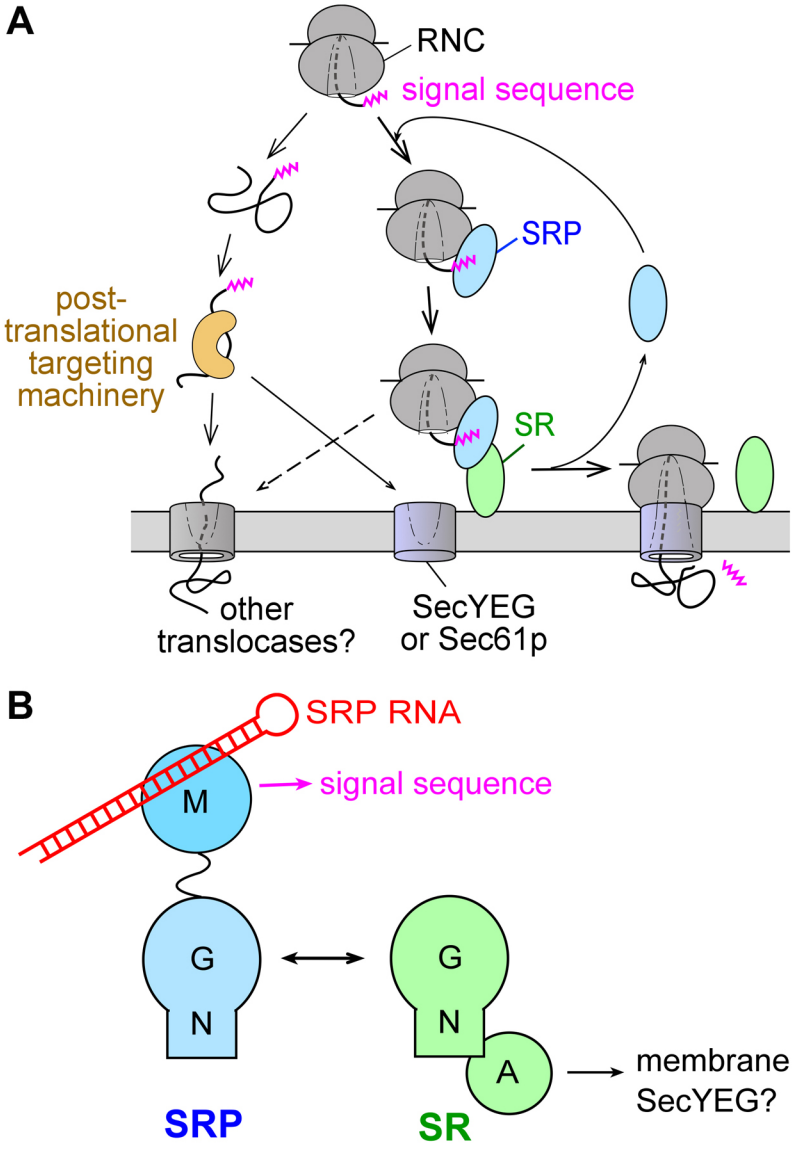

Figure 1.1 Overview of the pathways and components of SRP. (A) Multiple pathways deliver newly synthesized proteins to the ER or plasma membrane, with the SRP pathway mediating the co-translational targeting of translating ribosomes (right) whereas post-translational targeting machineries mediating the targeting of proteins released from the ribosome. (B) Domain structures of the ribonucleoprotein core of SRP, comprised of the SRP54 (or Ffh) protein and the SRP RNA (left), and the bacterial SRP receptor (right).

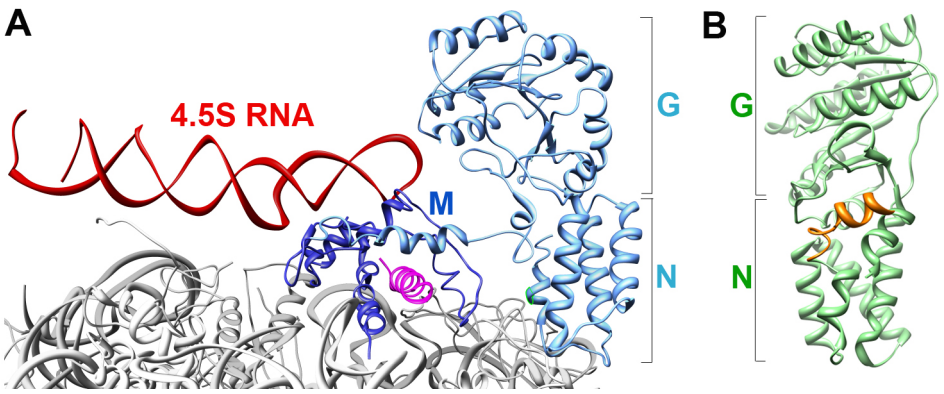

Figure 1.2 (A) Molecular model for interaction of the bacterial SRP with the translating ribosome (grey; PDB 2J28), derived from cryo-EM reconstruction and docking of the crystal structures of individual protein fragments as described in (Halic 2006b). The M- and NG-domains of the SRP are in dark and light *blue*, respectively, the SRP RNA is in *red*, and the signal sequence is in *magenta*. (B) Crystal structure of the bacterial FtsY (NG+1) construct (PDB 2QY9) highlighting its lipid-binding helix at the N-terminus (*orange*).

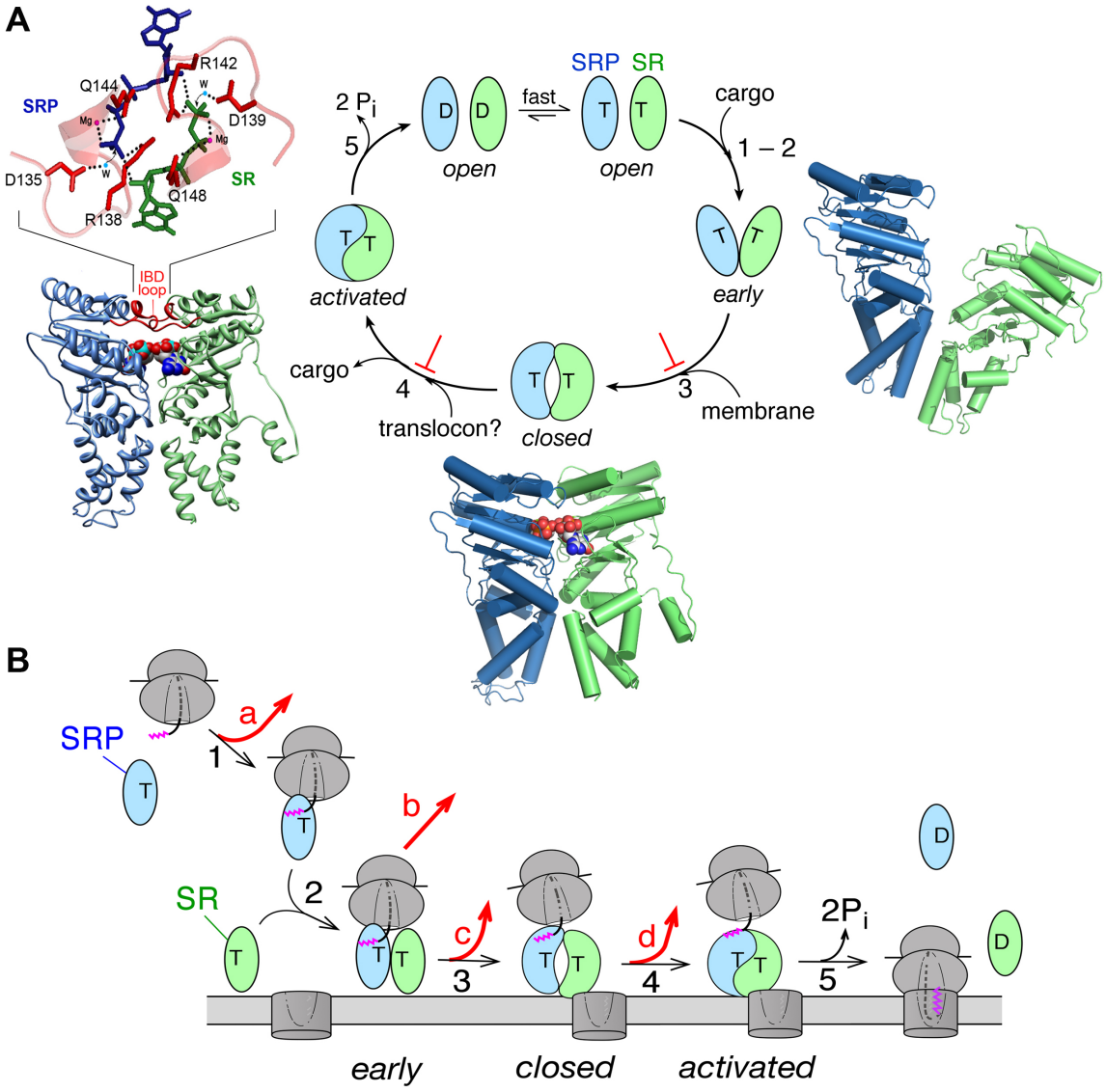

Figure 1.3 Conformational changes in the SRP and SR GTPases ensure the efficiency and fidelity of protein targeting. The steps are numbered to be consistent between parts (A) and (B). The Ffh- and FtsY-NG-domains are in *blue* and *green*, respectively. T and D denote GTP and GDP, respectively. (A) A series of discrete rearrangements drive the SRP-SR GTPase cycle, which are regulated by the cargo and target membrane. ⊥ denotes the pausing effect of cargo in disfavoring the conformational rearrangements. Right: molecular model of the early intermediate (PDB 2XKV). Bottom panel: Co-crystal

structure of the Ffh-FtsY-NG-domain complex in the closed/activated conformation (PDB 1RJ9). The two GTP analogues are in spacefill. Left panel: Zoom-in of the composite active site formed at the dimer interface required for GTPase activation, with the GMPPCP molecules from Ffh and FtsY in *blue* and *green*, respectively, active site Mg^{2+} in *magenta*, nucleophilic waters (W) in *blue*, and catalytic residues in the IBD loops in *red*. (B) GTPase rearrangements provide the driving force and ensure the fidelity of protein targeting. Step 1, RNC with a signal sequence (magenta) binds the SRP. Step 2, cargo-loaded SRP forms a stabilized *early* targeting complex with FtsY. Step 3, membrane association of FtsY drives rearrangement to the *closed* state, which weakens SRP's affinity for the cargo. Step 4, interaction of SR with the SecYEG translocon is proposed to drive GTPase rearrangements to the *activated* state required for cargo handover. Step 5, the cargo is unloaded from the SRP to SecYEG, and GTP hydrolysis drives the disassembly and recycling of SRP and SR. At each step, the cargo can be either retained in (black arrows) or rejected from (red arrows) the SRP pathway.

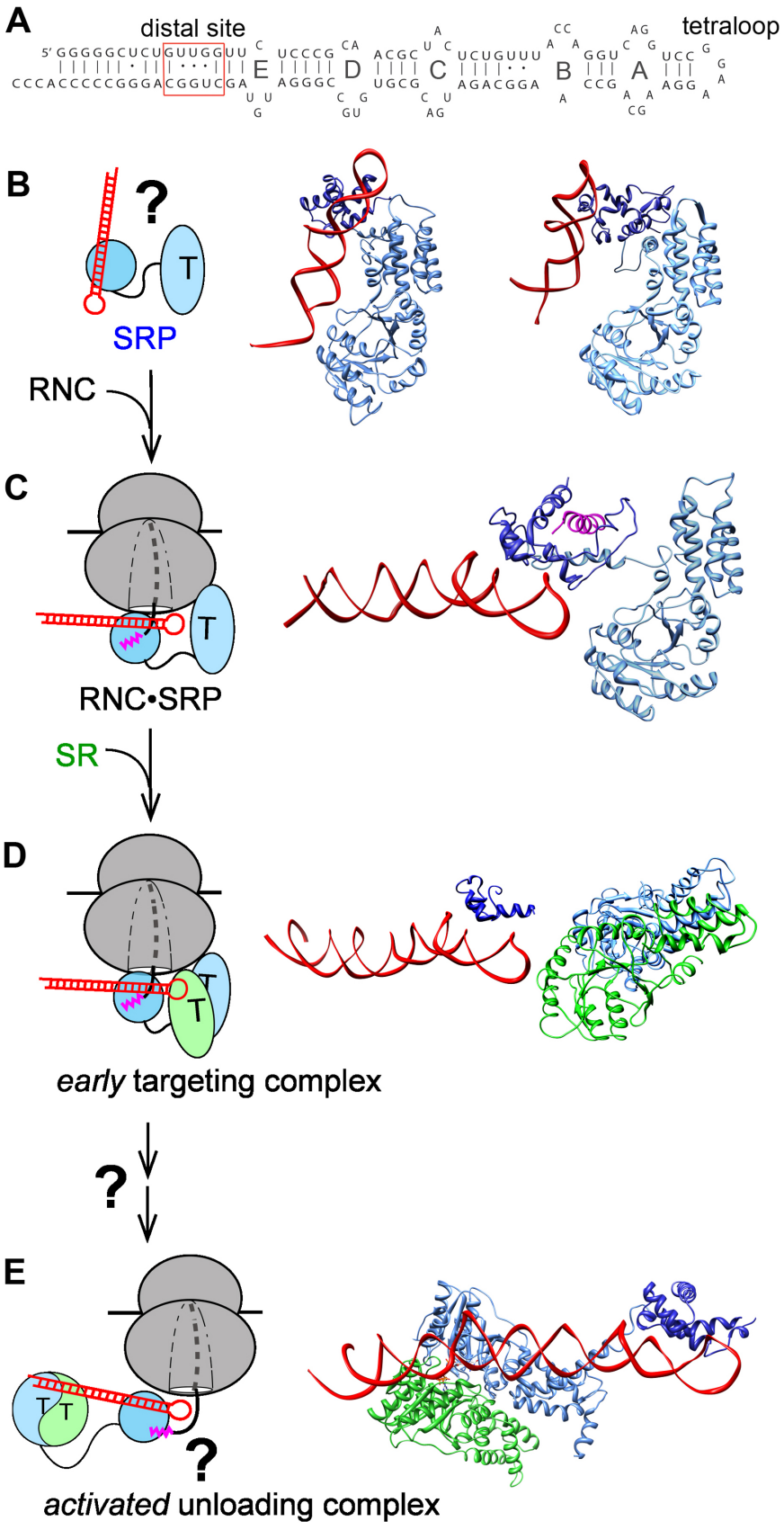
A
distal site
tetraloop
B
SRP
RNC
C
RNC•SRP
SR
D
early targeting complex
E
activated unloading complex

Figure 1.4 RNA-mediated global reorganization of the SRP couples the GTPase cycle to the cargo loading and unloading events during protein targeting. (A) Secondary structure of the *E. coli* 4.5S SRP RNA. The internal loops A–E, the GGAA tetraloop and the distal site near the 5',3'-end of this RNA are denoted. (B) Free SRP exist in a variety of 'latent' conformations in which the SRP RNA tetraloop is not positioned to contact SR. Two representative structures of SRP from *Methanococcus jannaschii* (left; PDB 2V3C) and *Sulfolobus solfataricus* (right; PDB 1QZW) are shown. (C) Binding of RNC induces SRP into a more active conformation, in which the SRP RNA tetraloop is properly positioned to interact with the G-domain of the incoming SR to form a stabilized *early* targeting complex in (D). Both panels show the molecular model derived from cryo-EM reconstructions of the RNC-SRP or RNC-SRP-FtsY early complex; the ribosome was not shown for clarity. (E) GTPase activation is potentially coupled to relocalization of the SRP•SR NG-domain complex to the distal end of SRP RNA, a conformation that is more conducive to cargo unloading (PDB 2XXA). The structures in (B) and (C) are aligned with respect to the SRP54-NG-domain, and the structures in (C)–(E) are aligned with respect to the SRP RNA. Color codings are the same as in Figure 2.

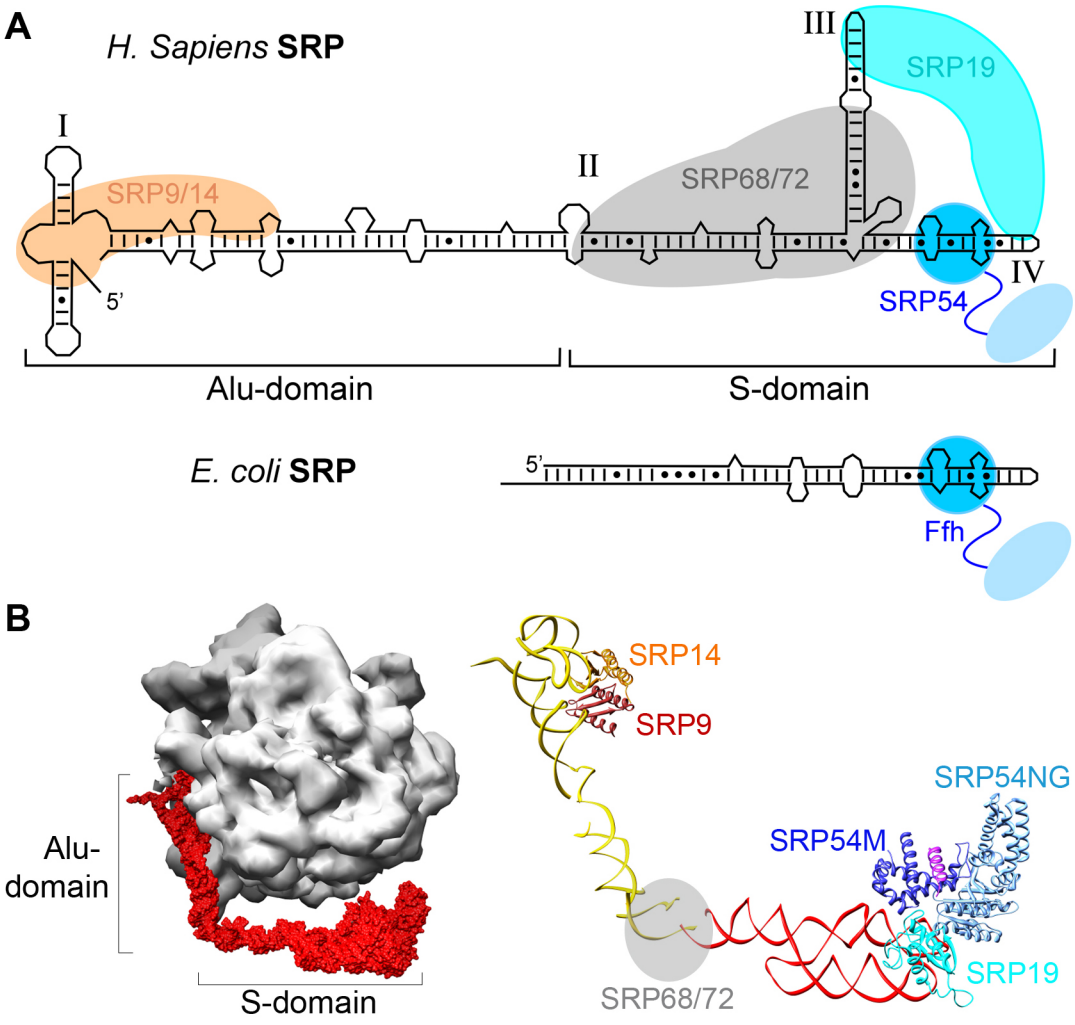

Figure 1.5 Organization of the mammalian SRP. (A) Comparison of the RNA secondary structure and composition of the mammalian and bacterial SRP. The SRP54 M- and NG-domains are in dark and light *blue*, respectively, SRP19 is in *cyan*, SRP9 is in *brown*, SRP14 is in *orange*, and the SRP68/72 complex, which lacks a crystal structure, is represented as a *grey* sphere. (B) Cryo-EM reconstruction of the mammalian SRP bound to the RNC (left; EMD-1063), and molecular model of the mammalian SRP derived from the cryo-EM and docking of the crystal structures of the individual proteins (right; PDB 1RY1). The S- and Alu-domains of the SRP RNA are in *red* and *yellow*, respectively, the protein subunits are colored as in (A).

2

SRP RNA tetraloop accelerates SRP-SR complex formation[†]

[†] A modified version of this section was published as: ***Transient tether between the SRP RNA and SRP receptor ensures efficient cargo delivery during cotranslational protein targeting***, Kuang Shen and Shu-ou Shan, *Proc Natl Acad Sci USA*, **2010**, *107*(17):7698–7703.

2.1 Abstract

Kinetic control of macromolecular interactions plays important roles in the regulation of biological systems. An example of such control occurs in co-translational protein targeting by the signal recognition particle (SRP), during which the SRP RNA and the cargo both accelerate complex assembly between the SRP and SRP receptor FtsY 10^2-fold. The molecular mechanism underlying these rate accelerations remains unclear. Here we provide biochemical, biophysical, and phylogenetic evidence that a highly conserved basic residue, Lys399, on the lateral surface of FtsY serves as a novel RNA tetraloop receptor that mediates the SRP RNA-induced acceleration of complex assembly between the SRP and FtsY. Further, mutation of this residue abolishes the ability of cargo to stimulate SRP-FtsY complex assembly, indicating that FtsY-Lys399 provides a key site that mediates the cargo-induced acceleration of complex assembly. We propose that FtsY-Lys399 makes a transient interaction with the SRP RNA tetraloop during the early stages and transition state of complex formation; this accelerates the assembly of a stable SRP•FtsY complex and allows the loading of cargo to be efficiently coupled to its membrane delivery. The use of a transient 'tether' to increase the lifetime of transient intermediates and reduce the dimension of diffusional search represents a novel and effective mechanism to accelerate macromolecular interactions.

2.2 Introduction

Macromolecular assembly processes mediate numerous essential biological processes. As cellular systems are seldom at equilibrium, controlling the kinetics of macromolecular interactions plays important roles in the regulation of cellular pathways. An example of such kinetic control is found during the interaction of the signal recognition particle (SRP) with the SRP receptor, which together comprise the major molecular machinery that mediates the co-translational targeting of proteins to cellular membranes (Walter and Johnson 1994). Protein targeting begins when the SRP recognizes ribosome-nascent chain complexes (RNCs) containing signal sequences (Walter and Blobel 1981; Walter 1981; Pool 2002; Halic 2004; Halic 2006; Schaffitzel 2006). The interaction of SRP with the SRP receptor, localized on the target membrane, is responsible for delivering the RNC to the membrane (Gilmore 1982; Walter 1984). After extensive rearrangements in the SRP•SRP-receptor complex (Shan 2004; Zhang 2009), the RNC is unloaded from the SRP onto a protein translocation machinery, through which the nascent polypeptide chain is either integrated into the membrane or translocated across the membrane to enter the secretory pathway (Simon and Blobel 1991; Beckmann 1997; Menetret 2000; Beckmann 2001; Van den Berg 2004). SRP and SRP receptor then dissociate from one another, a process driven by GTP hydrolysis (Connolly 1991; Peluso 2001), and a new cycle of protein targeting and translocation ensues.

The functional core of SRP is comprised of an SRP54 protein (called Ffh in bacteria) and an SRP RNA. SRP54 (or Ffh) contains a methionine-rich M-domain that recognizes signal sequences and binds the SRP RNA (Zopf 1990; Keenan 1998; Batey

2000). In addition, a GTPase NG-domain in Ffh binds the SRP receptor, called FtsY in bacteria, which also contains an NG-domain highly homologous to that in Ffh (Freymann 1997; Montoya 1997). SRP and FtsY form a stable complex through extensive interactions between their NG-domains (Egea 2004; Focia 2004), and this process is responsible for delivering the cargo to the target membrane.

Previous work showed that formation of a stable SRP-FtsY complex is a multi-step process that involves at least two distinct stages (Shan 2004; Zhang 2008). In the first stage, the two proteins rapidly associate to form a GTP-independent *early* intermediate (Zhang 2008). This intermediate is characterized by loose interactions between the two GTPases and is highly transient in nature, with a lifetime of ~ 16 milliseconds (Zhang 2008). In the second stage of complex assembly, the *early* intermediate undergoes extensive rearrangements to form a stable complex (Shan 2004; Zhang 2008). This rearrangement requires the removal of steric blocks imposed by the N-terminal α-helices of both Ffh and FtsY (Focia 2006; Gawronski-Salerno and Freymann 2007; Neher 2008). In addition, the N-domains of both proteins need to move closer to one another and form additional stabilizing interactions at the heterodimer interface (Egea 2004; Focia 2004). Finally, the two bound GTP molecules need to be correctly aligned, forming a cyclic pair of hydrogen bonds between each other across the dimer interface that stabilize the complex (Egea 2004). Together, these structural adjustments convert the GTP-independent *early* intermediate to a GTP-dependent, stable SRP•FtsY complex.

Due to the extensive rearrangements required for formation of a stable SRP•FtsY complex, this process is extremely slow, with a rate constant of 10^2 –10^3 $M^{-1}s^{-1}$ (Peluso

2000; Peluso 2001). This barrier is overcome by the SRP RNA, which accelerates complex formation 200-fold (Peluso 2000; Peluso 2001). Intriguingly, the effect of the SRP RNA is purely catalytic, as it also accelerates complex disassembly without changing the equilibrium stability of the SRP•FtsY complex (Peluso 2000). This indicates that any interaction(s) that the SRP RNA makes with the GTPases is transient and occurs only before or during the rate-limiting transition state for complex assembly; once a stable *closed* complex is formed this interaction likely dissolves. This is the first example of an RNA molecule catalyzing a protein-protein interaction, and different models have been suggested to explain how the SRP RNA exerts its catalytic effect. One class of models postulates that the SRP RNA pre-organizes the Ffh-NG-domain into a conformation more conducive to stable interaction with FtsY. A second class of models suggests that the SRP RNA provides a transient tether, either directly or indirectly, that holds the two GTPases together during the rate-limiting transition state of the SRP-FtsY interaction, thus lowering the free energy barrier for stable complex formation (Peluso 2000). Recently, it was found that the SRP RNA stabilizes the *early* intermediate preceding the rate-limiting rearrangement to form the stable SRP•FtsY complex, and the degree to which the *early* intermediate is stabilized directly correlates with the degree to which stable complex assembly is accelerated (Zhang 2008). Thus stabilization of the *early* intermediate provides an important mechanism to accelerate the assembly of a stable SRP•FtsY complex. Nevertheless, the molecular interactions that mediate the RNA-induced stabilization of the *early* intermediate and transition state for complex assembly has not be identified; and no direct evidence is available to support either the 'pre-organization' or 'transient tether' model.

To distinguish between these models and understand the precise mechanism underlying the effect of SRP RNA, one needs to identify the structural motifs and the molecular interactions essential for mediating the catalytic role of SRP RNA. Thus far, the conserved terminal tetraloop (GGAA) of the SRP RNA provides the strongest candidate. This tetraloop is phylogenetically conserved throughout bacterial, archaeal, and eukaryotic SRPs (Selinger 1993; Jagath 2001). Mutations in the RNA tetraloop specifically abolishes the ability of the RNA to mediate efficient SRP-FtsY complex formation *in vitro* (Jagath 2001; Zhang 2008), and blocks protein targeting and translocation *in vitro* and *in vivo* (Siu 2007). Hydroxyl radical probing experiments further suggest that the tetraloop is located near the heterodimer interface between SRP and FtsY (Spanggord 2005), supporting the possibility that the tetraloop has the ability to serve as a transient tether between the two GTPases.

In addition to the SRP RNA, the cargo for the SRP pathway, ribosome•nascent chain complex containing a strong SRP signal sequence (RNC), provides an additional 100–400 fold acceleration of the SRP-FtsY interaction (Zhang 2009). Together, the SRP RNA and the cargo raise the association rate constant between the two GTPases to over 4 $\times 10^6$ $M^{-1}s^{-1}$ (Zhang 2009). As the SRP-mediated protein targeting reaction needs to be completed within a time window of 3–5 seconds before the nascent polypeptide exceeds ~ 140 amino acids in length (Siegel and Walter 1988; Flanagan 2003), the SRP-FtsY complex assembly kinetics would be fast enough to support co-translational protein targeting only when it is accelerated by both the cargo and the SRP RNA. The molecular mechanism by which the cargo stimulates complex assembly between the two GTPases is not understood. Nevertheless, the SRP RNA, through its close proximity to the signal

sequence binding site (Batey 2000) and the ribosome (Rinke-Appel 2002; Halic 2006; Schaffitzel 2006) and its ability to communicate with the GTPases, provides a likely candidate to mediate the cargo-induced stimulation. This is supported by the recent observation that a signal peptide stimulates SRP-FtsY complex formation only in the presence of the SRP RNA (Bradshaw 2009).

In this work, we provide evidence that a highly conserved basic residue, Lys399 on FtsY, mediates the RNA- and cargo-induced efficient assembly of the SRP•FtsY complex. Biochemical analyses and phylogenetic comparisons strongly suggest that FtsY-Lys399 makes a transient interaction with the SRP RNA that stabilizes the *early* intermediate and the transition state of SRP-FtsY complex assembly. These data for the first time provide direct evidence for a 'transient tether' mechanism that allows the SRP RNA to exert its catalytic role on this protein-protein interaction. Further, mutation of FtsY-Lys399 largely abolishes the ability of cargo to stimulate the SRP-FtsY interaction, indicating that the RNA tetraloop interaction with FtsY-Lys399 provides a key site that mediates the cargo-induced stimulation of SRP-FtsY complex assembly.

2.3 Results

2.3.1 Basic residues away from the Ffh-FtsY dimer interface enable efficient complex formation

In a previous structure-function analysis of the interaction between SRP and FtsY, the results of biochemical analyses agree well with the co-crystal structure of the Ffh•FtsY complex: Mutation of conserved residues located at or near the heterodimer interface severely disrupt complex formation, whereas mutation of residues away from the dimer interface generally have no significant effects (Egea 2004). A notable exception to this, and a conundrum never explained, are the three mutants K399A (Egea 2004), R402A and K406A (this work). These residues are located on the lateral surface of FtsY and together form a continuous patch of positively charged surface on the Gα2-helix (Figure 2.1A, shown in *spacefill*). Although these residues are ≥ 15 Å away from the heterodimer interface, their mutations severely disrupt the kinetics of stable SRP-FtsY complex formation. In a well-established GTPase assay, the rate constant of the reaction: SRP + FtsY → products (k_{cat}/K_m) is reduced 82-fold for mutant FtsY-K399A. FtsY-R402A and K406A also cause significant, albeit modest reductions in k_{cat}/K_m (six- and fivefold, respectively). Since the rate constant k_{cat}/K_m in this assay equals the association rate constant to form an active SRP•FtsY complex (Peluso 2001), these results suggest that this patch of basic residues, especially FtsY-Lys399, plays a critical role during SRP-FtsY complex formation.

To provide an independent test for this conclusion, we directly measured the rate of SRP-FtsY complex formation using fluorescence resonance energy transfer (FRET) between donor and acceptor labeled Ffh and FtsY (Figure 2.1B) (Zhang 2008). To uncouple complex formation from GTP hydrolysis, the non-hydrolyzable GTP analog 5'-

guanylylimido-diphosphate (GppNHp) was used to assemble a stable SRP•FtsY complex, and complex assembly was monitored as a gain in FRET (Zhang 2008). The complex assembly rate constant is 120-fold slower with mutant FtsY-K399A than with wild-type FtsY (Figure 2.1B), providing direct evidence that FtsY-Lys399 plays an essential role in accelerating complex formation. Mutant FtsY-K399A also has a deleterious effect on complex disassembly, reducing the dissociation rate constant 36-fold (Figure 2.1C). In contrast, the equilibrium stability of the SRP•FtsY complex, either calculated from the ratio of the dissociation and association rate constants or directly measured by equilibrium titration, is only moderately affected by this mutation. The equilibrium dissociation constant (K_d) of the SRP•FtsY(K399A) complex is 97 nM, only ~ threefold higher than that of 36 nM for the wild-type complex (Peluso 2001).

2.3.2 FtsY-Lys399 functionally interacts with the 4.5S RNA tetraloop during complex assembly.

The roles of FtsY-Lys399 are reminiscent of those played by the 4.5S SRP RNA, i.e., accelerating both SRP-FtsY complex formation and dissociation without significantly changing the equilibrium stability of the complex. This suggests that Lys399 interacts, directly or indirectly, with the GGAA tetraloop of the SRP RNA that mediates the RNA-induced acceleration of complex assembly. If this were true, then the effects of FtsY-Lys399 and the RNA tetraloop should be synergistic with one another, i.e., these residues or motifs contribute to complex assembly only when both of them are present. To test this hypothesis, we compared the effect of the FtsY-K399A mutation with wild-type SRP and mutant SRP(GAAU), in which the GGAA tetraloop in the SRP

RNA has been changed to GAAU. This mutation has a deleterious effect on SRP-FtsY complex formation, decreasing their association rate constant 120-fold (Figure 2.2A, squares). Indeed, the large deleterious effect of the SRP(GAAU) mutation on complex formation is largely abolished when the FtsY-K399A mutation is present (Figure 2.2A). Analogously, FtsY-Lys399 no longer contributes to complex formation in the presence of mutant SRP(GAAU) (Figure 2.2A). As a control, mutation of other residues that disrupt the SRP-FtsY interaction, such as FtsY-E475K or FtsY-T307W (Egea 2004; Shan 2004), further slows down complex assembly with SRP(GAAU) (Supplementary Figure 2.1). Notably, although he FtsY-E475K mutation has a much smaller effect on complex assembly than FtsY-K399A in reactions with wild-type SRP (6- vs. 120-fold, respectively) (Shan 2004), additional deleterious effect could still be observed for FtsY-E475K (Supplementary Figure 2.1, open squares) but not for FtsY-K399A (Figure 2.2A and Supplementary Figure 2.1, closed circles) in reactions with mutant SRP(GAAU). These results provide strong evidence for a functional interaction between FtsY-Lys399 and the RNA tetraloop during the transition state of complex formation.

We recently showed that an important mechanism for the SRP RNA to accelerate stable SRP-FtsY complex formation is by stabilizing the GTP-independent *early* intermediate that precedes the rate-limiting rearrangement to the GTP-dependent stable complex (Zhang 2008). If FtsY-Lys399 mediates the RNA-induced acceleration of complex formation, then FtsY-Lys399 should also play an important role in stabilizing the *early* intermediate. To test this possibility, we isolated the *early* intermediate by performing complex assembly in the absence of nucleotides, thus blocking the rearrangement of the *early* intermediate to the *closed* complex (Zhang 2008). Formation

of the *early* intermediate was monitored using FRET. The *early* complex formed by FtsY-K399A has an estimated K_d value of ≥ 48 μM, over sixfold weaker than that formed by wild-type FtsY (Figure 2.2B). Furthermore, while either the FtsY-K399A or the SRP(GAAU) mutation alone significantly destabilizes the *early* complex, these mutations do not cause additional defects when the other mutation is already present (Figure 2.2C). Thus, FtsY-Lys399 also functionally interacts with the RNA tetraloop to stabilize the *early* intermediate.

2.3.3 An A → K reversal mutant of chloroplast FtsY allows its interaction with Ffh to be stimulated by the SRP RNA.

To provide independent evidence that FtsY-Lys399 provides a response element for the SRP RNA tetraloop, we explored an RNA-less SRP pathway in chloroplast (cpSRP). This pathway uses the chloroplast homologues of the SRP and FtsY GTPases (cpSRP54 and cpFtsY, respectively), but cpSRP54 does not bind the SRP RNA (Schuenemann 1999; Richter 2008). We recently showed that the NG-domains of the SRP and FtsY GTPases are highly conserved and can interact with their heterologous binding partners at rates comparable to that with their homologous binding partners (Jaru-Ampornpan 2009). However, the interaction of *E. coli* Ffh with cpFtsY cannot be stimulated by the SRP RNA (Jaru-Ampornpan 2009), suggesting that cpFtsY has lost the structural element that responds to the SRP RNA. Sequence analysis showed that Lys399 is highly conserved among prokaryotic and eukaryotic SRP receptors, but is replaced by uncharged amino acids in cpFtsYs (Figure 2.3A). We therefore reasoned that, if FtsY-Lys399 interacts with the SRP RNA, then mutation of the corresponding Ala233 to lysine

in *A. thaliana* cpFtsY should allow its interaction with Ffh to be stimulated by the SRP RNA.

We therefore characterized the ability of the reversal mutant cpFtsY-A233K to interact with *E. coli* Ffh in the presence and absence of the SRP RNA (Figure 2.3B). Values of k_{cat}/K_m in the GTPase assay were used as indices for the rate of stable complex formation between Ffh and cpFtsY. Mutant cpFtsY-A233K can interact with and stimulate the GTPase activity of Ffh, with rate constants comparable to that of wild-type cpFtsY (Figure 2.3B, open circles) (Jaru-Ampornpan 2009a). Interestingly, whereas the reaction of wildtype cpFtsY with Ffh is RNA-independent (Jaru-Ampornpan 2009), the SRP RNA stimulates the reaction of mutant cpFtsY-A233K with Ffh by eightfold (Figure 2.3B, closed circles). Although we did not restore the full extent of stimulatory effect from the SRP RNA, this is not unexpected given the heterologous nature of the *E. coli* Ffh-cpFtsY interaction and the evolutionary divergence in the precise location or orientation of cpFtsY residue 233 that could have occurred in the RNA-less cpSRP pathway. The ability of the SRP RNA to stimulate complex assembly with the cpFtsY-A233K reversal mutant provides independent evidence that the SRP RNA interacts with FtsY-Lys399 to stimulate complex formation between the SRP and SRP-receptor GTPases.

2.3.4 Electrostatic interactions drive SRP RNA-stimulated complex assembly.

The high density of positive charge on and surrounding FtsY-Lys399 (Figure 2.1A) raises the possibility that electrostatic interactions between this basic residue and the backbone phosphates of the SRP RNA play a major role in accelerating SRP-FtsY

complex assembly. A hallmark of macromolecular assembly processes driven by electrostatic attractions is that their rate constants are highly sensitive to ionic strength (Schreiber and Fersht 1996). To evaluate the contribution of electrostatic effects to complex assembly, we tested the effects of varying ionic strength on the rate constants of SRP-FtsY complex formation using the FRET assay (Figure 2.4 and Supplementary Figure 2.2). Indeed, the complex assembly rate constants decreased 15-fold when the NaCl concentration was increased from 0 to 200 mM (Figure 2.4A and Supplementary Figure 2A). In contrast, complex assembly in the absence of the SRP RNA is affected less than twofold (Figure 2.4B and Supplementary Figure 2.2B), indicating that interactions with the SRP RNA is responsible for the ionic strength dependence of SRP-FtsY complex assembly observed in Figure 2.4A. These results strongly suggest that the rate-limiting step for complex assembly is strongly dictated by electrostatic interactions with the SRP RNA.

2.3.5 FtsY-Lys399 mediates the cargo-induced stimulation of SRP-FtsY complex assembly.

The cargo for SRP, RNC exposing the signal sequence from FtsQ (RNC_{FtsQ}), accelerates complex formation between SRP and FtsY another 100–400-fold (Zhang 2009). Importantly, in the presence of RNC_{FtsQ} mutant FtsY-K399A has an even greater deleterious effect, reducing the complex assembly rate constant by 1800-fold (Figure 2.5A). Further, the stimulatory effect from the cargo is reduced to only ~ fivefold in the presence of mutant FtsY-K399A (Figure 2.5A), in contrast to the 100-fold stimulatory effect of RNC_{FtsQ} in the presence of wild-type FtsY (Figure 2.5A, bottom panel) (Zhang

2009). Thus FtsY-Lys399 plays a crucial role in mediating the cargo-induced stimulation of SRP-FtsY complex assembly.

We showed that RNC_{FtsQ} substantially stabilizes the *early* intermediate (Zhang 2009), and this stabilization is a key to the cargo-induced acceleration of SRP-FtsY complex assembly. We therefore tested whether the interaction with Lys399 is also required to stabilize the RNC•SRP•FtsY *early* targeting intermediate. With wild-type FtsY, cargo-loaded SRP forms a stabilized *early* complex with a K_d value of 76 nM (Figure 2.5B, circles). In contrast, the *early* targeting intermediate formed by FtsY-K399A is 26-fold less stable than that by wild-type FtsY (Figure 2.5B). Moreover, the FRET value of the RNC•SRP•FtsY-K399A *early* intermediate is only ~ 0.3 (Figure 2.5B, inset), much lower than that formed by wild-type FtsY (~ 0.7; Figure 2.5B, circles) (Zhang 2009). This observation, together with the slower rate of stable complex assembly with FtsY-K399A, suggests that the *early* targeting intermediate formed by FtsY-K399A is in a different conformation and likely mispositioned. Thus, FtsY-Lys399 is crucial for stabilizing and properly orienting the GTPases in the *early* targeting intermediate. Together, the results in this section strongly suggest that FtsY-Lys399 plays an essential role in mediating many of the cargo-induced allosteric regulations on the SRP•FtsY GTPase complex. Consistent with its crucial roles, mutant FtsY-K399A severely inhibits the targeting and translocation of SRP-dependent protein substrates across the microsomal membrane (Figure 2.5C) (Shan 2007).

2.4 Discussion

The SRP RNA is evolutionarily conserved and essential for co-translational protein targeting mediated by the SRP. An important role of this RNA is to accelerate the interaction between the SRP and SRP-receptor GTPases, allowing them to form a stable complex at a rate suitable for co-translational protein targeting. This is the first example of an RNA molecule accelerating a protein-protein interaction, and the precise molecular mechanism by which the RNA exerts this unprecedented catalytic effect was not completely understood. In this work, we showed that FtsY-Lys399, a basic residue on the lateral surface of the FtsY G-domain, provides a key site that mediates the SRP RNA-induced stimulation of complex assembly. Further, this site also provides a key link that allows information about cargo binding to be transmitted to the SRP and SRP-receptor GTPases.

How does FtsY-Lys399 mediate the stimulatory effect of the SRP RNA? Although several mechanisms are possible, a direct interaction between the RNA tetraloop and FtsY-Lys399 provides the simplest and most likely model. This is supported by multiple evidences: (i) Our results here established a functional link between the SRP RNA tetraloop and FtsY-Lys399: Neither site contributes to complex assembly by itself, and their effects are only observed when both sites/motifs are present and functional. Further, both sites affect the same stages of the SRP-FtsY interaction, stabilizing the *early* intermediate and the transitions state for stable complex assembly, without affecting other stages of the SRP-receptor interaction. (ii) Structural probing experiments have shown that several residues in the FtsY G-domain are in close proximity to the RNA tetraloop in the SRP•FtsY complex (Spanggord 2005). Notably,

residue 359, adjacent to the amino group of Lys399 (Figure 2.1A, magenta), cleaves the RNA tetraloop when tethered with Fe-EDTA. Residue 392, which is closer to the Ffh-FtsY interface (Figure 2.1A, magenta), cleaves nucleotides immediately preceding the tetraloop. (iii) Comparisons with the RNA-less cpSRP system further support a direct Lys399-RNA interaction. In cpSRP, the M-domain of cpSRP54 functionally replaces the SRP RNA to accelerate complex assembly between the cpSRP54 and cpFtsY GTPases ~ 100-fold (Jaru-Ampornpan 2009). Intriguingly, the SRP RNA only stimulates complex assembly with bacterial FtsY, whereas the cpSRP54 M-domain only stimulates complex assembly with cpFtsY (Jaru-Ampornpan 2009). This specificity strongly suggests that specific sites have coevolved in FtsY that allow each receptor to interact with the SRP RNA or the M-domain in their respective pathway. The findings here that Lys399 is conserved among cytosolic SRP receptors but diverged in the cpFtsYs, and that mutation of the corresponding alanine in cpFtsY to lysine restores the RNA-induced stimulation of complex assembly strongly supports Lys399 as the RNA-interaction site. Finally, the high density of positive charges on and surrounding Lys399 provides an attractive site that can electrostatically interact with the negatively charged RNA backbone, and the rate constants of SRP-FtsY complex assembly exhibits a strong dependence on ionic strength that is consistent with a major role of electrostatic interactions during complex assembly. Alternatively, more complex models to explain the effects of FtsY-Lys399 are possible, but such models would invoke a role of Lys399 in mediating conformational changes in FtsY that, in turn, allows the SRP RNA to interact with another site. However, extensive mutational analysis thus far have implicated FtsY-Lys399 as the only residue in the SRP

or FtsY-NG-domain that substantially contribute to the stability of the *early* intermediate (X.Z. and S.S., unpublished), rendering these indirect models less likely.

A direct interaction between the SRP RNA and FtsY-Lys399 provides strong support for the 'transient tether' model, and suggests a simple and elegant mechanism to account for the catalytic effect of the SRP RNA on SRP-FtsY complex formation (Figure 2.6). Since free Ffh and FtsY by themselves exist in conformations suboptimal for stable complex assembly (Freymann 1997; Rosendal 2003; Shan and Walter 2003), their initial association to form the *early* intermediate, though rapid (Zhang 2008), is not sufficient to give a stable complex. Extensive conformational changes have to occur in both proteins to form the stable complex; this rearrangement is slow (~ 1 s^{-1}) and presents the rate-limiting step for stable complex assembly (Zhang 2008). Hence the overall rate to form a stable SRP•FtsY complex is determined by the stability of the *early* intermediate (which establishes a rapid but unfavorable pre-equilibrium) and the rate at which it rearranges to the stable complex. The SRP RNA, by interacting with FtsY-Lys399 in the *early* intermediate, can temporarily hold both proteins together and prevent their premature dissociation (Figure 2.6, upper vs. lower pathways). This prolongs the lifetime of the intermediate, during which both proteins explore different conformations, thus increasing the probability that a successful rearrangement takes place before the intermediate disassembles. This tethering interaction might also restrict the translational and rotational degrees of freedom for the two GTPase domains (Figure 2.6, upper vs. lower pathways) and thus facilitates their subsequent rearrangement. Once the stable complex is formed, the interaction between the RNA tetraloop and Lys399 likely dissolves (Figure 2.6), as the RNA tetraloop does not significantly affect the stability of the final stable complex.

Macromolecular assemblies often begin with transient intermediates formed by inelastic collisions during which both binding partners engage in relative rotatory diffusions to bring the correct interacting surfaces into appropriate opposition. The principle that formation of such intermediates could reduce the dimensionality of diffusional search and thereby provide significant rate enhancements is supported by both theoretical and experimental work (Zhou 1993; Iwahara and Clore 2006; Tang 2006; Volkov 2006). Our finding here, that a transient tether can be used to increase the lifetime of transient intermediates and thereby significantly accelerate protein-protein interactions, represents a natural extension of this principle and a simple and effective mechanism to enhance the kinetics of macromolecular recognition. This mechanism bears some resemblance to facilitated target site binding by the *lac* repressor and other transcriptional factors (von Hippel and Berg 1989), in that in both cases the initial interactions are low affinity but serves to effectively reduce the dimension of 'search' by the proteins in achieving the final, correct interaction. In principle, such a transient tether can be provided by either a nucleic acid or protein molecule (see section below). Nevertheless, the polyanionic nature of RNA molecules could allow them to engage in relatively long-range electrostatic interactions that do not have highly stringent stereochemical requirements, and hence might make them particularly suitable for providing such transient tethering interactions that needs to be broken at later stages of complex assembly.

The SRP and SRP receptor belong to a novel family of GTPases activated by nucleotide-dependent dimerization (GADs) (Gasper 2009). Intriguingly, although direct interaction between the GTPase sites occur or have been proposed in almost all members

of this GTPase family, dimerization of these GTPases are often mediated at least in part by motifs away from the GTPase module. For example, dimerization of MnmE is driven primarily by interactions between its N-terminal domains whereas the GTPase sites only transiently interact with one another during the transition state of GTP hydrolysis (Meyer 2009). In the case of a bacterial dynamin-like protein, although the GTPase sites gain close approach to one another in the dimer, motifs away from the GTPase domain–the paddle and tip domains–engage in more extensive intermolecular interactions at the dimer interface (Low and Lowe 2006). Likewise, during the SRP-FtsY interaction, although formation of the final stable complex is mediated by direct contacts through the NG-domains, formation of the *early* intermediate is primarily driven by the RNA tetraloop-Lys399 interaction whereas contacts between the G-domains are much looser (X.Z & S.S., unpublished results). We speculate that the use of tethering interactions from sites away from the GTPase active site could be an important mechanism that allows or facilitates 'kissing' between G-domains in the GAD family of proteins.

In the SRP pathway, the kinetics of the SRP-FtsY interaction is further regulated by the cargo, which accelerates SRP-FtsY complex assembly another 100–400 fold (Zhang 2009). Together, the combined effect of the cargo and the SRP RNA brings the interaction kinetics between SRP and FtsY to a rate constant ($> 10^6$ $M^{-1}s^{-1}$) appropriate for co-translational protein targeting in the cell. The mechanism underlying the cargo-induced stimulation was not understood. Here we found that with cargo-loaded SRP, FtsY-Lys399 plays an even more important role in stabilizing a productive *early* intermediate and in accelerating stable SRP-FtsY complex assembly than with free SRP. Further, removal of the RNA tetraloop-Lys399 interaction largely abolishes the cargo-

induced stimulation of the GTPase interactions. These findings demonstrate that the RNA tetraloop-Lys399 interaction provides a key contact that mediates the cargo-induced acceleration of SRP-FtsY complex assembly. These findings also strongly suggest that the intrinsic energetic contribution of the RNA tetraloop-Lys399 interaction is significantly larger than that observed with free SRP. It is possible that only a fraction of free SRP molecules exist in the productive conformation in which the RNA tetraloop is correctly positioned to contact FtsY during complex assembly, whereas the presence of cargo could help pre-organize the SRP such that the RNA tetraloop is pre-positioned to interact with FtsY-Lys399, thus further activating the SRP for complex formation. In this way, the RNA tetraloop-Lys399 interaction provides a key link that transmits the information about cargo binding in the SRP M-domain to the SRP and FtsY GTPases, thus turning on their GTPase cycles and driving the rapid delivery of cargo to the target membrane.

2.5 Material and methods

2.5.1 Materials

E. coli Ffh, FtsY, and SRP RNA were expressed and purified using established procedures (Peluso 2001). Mutant proteins and SRP RNA were constructed using the QuikChange mutagenesis protocol according to manufacturer's instructions (Stratagene, La Jolla, CA). Fluorescent dyes 4,4-difluoro-1,3,5,7-tetramethyl-8-(4-maleimidylphenyl)-4-bora-3a,4a-diaza-s-indacene (BODIPY-FL) and N-(7-dimethylamino-4-methylcoumarin-3-yl)maleimide (DACM) were from Invitrogen (Carlsbad, CA). RNC_{FtsQ} was prepared and purified as described (Schaffitzel and Ban 2007).

2.5.2 GTPase assay

Rate constants for the stimulated GTP hydrolysis reaction between SRP and FtsY were determined using a well-established GTPase assay (Peluso 2001). In general, reactions contained 100 nM Ffh, 200 nM 4.5S RNA (where applicable), 100–200 μM GTP (doped with γ-^{32}P-GTP), and varying concentrations of wild-type or mutant FtsY.

2.5.3 Fluorescence experiments

Single cysteine mutants of Ffh and FtsY were labeled with DACM and BODIPY-FL, respectively, and purified as described previously (Zhang 2008). Labeling efficiency is usually ≥ 95%. Fluorescence measurements were carried out on a FluoroLog-3-22 spectrofluorometer (Jobin-Yvon, Edison, NJ) in assay buffer [50 mM KHEPES (pH 7.5), 150 mM KOAc, 2 mM $Mg(OAc)_2$, 2 mM DTT, and 0.01% Nikkol]. Rate and

equilibrium measurements using FRET were carried out as described (Zhang 2008). The association rate constants for SRP-FtsY complex formation were determined by mixing SRP with varying amounts of FtsY in the presence of 100 μM GppNHp and following the time course of FRET increase. Reactions used 50 nM Ffh (for wild-type FtsY) or 5 μM Ffh (for FtsY-K399A) in the presence of GppNHp (Figure 2.1B). Reactions in the presence of RNC_{FtsQ} were carried out using 150 nM Ffh and 150 nM RNC_{FtsQ} for FtsY-K399A. Linear fits of the observed rate constant as a function of FtsY concentration gives the association rate constant ($k_{obsd} = k_{on}$ [FtsY] + k_{off}), which were summarized in Figures 2.2A and 2.5A. The dissociation rate constant of the SRP•FtsY complex was measured by a pulse-chase experiment. SRP (2 μM) and FtsY (8 μM) were preincubated in the presence of 100 μM GppNHp for a sufficiently long time window (15 minutes for wild-type FtsY, and 1 hour for K399A mutant) to ensure complex formation. 5 mM GDP•Mg^{2+} is then added as a chase to drive the dissociation of the SRP•FtsY complex. The loss of FRET (gain in fluorescence of donor-labeled SRP; Figure 2.1C) after addition of chase was monitored to obtain the rate constant for complex disassembly (k_{off}).

2.5.4 Translocation assay

The protein targeting efficiency were determined using a co-translational translocation assay (Powers and Walter 1997; Shan 2007). Reactions were carried out using 1 μM FtsY and 2 eq of TKRM.

2.6 Acknowledgements

We thank William M. Clemons, Nenad Ban, Christiane Schaffitzel, and members of the Shan group for helpful comments on the manuscript. This work is supported by NIH grant GM078024 to S.S. S.S. was supported by a career award from the Burroughs Welcome Foundation, the Beckman Young Investigator award, the Packard and Lucile award in science and engineering, and the Henry Dreyfus teacher-scholar award.

2.7 Figures and figure legends

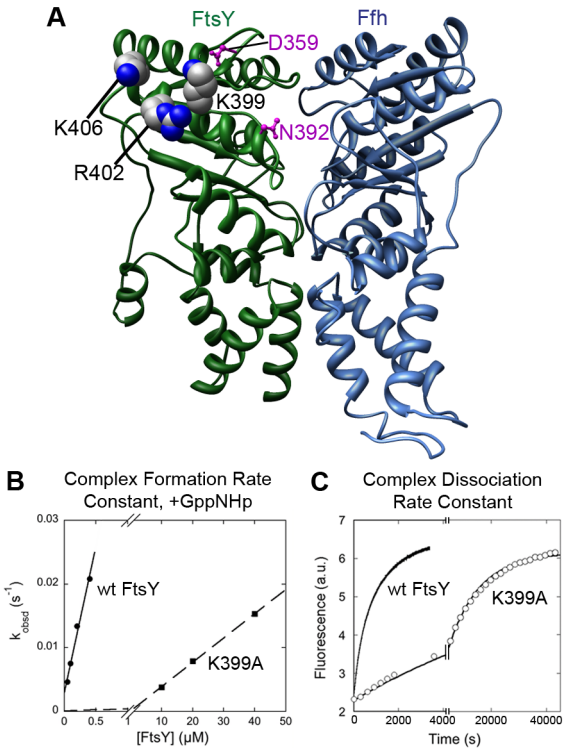

Figure 2.1 FtsY-Lys399 plays a crucial role in SRP-FtsY complex assembly. (A) The basic residues on the FtsY Gα2-helix are highlighted in *spacefill* in the crystal structure of the *T. aquaticus* Ffh•FtsY-NG-domain complex (PDB: 1RJ9). FtsY residues previously identified to be near the RNA tetraloop (Spanggord 2005a) are highlighted in *magenta*. (B) Mutant FtsY-K399A is defective in SRP-FtsY complex assembly. Linear fits of data gave rate constants of SRP-FtsY complex formation (k_{on}) of 4.58×10^{4} $M^{-1}s^{-1}$ for wild-type FtsY and 3.81×10^{2} $M^{-1}s^{-1}$ for mutant FtsY-K399A. (C) Rate constants of disassembly of the SRP•FtsY complex (k_{off}), which is 1.46×10^{-3} s^{-1} for wild-type FtsY and 4.05×10^{-5} s^{-1} for mutant FtsY-K399A.

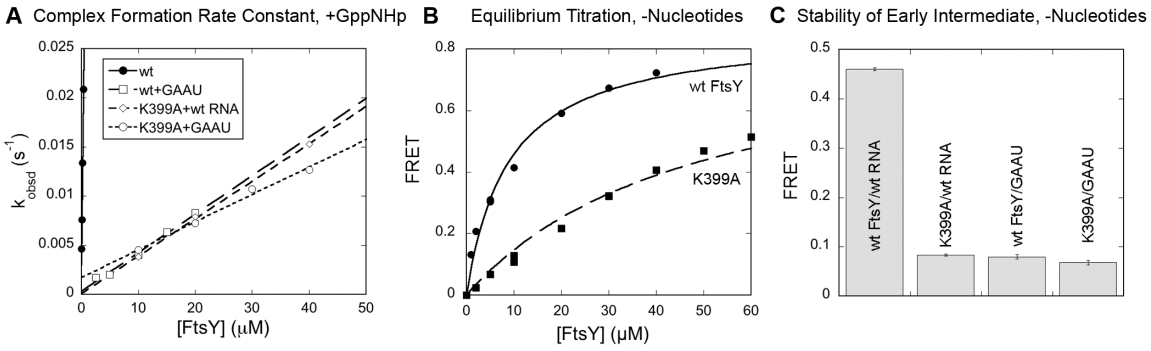

Summary of k_{on} (10^2 $M^{-1}s^{-1}$)

FtsY / RNA	wt	K399A
wt	458	3.81
GAAU	3.92	2.80

Figure 2.2 FtsY-Lys399 interacts with the SRP RNA tetraloop. (A) Effects of the FtsY-K399A and RNA(GAAU) mutations on the rate of stable complex formation, determined as described in the Methods. (B) The FtsY-K399A mutation destabilizes the GTP-independent *early* intermediate. Nonlinear fits of data gave K_d values of 8.85 μM for wild-type FtsY (●), and ≥48.4 μM for mutant FtsY-K399A (■). (C) Effects of the FtsY-K399A and RNA(GAAU) mutations on the stability of the *early* complex.

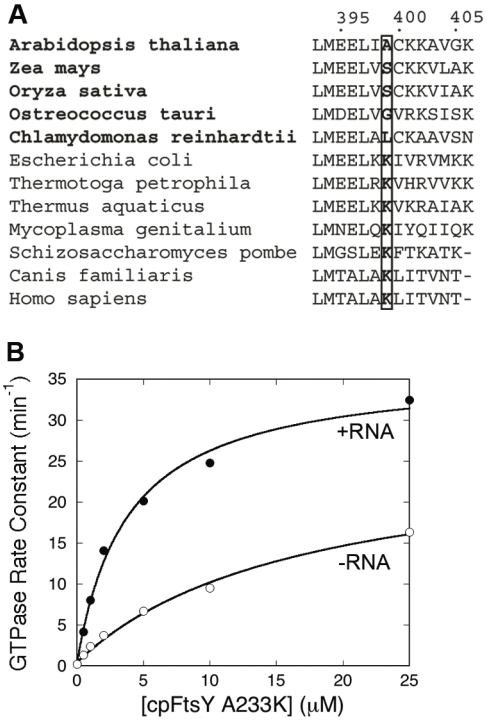

Figure 2.3 The cpFtsY-A233K reversal mutation allows complex formation with cpFtsY to be stimulated by the SRP RNA. (A) Sequence alignment of FtsY homologues. The residue numbering is for *E. coli* FtsY. Bold highlights the cpFtsY species. (B) GTPase assay to measure the interaction kinetics between cpFtsY-A233K and *E. coli* Ffh in the absence (○) and presence (●) of SRP RNA. Nonlinear fits of data gave k_{cat}/K_m values of 9.65×10^6 and 1.67×10^6 $M^{-1}min^{-1}$ with and without the SRP RNA, respectively.

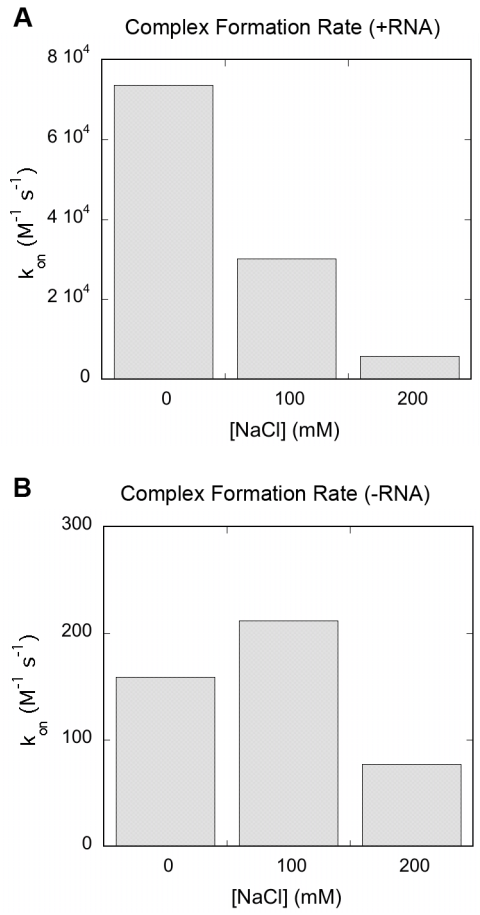

Figure 2.4 Effect of ionic strength on the rate constant of Ffh-FtsY complex assembly in the presence (part A) or absence (part B) of the SRP RNA, determined using the FRET assay. As all reactions also contain 50 mM K^+ and 2 mM Mg^{2+}, the ionic strength of the solution was increased from ~ 50 to ~ 250 mM in these experiments. The complex assembly rate constants were obtained from the data in Supplementary Figure 2.

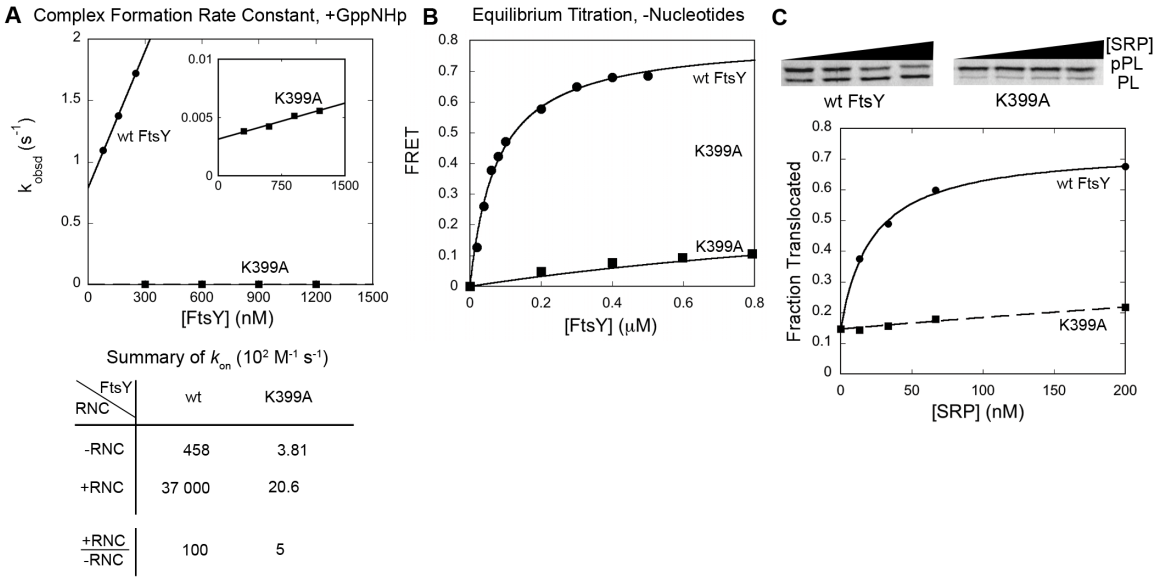

FtsY / RNC	wt	K399A
-RNC	458	3.81
+RNC	37 000	20.6
+RNC / -RNC	100	5

Figure 2.5 Mutation of FtsY-Lys399 diminishes the stimulatory effect of RNC on SRP-FtsY complex assembly. (A) Effect of FtsY-K399A on the rate constants for complex formation with cargo-loaded SRP. (B) Effect of FtsY-K399A on the equilibrium stability of the RNC•SRP•SR *early* targeting complex. Nonlinear fits of data gave K_d values of 76.5 nM (●) for wild-type FtsY and ~ 2 μM for mutant FtsY-K399A (■), and FRET end points of 0.72 for wild-type FtsY and 0.35 for mutant FtsY-K399A. (C) FtsY-Lys399 plays an essential role in co-translational protein targeting. Top, SDS-PAGE analysis of the translocation of pPL by wild-type FtsY and mutant FtsY-K399A. Bottom, quantitation of the results from SDS-PAGE.

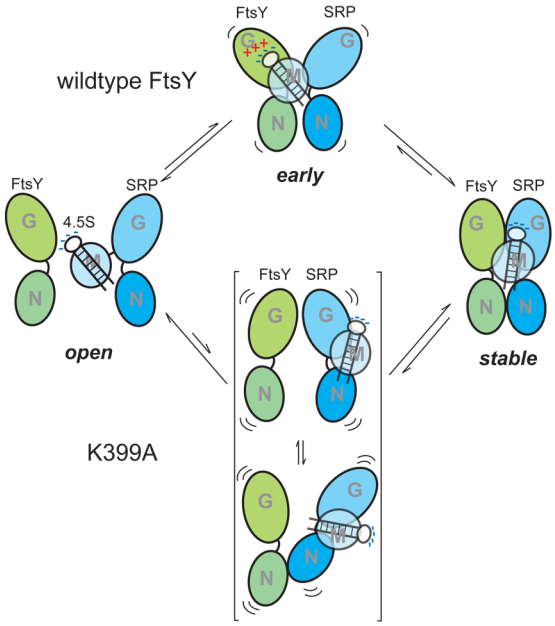

Figure 2.6 Model for the role of RNA tetraloop and FtsY-Lys399 on SRP-FtsY complex assembly, as described in the text. The top panel represents the complex assembly reaction with the assistance from the transient tether between the RNA tetraloop and FtsY-Lys399, and the bottom panel depicts the process in the absence of such a tethering interaction.

2.8 Supplementary figures legends

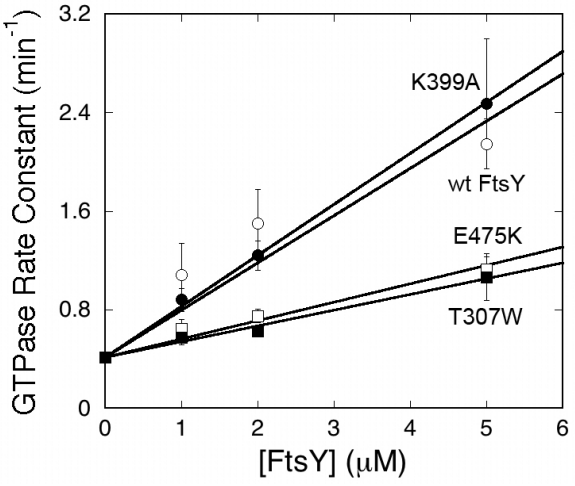

Supplementary Figure 2.1 Effect of FtsY mutations on the rate of complex assembly between mutant SRP(GAAU) and FtsY, determined from the k_{cat}/K_m values in the stimulated GTPase assay as described in the text. The data are fitted to the Michaelis-Menten equation, and gave k_{cat}/K_m values of 3.8×10^5, 4.1×10^5, 1.4×10^5, and 1.2×10^5 M^{-1} min^{-1} for wild-type FtsY (○), FtsY-K399A (●), FtsY-E475K (□), and FtsY-T307W (■), respectively.

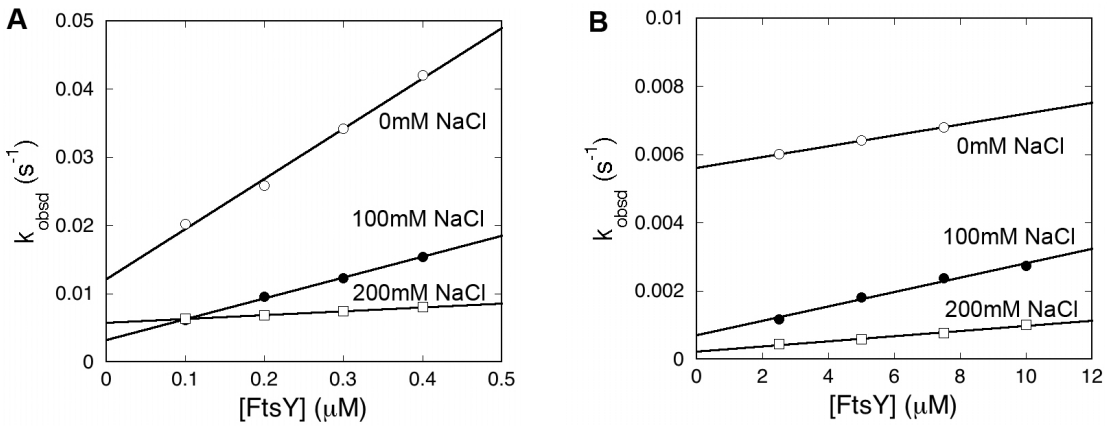

Supplementary Figure 2.2 Dependence of Ffh-FtsY complex assembly kinetics on the NaCl concentration in the presence (part A) and absence (part B) of SRP RNA. Complex assembly rate constants were determined using the FRET assay as described in the text. All reactions were carried out in solutions that contain a constant concentration of 50 mM KOAc and 2 mM $Mg(OAc)_2$. Linear fits of data gave complex assembly rate constants of 7.37×10^4, 3.05×10^4 and 5.09×10^3 $M^{-1}s^{-1}$ with 0, 100 and 200 mM NaCl, respectively, for reactions in the presence of the SRP RNA (A), and 159, 212 and 77 $M^{-1}s^{-1}$ with 0, 100 and 200 mM NaCl, respectively, for reactions in the absence of the SRP RNA (B).

3

Synergistic effect between SRP RNA and cargo[‡]

[‡] A modified version of this section was published as: ***Synergistic actions between the SRP RNA and translating ribosome allow efficient delivery of the correct cargos during cotranslational protein targeting***, Kuang Shen, Xin Zhang, and Shu-ou Shan, *RNA*, **2011**, *17*(5):892–902.

3.1 Abstract

During co-translational protein targeting by the signal recognition particle (SRP), the correct cargo accelerates stable complex assembly between the SRP and SRP receptor (FtsY) by several orders of magnitude, thus enabling rapid and faithful cargo delivery to the target membrane. The molecular mechanism underlying this cargo-induced rate acceleration has been unclear. Here we show that the SRP RNA allows assembly of the SRP-FtsY complex to be specifically stimulated by a correct cargo and reciprocally, a correct cargo enables the SRP RNA to optimize its electrostatic interactions with FtsY. These results combined with recent structural work led us to propose a 'conformational selection' model that explains the synergistic action of the SRP RNA with the cargo in accelerating complex assembly. In addition to its previously proposed role in preventing the premature dissociation of SRP and FtsY, we found that the SRP RNA also plays an active role in ensuring the formation of productive assembly intermediates, thus guiding the SRP and FtsY through the most efficient pathway of assembly.

3.2 Introduction

The signal recognition particle (SRP) is a key cellular machinery responsible for the co-translational targeting of proteins to their proper membrane destinations (Walter and Johnson 1994). SRP recognizes ribosome-nascent chain complexes (referred to as the RNC or cargo) carrying strong signal sequences (Pool 2002; Halic 2004; Halic 2006; Schaffitzel 2006) and delivers the cargo to protein translocation machineries on the target membrane (Gilmore 1982; Shan 2004). The simplest SRP, found in prokaryotes, is a ribonucleoprotein complex comprised of the SRP54 protein (called Ffh in bacteria) and the 4.5S SRP RNA (Walter and Johnson 1994). Ffh and the SRP receptor (called FtsY in bacteria) each contain a conserved NG-domain, comprised of a GTPase G-domain and a helical N-domain (Freymann 1997; Montoya 1997). Direct interaction between the NG-domains of Ffh and FtsY mediates the delivery of RNC to the target membrane (Egea 2004; Focia 2004). An additional M-domain in Ffh contains the binding sites for the SRP RNA and for the signal sequence emerging from the translating ribosome (Zopf 1990; Keenan 1998; Batey 2000; Janda 2010).

Previous kinetic and biophysical analyses showed that assembly of a stable SRP-FtsY complex is a dynamic process involving at least two distinct conformational stages (Zhang 2008; Zhang 2009). Complex assembly initiates with the formation of a transient 'early' intermediate, which forms quickly (k_{on} = 5.6 × 10^6 $M^{-1}s^{-1}$) but is highly labile (k_{off}= 62 s^{-1}); this intermediate has loose contacts between the NG-domains and hence can form in the presence or absence of GTP (Zhang 2008). Subsequently, extensive conformational changes are required to bring the NG-domains of both proteins into close contact with one another and to allow their bound GTP molecules to directly hydrogen

bond across the dimer interface, thus giving a highly specific, GTP-dependent stable complex (Egea 2004; Focia 2004). Due to the extensive rearrangements required to form these specific and extensive interface contacts, assembly of a stable complex by the free SRP and FtsY is thermodynamically favorable but kinetically very slow (Peluso 2001). In the presence of a correct cargo carrying a strong signal sequence, however, stable complex assembly between the SRP and FtsY is accelerated over 10^2-fold (Zhang 2009; Zhang 2010). This stimulation enables rapid delivery of the correct cargos to the target membrane, and provides kinetic discrimination against the incorrect cargos to improve the fidelity of protein targeting (Zhang 2009; Zhang 2010).

How does the cargo, whose signal sequence binds to the M-domain of the SRP, induce much more efficient assembly of the GTPase complex? The M-domain of SRP is connected to its NG-domain via a flexible linker and no direct interaction has been detected between these two domains, making a direct communication via the M-domain less likely. The other essential component of the SRP, the SRP RNA, is a more likely candidate to mediate the allosteric communication between the cargo and the GTPases. The SRP RNA binds to a helix-turn-helix motif in the M-domain close to the signal sequence binding site (Batey 2000), and cryo-EM and crosslinking analyses indicated that the SRP RNA forms close contacts with the ribosome (see next paragraph) (Gu 2003; Ullers 2003; Halic 2006; Schaffitzel 2006). On the other hand, the SRP RNA has also been shown to communicate with the GTPases, accelerating SRP-FtsY complex assembly ~ 10^2-fold (Peluso 2000; Peluso 2001). We recently showed that the conserved GGAA tetraloop of the SRP RNA makes a transient interaction with basic residues on the SRP receptor (primarily Lys399 in *E. coli* FtsY); this electrostatic interaction stabilizes

the early intermediate and prolongs its lifetime, thus giving the GTPases a longer time window to rearrange to the stable complex (Estrozi 2010; Shen and Shan 2010). Importantly, the stimulatory effect of the SRP RNA was only observed in the presence of a signal peptide or a stimulatory detergent, Nikkol, that mimics the effect of signal peptide (Bradshaw 2009), strongly suggesting that the SRP RNA can sense information about signal sequence binding in the M-domain and, in response, turns on its stimulatory activity on the GTPases. However, the mechanism by which the SRP RNA bridges between the cargo and the GTPases remains unclear.

Integrating the information from the recent cryo-EM structures of the RNC-SRP complex in the context of the biochemical results begins to shed light on this question. These structural analyses revealed extensive interactions between the RNC and the SRP including: (i) Contacts of the tip of Ffh-N-domain with ribosomal proteins L23p and L29p; (ii) Interaction of the emerging signal peptide with the signal sequence binding groove in Ffh-M-domain; and (iii) Contacts of the SRP RNA with ribosomal proteins L17p and L18p (Halic 2006; Schaffitzel 2006). Importantly, these contacts position the GGAA tetraloop of the SRP RNA next to the NG-domain of the SRP, which allow the electrostatic interaction between the GGAA tetraloop and the basic residues on FtsY to be more readily established (Estrozi 2010).

In this work, we tested this hypothesis and probed the mechanism of action of the SRP RNA by systematically examining how the ribosome, the signal sequence, and the SRP RNA cooperate with one another to provide maximal acceleration of SRP-FtsY complex assembly. We showed that the SRP RNA allows assembly of the SRP-FtsY complex to be specifically stimulated by a correct cargo and conversely, a correct cargo

enables the SRP RNA to optimize its electrostatic interaction with FtsY, and thus maximize its stimulatory effect on complex assembly. Moreover, in addition to acting as a passive tether that holds the SRP and FtsY GTPases together, the SRP RNA plays an essential role in preventing the formation of nonproductive intermediates, thus guiding the SRP and SR through the most efficient and productive pathway of assembly.

3.3 Results

3.3.1 SRP RNA does not affect the cargo-binding affinity of SRP

Previous chemical crosslinking (Gu 2003; Ullers 2003) and cryo-EM (Halic 2006; Schaffitzel 2006) studies suggested that the SRP RNA makes extensive contacts with the ribosome, which raises the possibility that the SRP RNA could enhance the binding affinity between the SRP and the RNC. To test this hypothesis, we used fluorescence anisotropy to determine the binding affinity between Ffh and purified RNCs in the absence and presence of the SRP RNA (Figure 3.1). Ffh was labeled with fluorescein at residue 421 in the M-domain, and the binding of RNC was detected as an increase in the fluorescence anisotropy of Ffh 421-fluorescein (Zhang 2010). Based on this anisotropy change, equilibrium titrations were carried out to test the effect of the SRP RNA on two different ribosomal complexes: (1) RNC_{FtsQ}, a correct cargo that carries the N-terminal 76 residues of FtsQ, a model SRP substrate (Figure 3.1A); and (2) $RNC_{Luciferase}$, an incorrect cargo that carries the N-terminal 50 amino acids of firefly luciferase, a cytosolic protein (Figure 3.1B). Consistent with previous observations (Zhang 2010), Ffh binds to RNC_{FtsQ} with an equilibrium dissociation constant (K_d) of 0.87 nM, ~ 10^2 fold lower than that to $RNC_{Luciferase}$. Unexpectedly, neither of these binding affinities were substantially enhanced by the SRP RNA (Figure 3.1A & B; summarized in Figure 3.1F, Ffh vs. SRP). Thus, the SRP RNA does not strengthen the binding affinity between Ffh and its cargo.

As most of the contacts between the SRP RNA and RNC are mediated by the ribosome, we further tested the effect of the SRP RNA on the binding affinity of Ffh to empty ribosomes. Binding of ribosomes to Ffh induced a significant change in the fluorescence anisotropy of a coumarin dye labeled at residue 153 in the Ffh G-domain;

based on this anisotropy change, the K_d value for Ffh-ribosome binding was determined to be 24 nM (Figure 3.1C & F). In the presence of the SRP RNA, however, the binding of ribosomes did not induce a sufficiently large anisotropy change to allow for accurate equilibrium titrations; therefore, the binding affinity of SRP for ribosomes was determined by using unlabeled SRP as a competitive inhibitor for the binding between Ffh C153-coumarin and the ribosome (Figure 3.1D; see Methods). This competition experiment gave a K_d value of 71 nM for SRP-ribosome binding, only threefold weaker than in the absence of the SRP RNA (Figure 3.1D & F). Together, these results indicate that the SRP RNA does not exert its stimulatory effect on the protein targeting reaction by helping to recruit Ffh to the ribosome. Instead, interactions of the SRP RNA with the ribosome may help position the SRP into a more active conformation that serves to stimulate subsequent steps in the pathway (see sections below).

It has been suggested that a stimulatory detergent included in previous biochemical assays, Nikkol, mimics the signal peptide and binds to the signal sequence binding groove of Ffh (Bradshaw 2009). If this were the case, Nikkol might compete with the RNC for binding to Ffh. To test whether this possibility interferes with the SRP-RNC binding measurements above, we compared the binding affinity of Ffh for RNC_{FtsQ} in the presence and absence of saturating (0.01%) Nikkol (Figure 3.1E). No significant difference was observed in these binding affinities (Figure 3.1E & F), suggesting that Nikkol does not directly or effectively compete with the RNC for binding Ffh.

3.3.2 A correct cargo enables the SRP RNA to most effectively stimulate SRP-FtsY complex formation

In the presence of the stimulatory detergent Nikkol, the SRP RNA has been shown to accelerate the assembly of a stable SRP-FtsY complex ~ 100-fold (Peluso 2000; Peluso 2001; Bradshaw 2009). A correct cargo, such as RNC_{FtsQ}, provides an additional 100–400 fold acceleration of complex assembly (Zhang 2009). As the SRP has a limited time window to complete the protein targeting reaction (~ 3–5 seconds) (Siegel and Walter 1988; Zheng and Gierasch 1996; Flanagan 2003), these rate accelerations are crucial for bringing the complex formation kinetics to values suitable for biological function. To test whether the SRP RNA is required for the cargo-mediated acceleration of complex assembly, we directly measured and compared the effect of these different activators using Forster Resonance Energy Transfer (FRET) between donor (DACM)- and acceptor (BODIPY-FL)-labeled Ffh and FtsY, respectively (Figure 3.2). In the absence of RNC_{FtsQ}, the SRP RNA induced a 165-fold stimulation of SRP-FtsY complex assembly (Figure 3.2A, +RNA –FtsQ (□) vs. –RNA –FtsQ (●), and Figure 3.2B), in agreement with previous studies (Zhang 2009). RNC_{FtsQ} had a marginal effect on the rate of complex assembly (~ twofold) in the absence of the SRP RNA, but provided an additional 80-fold acceleration of complex assembly in the presence of the SRP RNA. Thus, the correct cargo enabled a much larger stimulatory effect of the SRP RNA, 32,000-fold (Figure 3.2A, +RNA +FtsQ (◇) vs. –RNA +FtsQ (○), and Figure 3.2B).

To dissect the contributions of the signal sequence and the ribosome to the stimulatory effect of cargo, we measured and compared the complex assembly rates when SRP is bound with three distinct complexes: the empty ribosome, $RNC_{Luciferase}$, and RNC_{FtsQ}. Further, a recent study suggested that the detergent Nikkol partially mimics the

effect of signal peptides to stimulate SRP-FtsY complex assembly (Bradshaw 2009), and may thus mask the effect of the SRP RNA and cargo in stimulating complex assembly in previous (Zhang 2010) and the above (Figure 3.2) analyses. To uncover the full extent of stimulation provided by the cargo and the SRP RNA, we carried out these measurements in the absence of Nikkol (Figure 3.3).

In the absence of the ribosome complexes or signal peptides, complex assembly between Ffh and FtsY is extremely slow, with rate constants of ~ 3×10^2 $M^{-1}s^{-1}$, and the SRP RNA has only a small stimulatory effect on complex formation, ~ 3.3-fold (Figure 3.3A). In contrast, the correct cargo, RNC_{FtsQ}, allows the SRP RNA to accelerate complex assembly 96,000-fold (Figure 3.3B & E). Empty ribosomes and incorrect cargos such as $RNC_{Luciferase}$ allowed only partial stimulation by the SRP RNA, with the RNA providing rate enhancements of 65- and 48-fold, respectively (Figure 3.3C & D). In comparison, a signal peptide ΔEspP used in a previous study (Bradshaw 2009) and the signal peptide mimic, Nikkol, have been shown to provide partial rate accelerations by the SRP RNA of 160- and 820-fold, respectively (Figure 3.3E) (Bradshaw 2009). Finally, both the cargo and the SRP RNA were required for the observed rate accelerations, as in the absence of the RNA, neither the ribosomal complexes nor signal peptides (or signal peptide mimics) stimulated complex assembly; but rather, these components had a small inhibitory effect (Figure 3.3E, –RNA column). Taken together, these results demonstrate that the SRP RNA is essential for the cargo to stimulate the SRP-FtsY interaction, and reciprocally, a correct cargo enables the SRP RNA to maximize its stimulatory effect on assembly of the GTPase complex.

3.3.3 A correct cargo optimizes the electrostatic interaction of the SRP RNA with the SRP receptor

During complex formation between SRP and FtsY, a key electrostatic interaction between the GGAA tetraloop on the SRP RNA and Lys399 on FtsY must be established (Siu 2007; Zhang 2008; Shen and Shan 2010). This interaction provides a transient tether that holds the GTPases together during the transition state of complex assembly, and is essential for mediating the RNA-induced rate accelerations (Shen and Shan 2010). As the cargo makes extensive interactions with the SRP RNA and the M- and NG-domains of Ffh (Halic 2006; Schaffitzel 2006), we hypothesized that a correct cargo could help position the SRP into a more active conformation that optimizes the electrostatic interaction between the RNA tetraloop and the incoming FtsY (Estrozi 2010). If this were the case, then this electrostatic interaction would provide a much larger contribution to complex assembly with the correct than the incorrect cargos. To test this hypothesis, we used the FRET assay to measure and compare how the complex assembly rates were affected by either the mutant FtsY-K399A or an RNA tetraloop mutant, RNA-GAAU, which specifically disrupts this electrostatic interaction (Zhang 2008; Shen and Shan 2010).

In the presence of RNC_{FtsQ}, mutation of FtsY-Lys399 resulted in a 10^3-fold reduction in the rate constant of SRP-FtsY complex assembly (Figure 4 and Supplementary Figure 3.1, A & C). Mutation of the RNA tetraloop exhibited a similar phenotype (Supplementary Figure 3.1, A and C), and the combination of both mutations decreased the complex assembly rates another tenfold, approaching the value observed in the absence of the RNA (Supplementary Figure 3.1, A and C). In contrast, in the presence of an incorrect cargo, $RNC_{Luciferase}$, the FtsY-K399A mutation caused only a 18-

fold reduction in complex assembly rates (Figure 3.4 and Supplementary Figure 3.1, B and C). In the absence of cargo or stimulatory reagents (Nikkol or signal peptides) that mimic the effect of cargo, this interaction contributed only fourfold to SRP-FtsY complex assembly (Figure 3.4 and Supplementary Figure 3.1C). The reduced contribution of FtsY-Lys399 and RNA tetraloop to complex assembly in the absence of the correct cargo closely correlated with the reduced stimulatory effect of the SRP RNA under these conditions (compare Figure 3.4 with Figure 3.3E). Together, these results suggest that the electrostatic interaction between the RNA tetraloop and FtsY-Lys399 is most effectively established in the presence of a correct cargo, whereas incorrect cargos are much less effective in positioning the SRP to make this interaction.

3.3.4 The SRP RNA ensures the formation of a productive early intermediate

In the presence of the SRP RNA, assembly of a stable SRP-FtsY complex is preceded by a transient early intermediate (Zhang 2008). In previous work, we found that the SRP RNA stabilizes the early intermediate, which provides a longer time window for the intermediate to undergo its subsequent rearrangement and thus accelerates the formation of the stable complex (Shen and Shan 2010). We therefore asked if correct cargos are also essential for the ability of the SRP RNA to stabilize the early intermediate. To this end, we isolated the early intermediate by leaving out GTP or non-hydrolyzable GTP analogues, which blocks the rearrangement of this intermediate to the subsequent stable complex. FRET between SRP and FtsY was used to measure the equilibrium stability of the early intermediate. When SRP was loaded with RNC_{FtsQ}, SRP and FtsY formed a stable early complex in the presence of the SRP RNA, with a K_d value

of 57 nM (Figure 3.5A, open circles; and Figure 3.5C), 150-fold more stable compared to that without RNC (8.8 μM) (Shen and Shan 2010). In the absence of the SRP RNA, however, the early intermediate was considerably less stable, with a K_d value of ~ 2 μM (Figure 3.5A, squares; summarized in Figure 3.5C), indicating that the SRP RNA stabilizes the early intermediate ~ 40-fold when the SRP is loaded with a correct cargo. In contrast, when the SRP is loaded with empty ribosomes, the SRP RNA has a negligible effect on the stability of the early intermediate (Figure 3.5B & C). Thus, correct cargos bearing strong signal sequences also enable the SRP RNA to exert its stabilizing effect on the early intermediate.

We also noted that in the absence of the SRP RNA, the FRET end point of the early intermediate at saturating FtsY concentrations was much lower (~ 0.3; Figure 3.5A, squares and Figure 3.5C) than that in the presence of the SRP RNA (~ 0.7; Figure 3.5A, circles and Figure 3.5C). This indicates that the early intermediate formed in the absence of the SRP RNA has a different conformation than that formed in the presence of the RNA, and raised the question of whether the former are productive, 'on-pathway' intermediates, in other words, whether they can efficiently rearrange to form the stable complex. To address this question, we measured the rate constant of this rearrangement by pre-forming the early complex using saturating FtsY in the absence of nucleotides, and triggered the formation of the stable complex from this intermediate by the addition of GppNHp. Stable complex formation was detected using an environmentally sensitive dye, acrylodan labeled at residue 235 of Ffh, which specifically changes fluorescence upon formation of the stable complex (Zhang 2008). If the early intermediate is productive and on-pathway, the kinetics of stable complex formation should be

independent of FtsY concentration, reflecting the first-order rate constant for the early → stable rearrangement (Scheme 3.1, +RNA). This was indeed the case for the early complex formed with RNC_{FtsQ} in the presence of SRP RNA: the stable complex was quickly generated with a rate constant of 0.61 s^{-1}, and this rate constant is independent of FtsY concentration (Figure 3.5D & F, circles). In contrast, in the absence of the SRP RNA the kinetics for attaining the stable complex was ~ 10^4-fold slower (note the difference in time scales in Figure 3.5D *vs*. E). Further, the observed rate constants for formation of the stable complex became linearly dependent on FtsY concentration up to 80 μM and overlapped well with the second-order rate constants for assembly of this complex starting from free Ffh and FtsY (Figure 3.5E and F, squares). These results strongly suggest that in the absence of the SRP RNA, rearrangement of the early intermediate to the stable complex is extremely slow; instead, the GTPases must first dissociate into free Ffh and FtsY and then generate the stable complex via an alternative pathway (Scheme 3.1, –RNA). Thus, the SRP RNA not only stabilizes the early intermediate, but also ensures a productive conformation of this intermediate in the presence of a correct cargo.

Scheme 3.1

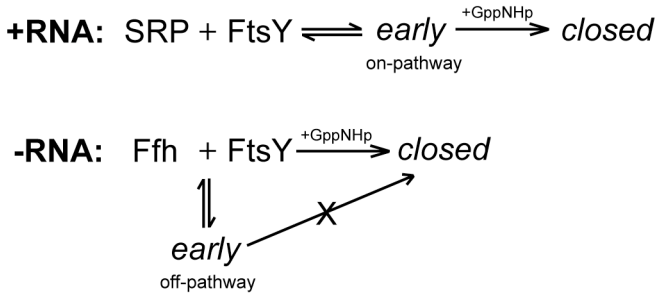

The notion that the SRP RNA can actively modulate the conformation of the early intermediate was further supported by observations under low salt (50 mM KOAc) conditions. Under these conditions, Ffh and FtsY assembled an extremely tight early complex (Figure 3.6A, open circles; K_d = 17 nM), presumably because the early encounter between these two GTPases are driven by electrostatic interactions (Zhang 2011) which is stabilized by decreasing ionic strength. However, this did not lead to a corresponding acceleration of the assembly of the stable complex (Figure 3.6C, -RNA) (Shen and Shan 2010), indicating that the early intermediate formed under these conditions, though stable, is also nonproductive and off-the-pathway. Intriguingly, the SRP RNA reduced the affinity of the early complex formed under low salt conditions by 150-fold (Figure 3.6A, squares), in contrast to the stabilizing effect of this RNA on the early complex at higher salt conditions (Figure 3.5A) (Zhang 2008; Shen and Shan 2010). The productivity of the early intermediate was also restored by the SRP RNA under these conditions. The early intermediate formed in the absence of the SRP RNA reaches the stable conformation slowly and with a strong FtsY concentration dependence, suggesting that it is off-the-pathway (Figure 3.6C, –RNA). The presence of SRP RNA allowed the intermediate to quickly and directly rearrange to the stable complex (Figure 3.6B and C, +RNA). Together, these results suggest that aside from preventing the premature disassembly of the early intermediate, the SRP RNA is essential for ensuring a productive conformation of this intermediate, such that it can readily rearrange to the subsequent conformations in response to its biological cues.

3.4 Discussion

Protein targeting by the SRP requires efficient and faithful delivery of translating ribosomes to the target membrane in response to correct signal sequences. Recent work strongly suggested that this is achieved, in part, by having an intrinsically slow rate of SRP-FtsY complex assembly that minimizes the delivery of incorrect cargos, and allowing efficient complex assembly only when RNCs carrying strong signal sequences are loaded on the SRP (Zhang 2010). In this work, we showed that the SRP RNA plays an essential role in enabling specific stimulation of SRP-FtsY complex formation by a correct cargo. The strong synergistic effect between the SRP RNA and the cargo, in combination with recent structural work, suggest a potential mechanism for how a correct cargo stimulates SRP-FtsY complex assembly. Finally, the SRP RNA actively modulates the conformation of the SRP-FtsY complex to guide complex assembly through the most efficient and productive pathway.

Previous work have reported that the cargo and the SRP RNA each accelerates SRP-FtsY complex assembly ~ 10^2-fold (Peluso 2000; Peluso 2001; Zhang 2008; Zhang 2009). A recent study, however, suggested that the full extent of their stimulatory effects might be masked because a detergent Nikkol used in previous studies mimics the effect of signal peptides (Bradshaw 2009). Indeed, omission of this detergent revealed much larger stimulatory effects from both the cargo and the SRP RNA, 10^4- (Zhang 2010) and 10^5-fold (herein), respectively. These results emphasize the essential role of the SRP RNA in co-translational protein targeting, and the specificity that it confers on the correct cargo during SRP-FtsY complex assembly.

Comparison of the complex assembly rates when the SRP is loaded with the correct or incorrect cargos illustrates the kinetic discrimination that the SRP RNA provides. The intrinsic complex assembly rate between Ffh and FtsY is extremely slow, on the order of 10^2 $M^{-1}s^{-1}$, and is only marginally (threefold) stimulated by the SRP RNA. In the presence of the SRP RNA, complex assembly is accelerated ~ 10^4-fold by the correct cargo but only ~ tenfold by empty ribosomes or incorrect cargos. This allows the correct cargo to gain a 10^3-fold kinetic advantage over incorrect cargos during its delivery to the target membrane. In contrast, in the absence of the SRP RNA none of the ribosomal complexes provides any rate acceleration and is, in fact, slightly inhibitory. The low efficiency of complex formation in the absence of the SRP RNA is accompanied by a loss of specificity. Thus the SRP RNA enables Ffh to sense the cues from correct signal sequences and to kinetically discriminate against incorrect signal sequences during the cargo delivery step, introducing both efficiency and specificity.

How is SRP-FtsY complex assembly specifically stimulated by a correct cargo? Recent biochemical and structural work has provided important clues. First, previous biochemical analyses and structural probing experiments have established an important role of the electrostatic interaction between the SRP RNA's GGAA tetraloop and FtsY-Lys399 in facilitating SRP-FtsY complex assembly (Siu 2007; Zhang 2008; Shen and Shan 2010). The analyses herein showed that a correct cargo maximizes the stimulatory effect of the SRP RNA on complex assembly, and this is paralleled by an optimization of the electrostatic interaction between the RNA tetraloop and FtsY-Lys399 in the presence of the correct cargo. Second, cryo-EM analyses of the RNC-SRP and RNC-SRP-SRP early complexes have revealed extensive interactions of the Ffh M- and NG-domains

with the nascent polypeptide and ribosomal proteins L23/ L29, respectively (Halic 2006; Schaffitzel 2006; Estrozi 2010); these interactions help position the SRP RNA's tetraloop adjacent to the Ffh-NG-domain, allowing it to be poised for contacting the incoming FtsY. In contrast, the free SRP has been found in at least four different conformations (Keenan 1998; Rosendal 2003; Buskiewicz 2005; Spanggord 2005); in each of these structures the SRP RNA was oriented differently with respect to the NG-domain and in most structures, the RNA tetraloop pointed away from the Ffh-FtsY interface (Figure 3.7A, bracket). Given these observations and the flexibility of the linker connecting the Ffh M- and NG-domains, we speculate that free SRP has a relative flat conformational space and is able to adopt a variety of 'latent' conformations in which the RNA tetraloop is not well positioned (Figure 3.7A, bracket). The action of the RNC could be likened to a conformational selection process (Figure 3.7A): A correct cargo selectively stabilizes the rare but active conformation of SRP in which the RNA tetraloop is optimally positioned to interact with FtsY, thereby activating the SRP RNA to achieve efficient SRP-FtsY complex assembly.

Using this model and the observed SRP-FtsY complex assembly rate constants, a rough estimate could be made for how the ribosome, signal peptides, and different cargos affect the conformational equilibrium of SRP (Figure 3.7A, right panel). As the complex assembly rate constant levels off at $\sim 9 \times 10^6$ $M^{-1}s^{-1}$ for RNCs with increasingly strong signal sequences, this value likely represents the rate of complex assembly from the 'active' SRP molecules (Figure 3.7A, k_2), and the SRPs bound to a correct cargo such as RNC_{FtsQ} are primarily in this conformation (Figure 3.7A, $K \geq 1$). With free SRP, however, only a small fraction of the molecules exist in the 'active' conformation ($K \leq 3$

$\times 10^{-5}$). The ribosome and signal peptides each shifts the conformational equilibrium of SRP towards the active state by ~ ten- and ~ 10^2-fold, respectively, but the SRP would still be primarily in the 'latent' conformations in the presence of these isolated components of the cargo. This analysis also shows that the additive effect of the ribosome and signal peptides (~ 10^3-fold) is at least an order of magnitude lower than that provided by a correct cargo (≥ 3×10^4-fold), suggesting a modest but significant degree of cooperativity between the different components of the RNC.

In previous studies, we attributed the catalytic effect of the SRP RNA to its role as a transient 'tether': by holding the Ffh and FtsY GTPases together in the early intermediate, the SRP RNA prevents the premature disassembly of this intermediate and thereby increases the probability of obtaining the stable complex (Peluso 2000; Shen and Shan 2010). In addition to this role, several observations in this work demonstrate that the SRP RNA also actively modulates the conformation of the early intermediate. First, the early intermediate formed in the absence of the SRP RNA has a much lower FRET value than that formed in the presence of the RNA. Second, the early intermediate formed in the presence of the SRP RNA directly and rapidly rearranges to the stable complex (0.5–1 s^{-1}), whereas in the absence of the SRP RNA, the intermediate is off-the-pathway and complex assembly has to go through an alternative pathway that bypasses this intermediate (Figure 3.7B, blue lines). Third, under low salt conditions Ffh and FtsY are trapped in a stable but off-pathway intermediate (Figure 3.7B, red lines), and the SRP RNA destabilizes this intermediate while restoring its kinetic competence to rearrange to the stable complex. Together, these results strongly suggest that the SRP RNA is essential for ensuring a productive conformation of the early intermediate, and actively

guides complex assembly through the most efficient and productive pathway (Figure 3.7B, black lines).

3.5 Materials and methods

3.5.1 Materials

E. coli Ffh, FtsY, and SRP RNA were expressed and purified using established protocols (Peluso 2001). Mutant proteins and SRP RNA were constructed using the QuikChange mutagenesis protocol (Stratagene, La Jolla, CA), and were purified as described previously (Peluso 2001). Fluorescent dyes fluorescein, BODIPY-FL, DACM, and acrylodan were purchased from Invitrogen (Carlsbad, CA). 70S ribosome was purified as described (Moazed and Noller 1989). RNCs were prepared and purified as described (Schaffitzel and Ban 2007).

3.5.2 Fluorescence experiments

Single cysteine mutants of Ffh and FtsY were labeled using maleimide chemistry and purified as described (Zhang 2008). Labeling efficiency was usually ≥ 95%. Fluorescence measurements were carried out on a FluoroLog-3-22 spectrofluorometer (Jobin-Yvon, Edison, NJ) in assay buffer [50 mM KHEPES (pH 7.5), 150 mM KOAc, 10 mM $Mg(OAc)_2$, 2 mM DTT, with or without 0.01% Nikkol].

The binding affinities of SRP for RNCs or ribosomes were determined using fluorescence anisotropy measurements, using either one of the two procedures below. (1) Varying concentrations of RNC_{FtsQ} or $RNC_{Luciferase}$ were added to a small, fixed amount of C421-fluorescein labeled Ffh or SRP. Anisotropy values were calculated and plotted against RNC (or ribosome) concentration, and quadratic fits of the data gave the K_d value of the complex (Zhang 2010). (2) Varying amounts of unlabeled SRP were added as competitive inhibitors to a ribosome-Ffh complex formed by C153-coumarin labeled Ffh

(Scheme II, Ffh*). Under conditions where the concentration of labeled Ffh (Ffh*) was low (10 nM) compared to that of ribosome (≥ 50 nM), the observed anisotropy value (A_{obsd}) as a function of competitor concentration can be approximated by Equation 3.1 and 3.2, derived from Scheme 3.2, to obtain the K_i value.

Scheme 3.2

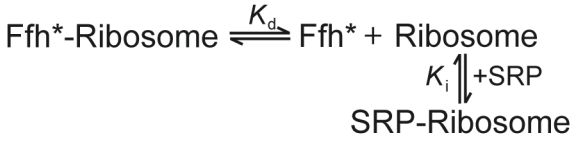

$$A_{obsd} \approx (A_1 - A_0) \times \frac{[\mathrm{R}]_0 - Y}{K_d + [\mathrm{R}]_0 - Y} + A_0 \qquad (3.1)$$

$$\text{where } Y = \frac{[\mathrm{SRP}]_0 + [\mathrm{R}]_0 + K_i - \sqrt{([\mathrm{SRP}]_0 + [\mathrm{R}]_0 + K_i)^2 - 4[\mathrm{SRP}]_0[\mathrm{R}]_0}}{2} \qquad (3.2)$$

In Equation 3.1 and 3.2, A_1 is the anisotropy value of the Ffh*-ribosome complex, A_0 is the anisotropy value of free Ffh*, $[\mathrm{SRP}]_0$ and $[\mathrm{R}]_0$ are the total concentrations of SRP and ribosome, respectively, and the equilibrium constants K_i and K_d are defined in Scheme 3.2.

Association rate constants for SRP-FtsY complex formation were determined using FRET. In all cases, saturating concentrations of ribosome or ribosomal complexes were used so that ≥90% of SRP is bound with the different cargos. Complex assembly was initiated by mixing SRP with varying amounts of FtsY in the presence of 100 μM GppNHp and the time course of fluorescence change was monitored using either a FluoroLog-3-22 spectrofluorometer (Jobin-Yvon, Edison, NJ) or a SF-2004 stopped-flow (KinTek, La Marque, TX). Linear fits of the observed rate constants as a function of

FtsY concentration gave the second-order association rate constant ($k_{obsd} = k_{on}$ [FtsY] + k_{off}). Equilibrium titrations of the early intermediate were carried out using FRET as described previously (Zhang 2008). Rate constants of stable complex formation from the early intermediate were measured using Ffh-C235 labeled with acrylodan. The reaction was initiated by mixing 500 μM GppNHp with a preformed early intermediate, assembled in the presence of saturating amount of SRP/Ffh and FtsY with respect to the K_d value of the early intermediate. The time course of fluorescence change was fit with single-exponential functions to give the observed rate constants. For experiments concerning SRP or Ffh loaded with different ribosome complexes, ribosome or RNC concentrations 5–100-fold above their respective K_ds for Ffh were used to ensure > 90% occupancy of SRP or Ffh by the cargo.

3.5.3 Estimation of the partition of SRP into the active conformation

The fractions of SRP molecules in the active conformation under different conditions in Figure 3.7A were estimated using the complex assembly rate constants determined here and previously (Zhang 2010). As the observed complex assembly rate constant levels off at a value of 9×10^6 $M^{-1} s^{-1}$ with increasingly strong cargos, this rate constant likely approximates the value of k_2 (Figure 3.7A) and SRP's bound with strong cargos such as RNC_{FtsQ} are primarily in the active conformation (Figure 3.7A, $K \geq 1$). In the absence of the SRP RNA, the observed complex assembly rate constant approximates the complex formation rate from the ensemble of inactive SRP conformations (Figure 3.7A, k_1). The observed complex assembly rate constants under different conditions are

therefore a weighted sum of the contributions from the active and inactive SRP populations according to Equation 3.3,

$$k_{on,obsd} = k_1 \times \frac{1}{K+1} + k_2 \times \frac{K}{K+1} \qquad (3.3)$$

From which the equilibrium to form the active conformation, K, can be calculated and the results were listed in Figure 3.7A.

3.5.4 Free energy diagram

The free energy surface in Figure 3.7B was constructed using Mathematica (Wolfram Research, Champaign, IL). The free energy profile in the lower panel of Figure 3.7B were constructed based on the experimentally determined rate and equilibrium constants using a standard state of 1 μM. $\Delta G = -RT \ln K$, in which $R = 1.987$ cal mol^{-1} K^{-1}, $T = 298.15$ K, and K is the experimentally measured equilibrium constant. $\Delta G^{\ddagger} = -RT \ln (kh/k_BT)$, in which $R = 1.987$ cal mol^{-1} K^{-1}, $T = 298.15$ K, $k_B = 3.3\times10^{-24}$ cal K^{-1}, $h = 1.58\times10^{-34}$ s, and k is the experimentally measured rate constant.

3.6 Acknowledgement

We thank members of the Shan group for helpful comments on the manuscript. This work was supported by NIH grant GM078024 to S.S. S.S. was supported by a career award from the Burroughs Wellcome Foundation, the Beckman Young Investigator award, the Packard and Lucile award in science and engineering, and the Henry Dreyfus teacher-scholar award.

3.7 Figures and figure legends

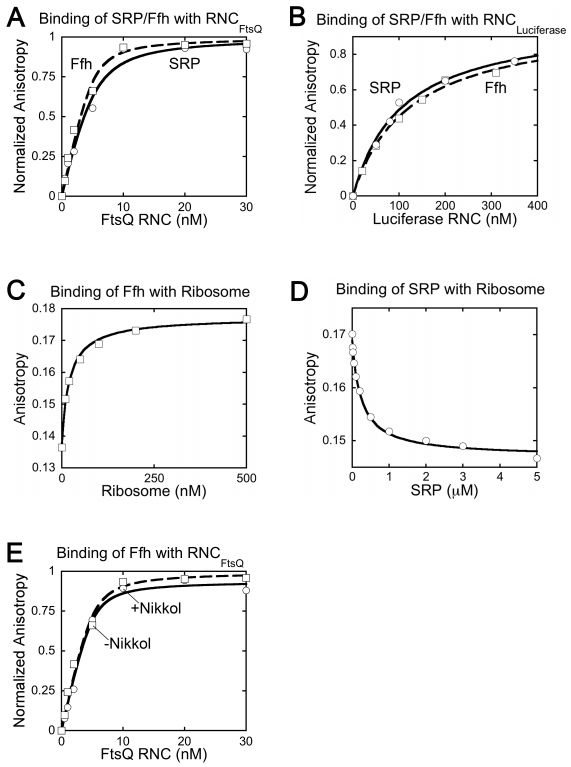

F

K_d (nM)	-Nikkol			+Nikkol
	Ribosome	$RNC_{Luciferase}$	RNC_{FtsQ}	RNC_{FtsQ}
Ffh	24	123	0.87	0.48
SRP	71	107	2.14	

Figure 3.1 The SRP RNA does not strengthen the binding between SRP and the RNC. (A) Equilibrium titrations for the binding of Ffh (□ and dashed line) or SRP (○ and solid line) to RNC_{FtsQ} , carried out and analyzed as described in the Methods. (B) Equilibrium titrations for the binding of Ffh (□ and dashed line) or SRP (○ and solid line) to $RNC_{Luciferase}$. (C & D) Binding of empty ribosomes to Ffh (C) or SRP (D), determined using equilibrium titrations and competition experiments, respectively, as described in the Methods. (E) Binding of Ffh to RNC_{FtsQ} in the presence (○ and solid line) and absence (□ and dashed line) of Nikkol. (F) Summary of the K_d values obtained from (A) to (E).

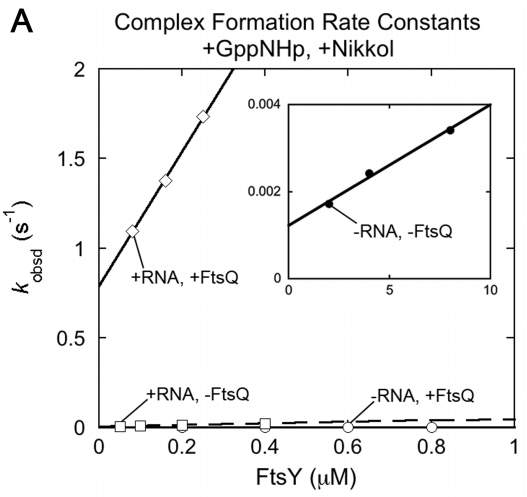

RNA / RNC	-RNA	+RNA	+RNA / -RNA
$-RNC_{FtsQ}$	277	45,800	165
$+RNC_{FtsQ}$	116	3,700,000	32,000
+RNC / -RNC	0.42	80.8	

Figure 3.2 A correct cargo allows the SRP RNA to more strongly stimulate SRP-FtsY complex assembly. (A) SRP-FtsY complex formation rates in the presence and absence of the SRP RNA and RNC_{FtsQ}, measured using the FRET assay as described in the Methods. All measurements in this figure were carried on in the *presence* of 0.01–0.02% Nikkol. (B) Summary of complex formation rate constants from (A).

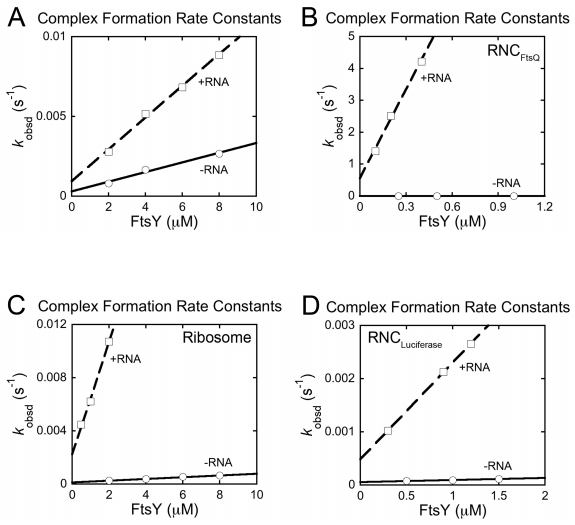

E

k_{on} Summary (M^{-1} s^{-1})

RNA / stimulants	-RNA	+RNA	+RNA / -RNA
–	304 (1.0)	994 (3.3)	3.3
RNC_{FtsQ}	95.9 (0.32)	9,250,000 (30,000)	96,000
Ribosome	65.3 (0.21)	4,220 (14)	65
$RNC_{Luciferase}$	38.2 (0.13)	1,820 (6.0)	48
+Nikkol *	*277* (0.91)	*45,800* (150)	*170*
+ΔEspP #	*44* (0.14)	*36,000* (118)	*820*

Figure 3.3 Both the ribosome and a strong signal sequence are required to maximize the stimulatory effects of the SRP RNA on SRP-FtsY complex assembly. All experiments in this figure were performed in the *absence* of Nikkol. (A-D) SRP-FtsY complex assembly rates with (□ and dashed line) or without (○ and solid line) the SRP RNA, in the presence of (A) no stimulants, (B) RNC_{FtsQ}, (C) empty ribosome, and (D) $RNC_{Luciferase}$. (E) Summary of complex formation rates constants from (A)–(D). The rate constants in the presence of Nikkol (*) are from Figure 3.2 and data of ΔEspP (#) are from reference (Bradshaw 2009).

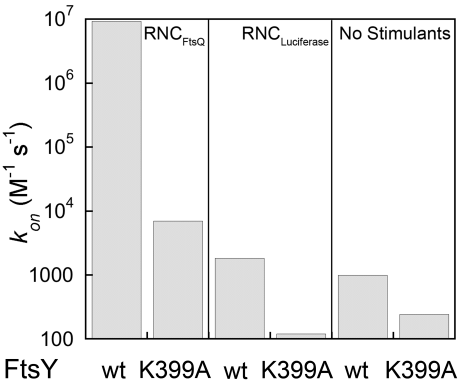

Figure 3.4 A correct cargo optimizes the electrostatic interaction of the SRP RNA tetraloop with FtsY-K399 during SRP-FtsY complex formation. The contribution of this electrostatic interaction is compared in the presence of RNC_{FtsQ} (left), $RNC_{Luciferase}$ (middle), and no stimulants (right). The rate constants are from the data in Supplementary Figure 3.1.

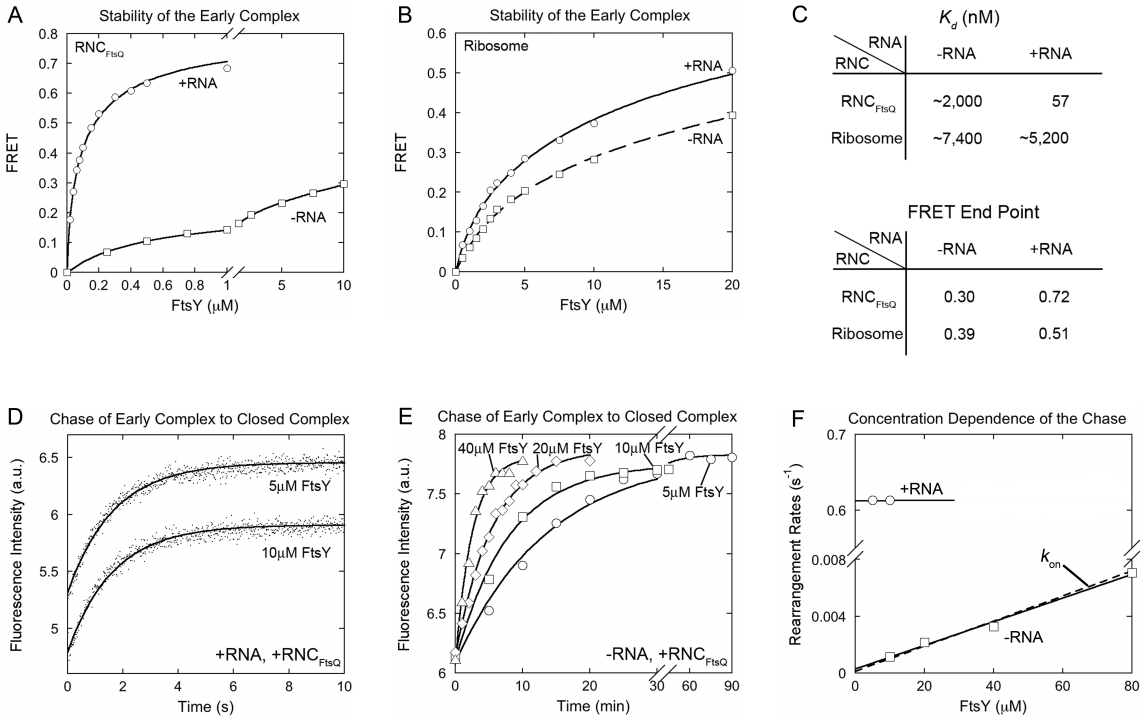

Figure 3.5 The SRP RNA ensures the formation of a stable and productive early intermediate. (A & B) Effects of the SRP RNA on the equilibrium stability of the early complex in the presence of RNC_{FtsQ} (A) or the empty ribosome (B). (C) Summary of the K_d values and FRET end points of the early complex from (A) and (B). (D & E) Rate constants for formation of the stable complex starting from a preformed cargo•Ffh•FtsY early complex in the presence (D) and absence (E) of the SRP RNA. (F) Dependence of the rearrangement rate constants on FtsY concentration, obtained from (D) and (E), in the presence (○) and absence (□) of the SRP RNA. The dashed line shows the rate constant for complex assembly starting from free Ffh and FtsY.

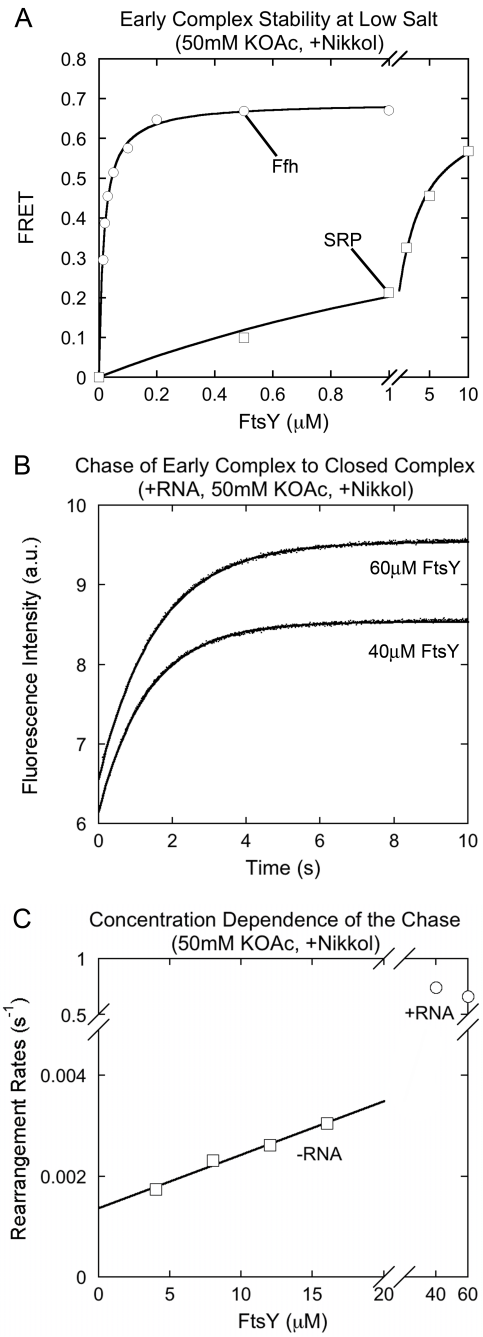

Figure 3.6 SRP RNA prevents the formation of a nonproductive early intermediate at low salt concentrations. (A) The stability of the early intermediate at 50 mM KOAc. The K_d values are 17 nM for Ffh (○) and 2.5 μM for SRP (□). (B) Rate constants for formation of the stable complex from a pre-assembled early intermediate in the presence

of the SRP RNA. Exponential fits of data gave rearrangement rate constants of 0.74 s^{-1} and 0.66 s^{-1} at 40 and 60 μM FtsY, respectively. (C) FtsY concentration dependence of the rate constants for formation of the stable complex starting from the early intermediate in the presence (○) and absence (□) of the SRP RNA. Linear fit of the –RNA data gave a slope of 106 $M^{-1}s^{-1}$, consistent with the k_{on} value of 159 $M^{-1}s^{-1}$ measured in reference (Shen & Shan 2010).

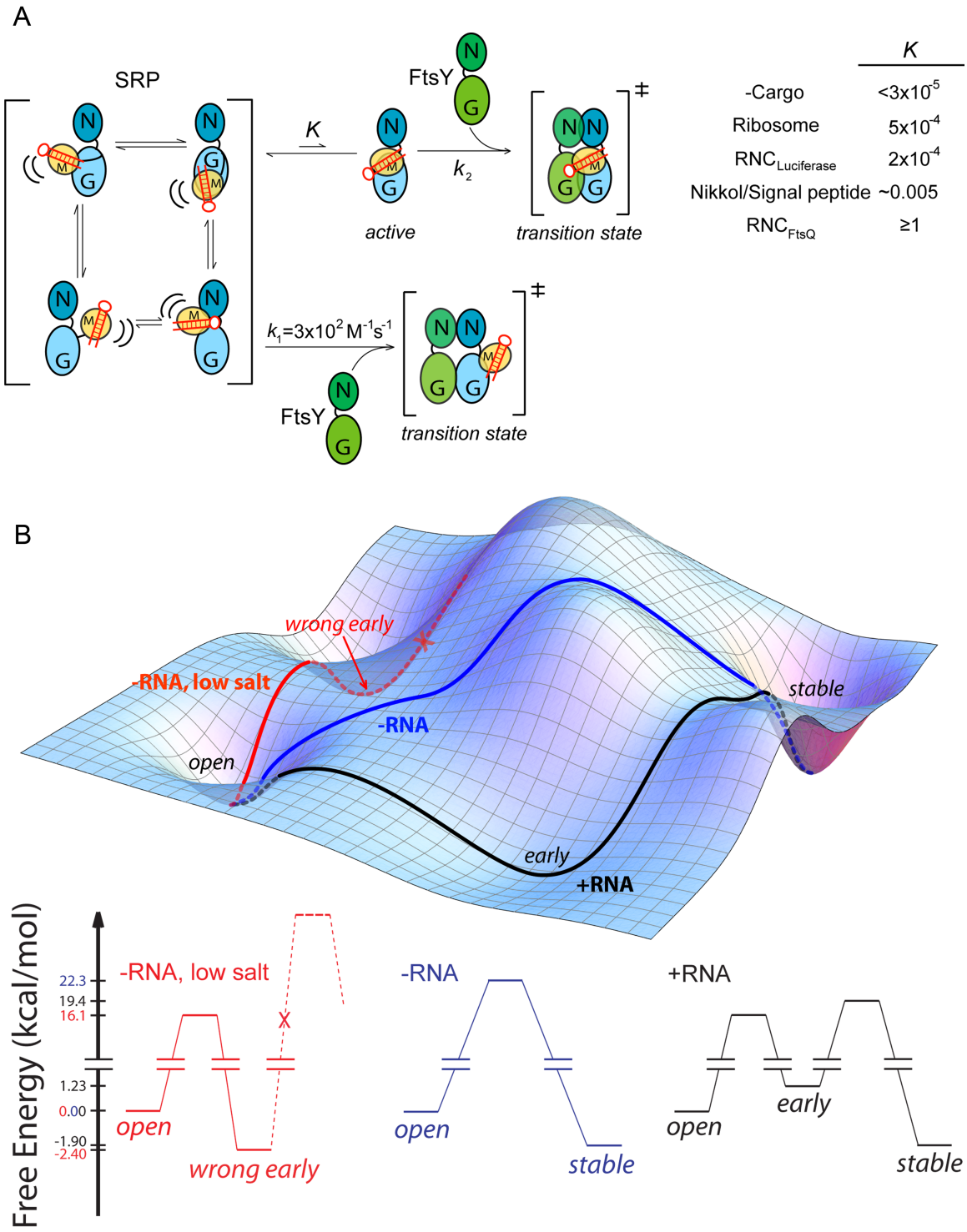

Figure 3.7 Model for how the SRP RNA and cargo act synergistically to stimulate complex assembly. (A) The SRP exists in an equilibrium (*K*) between an active

conformation, in which the SRP RNA tetraloop is positioned to contact the incoming FtsY, and an ensemble of latent conformations (bracket on left) in which the RNA is not properly oriented. The observed rate constant for complex assembly is a weighted average of complex assembly rates from these different conformations. Using this model, the effects of different stimulatory factors on the conformational equilibrium of SRP were estimated from their respective complex assembly rate constants, as described in the Methods. (B) The SRP RNA guides complex assembly through a more efficient pathway. In the presence of the SRP RNA, efficient complex assembly occurs through formation of a productive and stabilized early intermediate, which can readily rearrange to the stable complex (black). Without the SRP RNA, however, the early complex is unstable and nonproductive; hence stable complex assembly likely proceeds through an alternative pathway that bypasses this intermediate (blue). Under low salt conditions, Ffh and FtsY could be trapped in a tight but nonproductive early complex (red) without the SRP RNA. All three cases refer to reactions with cargo (black or blue) or Nikkol (red) present.

3.8 Supplementary figures and legends

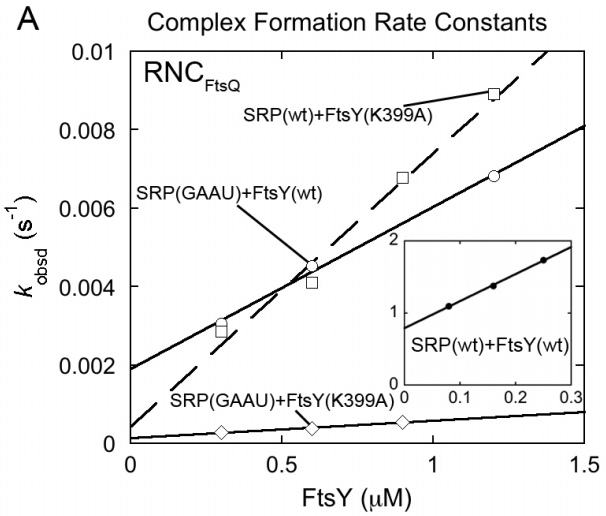

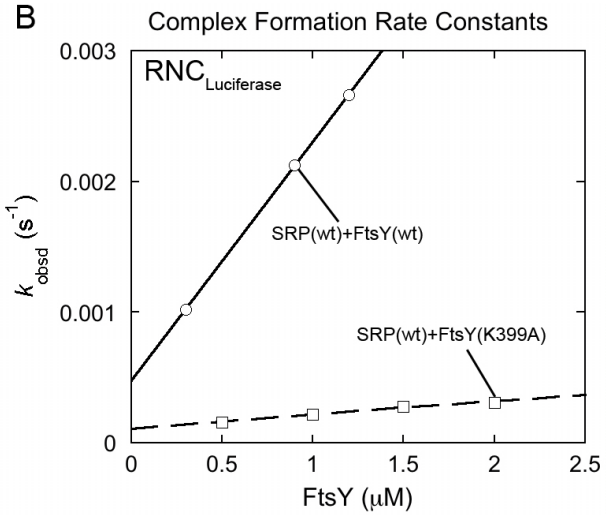

C

k_{on} summary (M^{-1} s^{-1})

cargo / FtsY	RNC_{FtsQ} wt	RNC_{FtsQ} GAAU	$RNC_{Luciferase}$ wt	– wt
wt	9,250,000	4,120	1,820	994
K399A	6,950	440	103	241
wt / K399A	1,330	9.4	18	4.1

Supplementary Figure 3.1 A correct cargo optimizes the electrostatic interaction of the SRP RNA tetraloop with FtsY-K399. All experiments in this figure were performed in the *absence* of Nikkol. (A) SRP-FtsY complex assembly rates in the presence of RNC_{FtsQ}

with mutant FtsY-K399A (□), SRP RNA tetraloop mutant (GAAU, ○), both mutants (◇), or with wild-type FtsY and RNA (inset, ●). (B) SRP-FtsY complex assembly rates in the presence of $RNC_{Luciferase}$ with wild-type FtsY (□) or mutant FtsY-K399A (○). (C) Summary of complex formation rates constants from (A) & (B).

4

Global relocalization of the GTPase along the SRP RNA [§]

[§] A modified version of this section was published as: ***Activated GTPase movement on an RNA scaffold drives co-translational protein targeting***, Kuang Shen, Sinan Arslan, David Akopian, Taekjip Ha, and Shu-ou Shan, *Nature*, **2012**, *492*(7428):271–275.

4.1 Abstract

Roughly one third of the proteome is initially destined for the eukaryotic endoplasmic reticulum or the bacterial plasma membrane (Keenan 2001). The proper localization of these proteins is mediated by a universally conserved protein targeting machinery, the signal recognition particle (SRP), which recognizes ribosomes carrying signal sequences (Pool 2002; Halic 2006; Schaffitzel 2006) and, via interactions with the SRP receptor (Egea 2004; Focia 2004), delivers them to the protein translocation machinery on the target membrane (Becker 2009). The SRP is an ancient ribonucleoprotein particle containing an essential, elongated SRP RNA whose precise functions have remained elusive. Here, we used single-molecule fluorescence microscopy to demonstrate that the SRP-receptor GTPase complex, after initial assembly at the tetraloop end of SRP RNA, travels over 100 Å to the distal end of this RNA where rapid GTP hydrolysis occurs. This movement is negatively regulated by the translating ribosome and, at a later stage, positively regulated by the SecYEG translocon, providing an attractive mechanism to ensure the productive exchange of the targeting and translocation machineries at the ribosome exit site with exquisite spatial and temporal accuracy. Our results show that large RNAs can act as molecular scaffolds that enable the facile exchange of distinct factors and precise timing of molecular events in a complex cellular process; this concept may be extended to similar phenomena in other ribonucleoprotein complexes.

4.2 Results and discussion

Co-translational protein targeting face fundamental challenges in both spatial and temporal coordination. Spatially, both the SRP (Pool 2002; Halic 2006; Schaffitzel 2006) and SecYEG (or Sec61p) translocon (Becker 2009) contact the L23 ribosomal protein and the signal sequence, raising puzzling questions about how the translating ribosome is transferred from the targeting to translocation machinery. Temporally, guanosine-5'-triphosphate (GTP) hydrolysis by the SRP-SRP-receptor complex, which drives its irreversible disassembly (Peluso 2001), must be accurately timed during cargo delivery and unloading to avoid abortive reactions (Zhang 2010). Such accurate spatial and temporal coordination is required in all protein targeting pathways, but its underlying molecular mechanism is not understood. Here, single-molecule experiments reveal large-scale rearrangements in the SRP, providing a unifying molecular mechanism to explain how such coordination is achieved during co-translational protein targeting.

The bacterial SRP is comprised of an SRP54 protein subunit, Ffh, and a 114-nucleotide SRP RNA (Keenan 200). Ffh contains two domains connected by a flexible linker: a methionine-rich M-domain, which recognizes the signal sequence (Janda 2010) and binds the SRP RNA (Batey 2000), and a GTPase, NG-domain that interacts with a homologous NG-domain in the SRP receptor, FtsY (Egea 2004; Focia 2004) (Figure 4.1a). The SRP RNA is a universally conserved and essential SRP component, but its precise roles are not completely understood. Most previous work (Zhang 2008; Shen and Shan 2010; Estrozi 2011; Shen 2011) focused on the GGAA tetraloop that caps one end of this RNA, which accelerates the initial SRP-FtsY assembly by electrostatically interacting with FtsY (Shen and Shan 2010). These findings, however, do not explain

why the SRP RNA has a conserved elongated structure (Althoff 1994). Valuable clues come from a recent crystal structure that found the Ffh-FtsY GTPase complex at another docking site near the 5',3'-distal end of this RNA, where mutations disrupt GTPase activation (Ataide 2011) (Figure 4.1a, distal state). This posits an attractive hypothesis in which the Ffh-FtsY GTPase complex, after initial assembly near the tetraloop (Zhang 2008; Shen and Shan 2010; Estrozi 2011; Shen 2011), can re-localize to the distal site of the SRP RNA ~ 100 Å away (Ataide 2011). Nevertheless, no functional evidence for the relocalization is available, nor are the importance, timing, mechanism, and regulation of such a large-scale movement understood.

To address these questions, we used single-molecule fluorescence resonance energy transfer (smFRET) and total internal reflection fluorescence (TIRF) microscopy to directly detect conformational dynamics of individual SRPs (Ha 1996; Roy 2008). Migration of the SRP-FtsY GTPase complex on the SRP RNA was tracked using FRET between a donor (Cy3) attached to the FtsY-NG-domain and an acceptor (Quasar670) labeled near the RNA distal end (Figure 4.1a). Stable SRP-FtsY complexes, formed with the non-hydrolyzable GTP analogue 5'-guanylyl-imidodiphosphate (GMPPNP), displayed rapid transitions among multiple FRET states (Figure 4.1b, c). A low FRET (~ 0.1) state, ***L***, was assigned to the proximal state in which the GTPase complex resides near the SRP RNA tetraloop (Shen and Shan 2010). A high FRET (~ 0.8) state, ***H***, was attained ~ 20% of the time and assigned to the distal state in which the GTPase complex stably docks at the distal site, as verified below. Cy3 attached to the Ffh-NG-domain showed similar transitions but with a lower FRET value in the ***H*** state (Supplementary Figure 4.2a, b), consistent with Ffh being further from the distal site than FtsY (Ataide

2011). These results directly demonstrate dynamic movements of the SRP-FtsY GTPase complex on the SRP RNA that span over 100 Å.

We used hidden Markov modeling (HMM)-based statistical analyses to determine the most likely sequence of FRET transitions (McKinney 2006). This revealed an ensemble of additional states with intermediate FRET values (0.3–0.6; ***M1*** and ***M2***) and extremely short lifetimes (Figure 4.1b–d and Supplementary Figure 4.2b–g, 4.3a–c), representing alternative binding modes of the GTPase complex on the SRP RNA. The transition information was pooled into a transition density map (TDP) that describes the number of distinct FRET states, their FRET values, and their transition frequencies (Figure 4.1e and Supplementary Figure 4.2h). Additionally, the kinetics of FRET transitions was obtained from dwell time analyses (Figure 4.1f–g and Supplementary Figure 4.2i–o, 4.3d–h). While molecules leaving ***L*** rapidly transitioned to all the other states, the ***H*** state had a longer lifetime than ***M1*** and ***M2*** and was hence more populated (Figure 4.1d), indicating more stable docking of the GTPase complex in this state. 58% of transitions to ***H*** occurred directly from ***L***, whereas molecules in the intermediate FRET states transitioned primarily back to ***L*** (Figure 4.1e and Supplementary Figure 4.2h). Thus, correct docking at the RNA distal site requires extensive searching that involves frequent trial and error.

To test whether the ***H*** state is responsible for GTPase activation, we isolated mutant RNAs that specifically perturb the distal docking site. The 82mer RNA, which lacks this site(Ataide 2011), reduced GTPase activation sixfold, whereas a ‘superactive’ mutant, 99A, enhanced GTP hydrolysis 2.5-fold (Figure 4.2a, green bars and Supplementary Figure 4.1b, 4.4a). The GTPase activity of these mutants quantitatively

correlated with their efficiency of reaching the ***H*** state (Figure 4.2a and Supplementary Figure 4.5, 4.6), strongly suggesting that activated GTP hydrolysis occurs at the RNA distal site.

To test the importance of the RNA distal site in protein targeting, we measured the ability of SRP and FtsY to deliver a model substrate, preprolactin (pPL), to ER microsomes (Shan 2007). Translocation of pPL results in cleavage of its signal sequence, allowing the targeting and translocation efficiency to be quantified (Supplementary Figure 4.4). Further, the specificity of targeting was tested using pPL variants in which the signal sequence is systematically varied (Zhang 2010) (Supplementary Figure 4.4d). Mutant 82mer RNA significantly reduced the targeting of correct substrates (wild-type-, 8L- and 7L-pPL; Figure 4.2b, c and Supplementary Figure 4.4c, e). In contrast, the superactive 99A RNA targeted these substrates more efficiently than the wild-type SRP, without compromising the discrimination against incorrect substrates (Figure 4.2b, c and Supplementary Figure 4.4c, e). Thus the SRP RNA distal site, though not essential for cell survival (Batey 2000), does enhance efficient and accurate co-translational protein targeting.

SRP and FtsY undergo an unusual GTPase cycle, driven by multiple conformational rearrangements in their heterodimer that culminate in GTPase activation (Figure 4.3a–d, cartoon) (Shan 2004; Zhang 2009; Zhang 2011). We asked how these rearrangements *within* the GTPase complex drive its *global* movements on the SRP RNA, using conditions that block the GTPase cycle at distinct stages (Shan 2004; Zhang 2009). SRP by itself exhibited no movements on the RNA (Figure 4.3a and Supplementary Figure 4.7a). Recruitment of FtsY begins with a transient *early*

intermediate, which lacks close contacts between the G-domains and hence can be isolated by leaving out GTP analogues (Zhang 2008; Zhang 2011). No GTPase movement was observed at this stage either (Figure 4.3b and Supplementary Figure 4.7b). Subsequently, GTP-dependent rearrangements give a stable *closed* complex, which lacks optimal positioning of the catalytic loops and can be isolated by a mutation, FtsY(A335W), in the catalytic loop (Figure 4.3c, d) (Shan 2004; Zhang 2009). Although GTPase movements were observed in the *closed* complex, most of them only reached ***M1*** and ***M2*** but did not significantly populate the ***H*** state (Figure 4.3c–e and Supplementary Figure 4.7c, d). Thus, GTP-induced rearrangements within the NG-domain complex drive its global movements on the SRP RNA. Moreover, stable GTPase docking at the RNA distal site requires optimal positioning of the catalytic loops, explaining why mutants that block GTPase activation, such as FtsY(A335W), severely impair protein targeting (Shan 2007).

If the GTPase complex only transiently reaches the SRP RNA distal site where GTPase activation occurs, previous ensemble measurements (Peluso 2001) would have significantly underestimated the hydrolysis rate. We therefore performed real-time GTPase assays using the smFRET setup. If GTP hydrolysis at the distal site, which drives irreversible SRP-FtsY dissociation, occurred faster than their return to the proximal state, we would observe high FRET 'bursts' with GTP instead of the reversible transitions with GMPPNP. This was indeed observed (Figure 4.3f). The duration between these bursts has a rate constant (0.59 s^{-1}; Supplementary Figure 4.8b) expected for rearrangement to the *activated* complex (~ 1 s^{-1}) (Zhang 2008) and is similar to the ensemble GTPase rate (0.7 s^{-1}) (Peluso 2001), strongly suggesting that the latter is rate-

limited by GTPase movement to the RNA distal site. The duration of the high FRET bursts includes GTP hydrolysis and subsequent SRP-FtsY disassembly and exhibits a rate constant of $7.1s^{-1}$ (Supplementary Figure 4.8a), providing a lower limit for the actual hydrolysis rate and is at least tenfold faster than ensemble measurements (Peluso 2001).

These results also show that GTP drives almost irreversible movement of the GTPases to the RNA distal site, necessitating accurate control of the timing of this movement. Indeed, ribosome-nascent chain complexes (RNC or cargo) delay GTPase activation in the SRP-FtsY complex (Zhang 2009; Zhang 2010) (Figure 4.4a, wt). This effect, termed 'pausing', prevents premature GTP hydrolysis and is essential for ensuring the efficiency and specificity of the SRP pathway (Zhang 2010). We asked whether the RNC negatively regulates the GTPase movement to the SRP RNA distal site. RNC_{FtsQ}, which carries an obligate SRP substrate FtsQ, completely abolished the GTPase movements on the RNA (Figure 4.4b and Supplementary Figure 4.9a–e). This is specific to the correct cargo, as $RNC_{Luciferase}$, which contains no signal sequence, exerted no effects (Figure 4.4c and Supplementary Figure 4.9f). Further, GTP hydrolysis in the presence of RNC is no longer affected by mutations in the RNA distal end (Figure 4.4a and Supplementary Figure 4.10a, b), but is still reduced by a mutation in FtsY active site (Shan 2004) (Supplementary Figure 4.10d, e). These results demonstrate that correct cargos stabilize the GTPase complex in the proximal state and prevent its relocalization to the RNA distal site, thus exerting the 'pausing' effect.

On the target membrane, RNC must be transferred from the targeting to the translocation machinery. The mechanism of this transfer and its timing have remained long-standing challenges. To test whether the translocon helps regulate these events, we

added the SecYEG complex to the RNC_{FtsQ}-SRP-FtsY complex (Supplementary Figure 4.11a). SecYEG restored the high FRET state (Figure 4.4d, e). It also reversed the cargo-induced 'pausing' and restored efficient GTP hydrolysis (Figure 4.4a) (Akopian 2013). Neither effect was observed with DDM alone (Supplementary Figure 4.11b) nor with mutant 82mer RNA (Figure 4.4f and Supplementary Figure 4.10c) or FtsY(A335W) (Supplementary Figure 4.11c). Thus, SecYEG drives productive docking of the GTPase complex at the RNA distal site and thus re-activates GTP hydrolysis.

How does SecYEG restore the GTPase movements? Although SecYEG could simply remove the RNC from the SRP-FtsY complex, the following strongly suggests that this is not the case. Compared to the SRP-FtsY complex alone, GTPase movements in the presence of RNC_{FtsQ} and SecYEG displayed a distinct pattern, characterized by fewer transitions to intermediate FRET states, more frequent docking (Figure 4.4g, h) and longer dwell times in the ***H*** state (Figure 4.4d, i). These SecYEG-induced changes were not observed without RNC (Supplementary Figure 4.11d, e). To directly test if RNC remains on the targeting complex, we labeled the RNC with Alexa647, which was found to co-localize with labeled SRP (Supplementary Figure 4.12). These co-localized spots remain after incubation with SecYEG (Supplementary Figure 4.12c, d), indicating that RNC was not displaced by SecYEG. These data imply that SecYEG forms a quaternary complex with RNC, SRP, and FtsY; which could represent a transient intermediate in the targeting and translocation reaction. These results also suggest that SecYEG drives the GTPase movement via two mechanisms: (i) displacing the GTPase complex from the proximal site, as indicated by the reappearance of ***H*** state even with RNC present (cf. Figure 4.4d vs. Supplementary Figure 4.9b); and (ii) prolonging productive docking at

the RNA distal site (Figure 4.4i). Finally, nonproductive movements to intermediate FRET states are minimized with RNC and SecYEG present (Figure 4.4g, h). Considering the size of SRP RNA relative to the ribosome, the RNC possibly masks nonproductive GTPase docking sites on the SRP RNA, which could also explain the conserved length of this RNA.

In summary, we demonstrate that the SRP RNA provides a molecular scaffold that mediates large-scale movements of the SRP-FtsY complex, which are tightly regulated by the GTPase cycle of SRP and FtsY, the translating ribosome, and the SecYEG translocon. Together with previous studies, we propose a molecular model for co-translational protein targeting (Figure 4.4j). Upon cargo recognition (step 1), the SRP RNA tetraloop is optimally positioned adjacent to the Ffh NG-domain, allowing efficient recruitment of FtsY near the ribosome exit site (Zhang 2008; Shen and Shan 2010; Estrozi 2011; Shen 2011) (step 2). GTP-induced rearrangements primes(Halic 2006; Zhang 2009) but is insufficient to release the SRP-FtsY GTPase complex from the vicinity of ribosome due to the RNC's 'pausing' effect. SecYEG is required to drive GTPase relocalization to the SRP RNA distal site (step 3). This vacates the ribosome exit site and allows SecYEG to initiate contacts with L23, thus enabling the coordinated transfer of RNC from the targeting to translocation machinery (step 4). Concomitantly, GTPase docking at the RNA distal site triggers rapid GTP hydrolysis, driving the disassembly and recycling of SRP and FtsY (step 4-5). This provides an attractive mechanism to allow the concerted exchange of SRP and SecYEG at the ribosome and the precise timing of GTP hydrolysis, thus minimizing abortive reactions due to premature SRP-FtsY disassembly or nonproductive loss of cargo.

Nucleic acid-mediated protein movement is a widespread phenomenon and has been observed with the spliceosome (Hoskins 2011), helicases (Lohman and Bjornson 1996; Yodh 2010), and type I restriction endonucleases (Yuan 1981; Murray 2000). Our results here enrich these findings and further suggest that large RNA molecules can provide useful molecular scaffolds to coordinate multiple protein interactions and large-scale protein rearrangements, thus enabling productive exchange of different factors and precise timing of molecular events in a cellular pathway. This may provide general principles for understanding similar phenomena in other ribonucleoprotein particles.

4.3 Material and methods

4.3.1 Plasmids

Plasmids for *in vivo* expression of Ffh, full-length FtsY, and SRP RNA and for *in vitro* transcription of FtsQ, luciferase, and pPL and its signal sequence variants have been described (Peluso 2001; Schaffitzel and Ban 2007; Zhang 2010). The pEK20 construct for SecYEG expression was a kind gift of Arnold Driessen (van der Sluis 2002). Plasmids for mutant SRP RNAs and mutant proteins were constructed using the QuikChange mutagenesis protocol (Stratagene) following manufacturer's instructions. The plasmid for *in vitro* transcription of Hammerhead-SRP RNA-HDV was a generous gift from Adrian Ferre-D'Amare (Ferre-D'Amare and Doudna 1996). The hammerhead coding sequence was removed and the 5'-end of SRP RNA was extended using the QuikChange mutagenesis protocol (Stratagene) to make *in vitro* transcription constructs for smRNA.

4.3.2 Protein preparations

Wild-type and single cysteine mutants of Ffh and FtsY were expressed and purified as described previously (Peluso 2001). Briefly, Ffh expression was induced in logarithmically growing BL21(DE3)pLysE cells with 1 mM IPTG. The soluble fraction from lysed cells were purified by cation-exchange chromatography on the SP-Sepharose Fast Flow resin (GE Healthcare) using a gradient of 0.25–1 M NaCl, and was further purified by gel-filtration chromatography on the Superose12 column (Amersham Biosciences). His_6-tagged full-length FtsY was expressed in BL21(DE3)pLysS cells by induction with 0.5 mM IPTG in logarithmically growing cells. The soluble fraction from

lysed cells was purified by anion exchange chromatography using Q Sepharose Fast Flow resin (GE Healthcare) with a gradient of 150–500 mM NaCl, followed by affinity purification using Ni-NTA resin (Qiagen). For GTPase assays, FtsY was further purified by anion exchange chromatography on the MonoQ column (Amersham Biosciences) using a gradient of 150–350 mM NaCl. All proteins were exchanged into SRP buffer (50 mM KHEPES, pH 7.5, 150 mM KOAc, 2 mM $Mg(OAc)_2$, 2 mM DTT, 0.01% Nikkol) before use.

Detergent-solubilized SecYEG was expressed in BL21(DE3) cells with 0.5 mM IPTG and was purified following published procedures (van der Sluis 2002; Van den Berg 2004; Dalal and Duong 2010). Cells were lysed by sonication and the membranes were collected by ultracentrifugation. SecYEG was extracted and purified by cation-exchange chromatography on the SP-Sepharose Fast Flow resin (GE Healthcare) followed by affinity purification with Ni-NTA (Qiagen). DDM (Affimetrix) was used for purification of solubilized SecYEG, which has been shown to be fully functional in binding RNC (Mothes 1998; Akopian 2013), in mediating nascent peptide translocation (Mothes 1998), and stimulating SecA ATPase activity (Duong 2003).

4.3.3 Fluorescence labeling

Single cysteine mutants of Ffh and FtsY were labeled with Cy3-maleimide (GE Healthcare) as described (Zhang 2008). Protein concentration during labeling was 50 – 100 μM, and the dye was in tenfold molar excess. Labeling reaction was carried out in buffer A (50 mM KHEPES, pH 7.0, 300 mM NaCl, 2 mM EDTA, 10% glycerol) with gentle shaking at room temperature for 2 hours. Unconjugated dyes were removed by gel

filtration chromatography using Sephadex G-25 resin (Sigma). Mass-spectrometry confirmed > 95% labeling efficiencies. Fluorescence labeling and modifications of the SRP RNA for surface immobilization (Figure 4.1a and Supplementary Figure 4.1b) did not affect the activity of SRP and FtsY (Supplementary Figure 4.1d).

Fluorescent DNA probes for hybridization with the mRNA on RNC were prepared by incubating NH_2-modified DNA oligo (IDT) with a tenfold excess of Alexa Fluor 647 carboxylic acid succinimidyl ester (Invitrogen) for an hour at 37 °C. Excess dyes were removed by HPLC.

4.3.4 RNA preparations

Wild-type SRP RNA was expressed *in vivo* and purified as described (Peluso 2001a). SRP RNAs for smFRET experiments (smRNA; Supplementary Figure 4.1b) were prepared by *in vitro* transcription using T7 polymerase according to the Megascript protocol (Ambion). The 3'-end of SRP RNA coding sequence was fused to that of an HDV ribozyme (sequence: GGG CGG CAT GGT CCC AGC CTC CTC GCT GGC GCC GCC TGG GCA ACA TTC CGA GGG GAC CGT CCC CTC GGT AAT GGC GAA TGG GAC C). Self-cleavage of the HDV ribozyme occurred during *in vitro* transcription to generate a homogeneous 3'-end of the SRP RNA. Purified smRNA was annealed to a complementary DNA splint by the following procedures: (1) heat the TE buffer (10 mM Tris-HCl, pH 7.0, 2 mM EDTA) containing 10 μM DNA and 20 μM smRNA for 5 minutes at 75 °C. (2) Gradually cool to 50 °C over a period of 30 minutes. (3) Add 12 mM $MgCl_2$ to the mixture. (4) Gradually cool to room temperature over a period of 30 minutes. The annealed DNA-smRNA hybrids were stored at -80 °C.

Messenger RNAs for *in vitro* translation were generated by *in vitro* transcription using T7 (for RNC prep) or SP6 (for targeting assays) polymerase following the Megascript protocol (Ambion).

4.3.5 RNC preparations

Synchronized RNCs with defined nascent chain length and sequence were prepared as described previously (Schaffitzel and Ban 2007). In short, mRNAs encoding a $Strep_3$ tag at the N-terminus, the first 74 amino acids of FtsQ or luciferase, and a SecM translation stall sequence at the C-terminus were translated by S100 extract as described (Schaffitzel and Ban 2007). RNC from the translation mixture was purified by affinity chromatography using the streptactin resin (IBA), collected by ultracentrifugation, and re-dissolved in SRP buffer and stored at -80 °C. RNCs used for GTPase assay were further purified by ultracentrifugation and fractionation on a 10–50% sucrose gradient as described (Schaffitzel and Ban 2007).

RNC_{FtsQ} was fluorescently labeled by incubation with fluorescent DNA probes complementary to the mRNA for 3 hours at room temperature. Labeled RNC was isolated by ultracentrifugation and re-dissolved in SRP buffer.

4.3.6 Single-molecule instrument

Objective-type TIRF microscope was home-built based on an Olympus IX-81 model as described (Roy 2008). Green (532 nm) and red (635 nm) lasers were focused in a 100x oil immersed objective. Scattering light was removed by a 560 nm and a 660 nm

long pass filters (Chroma) for the green and red lasers, respectively. Cy3 and Quasar670 signals were split by a dichroic mirror and simultaneously focused onto the Ixon 897 camera (Andor) through DV2 Dualview (Photometrics). Data were recorded at 30 ms time resolution.

4.3.7 PEGylated slides and coverslips

PEGylated slides and coverslips were prepared based on an existing protocol (Roy 2008). Briefly, quartz slides and coverslips were treated sequentially with 10% alconox, acetone, and 10 M KOH. The surfaces were then burnt with a propane torch to remove autofluorescence. Aminosilation reactions were carried out in methanol with 5% (v/v) HOAc and 1% (v/v) aminopropylsilane. PEGylation reactions were carried out in 100 mM $NaHCO_3$ buffer containing 20% (w/v) PEG and 0.6% (w/v) biotin-PEG. PEGylated slides and coverslips were stored in vacuum at -20 °C and assembled into flow chambers before use.

4.3.8 Single-molecule assay

To remove aggregates, all protein samples were ultracentrifuged at 100,000 rpm (Optima TLX, Beckman Coulter) for an hour before use. PEGylated slides and coverslips were assembled to form a flow chamber. 0.2 mg/ml neutravidin was applied to the chamber and incubated for 10 minutes before flowing in molecules of interest.

SRP complexes were assembled in SRP buffer under the following conditions. SRP-FtsY complex with labeled Ffh: 1 μM DNA-smRNA hybrid, 2 μM Ffh-Cy3, 5 μM

FtsY, 100 μM GMPPNP. SRP-FtsY complex with labeled FtsY: 1 μM DNA-smRNA hybrid, 2 μM Ffh, 3 μM FtsY-Cy3, 100 μM GMPPNP. RNC-SRP-FtsY complexes: 200 nM DNA-smRNA hybrid, 400 nM Ffh-Cy3, 500 nM RNC_{FtsQ} or 1 μM $RNC_{Luciferase}$, 1 μM FtsY, 100 μM GMPPNP. SecYEG solubilized in 0.02% DDM was added to RNC_{FtsQ}-SRP-FtsY complex at 10 μM. The samples were then diluted to 50 pM in imaging buffer (SRP buffer supplemented with 0.4% glucose and 1% Gloxy in Trolox), flowed onto the sample chamber and incubated for 5 minutes before imaging. Movies were recorded at 30 ms intervals for up to 3 minutes until most fluorescent molecules were photobleached. A red laser was applied at the end of the movie to confirm the presence of immobilized SRP.

4.3.9 Data analysis

Single-molecule data were processed by scripts written in IDL and MATLAB. Briefly, fluorescent peaks in the images were identified and traced throughout the trajectory. Traces that showed a single donor bleaching event were used for data analysis. Hidden Markov Modeling was calculated using the HaMMy program (McKinney 2006). Transition density map was generated by TDP program (McKinney 2006) using the output from HaMMy. FRET histograms were generated using home-written script in MATLAB (Roy 2008). Transition kinetics between different states was obtained by exponential fits to dwell time histograms. Two-dimensional scatter plots of the average dwell time of individual molecules during transitions were generated using the home-written script in MATLAB.

4.3.10 GTPase assay

GTPase rate constants were determined using a well-established GTPase assay (Peluso 2001). In general, reactions contained 100 nM Ffh, 200 nM SRP RNA, 100 μM GTP (doped with γ-^{32}P-GTP), varying concentrations of FtsY, and 250 nM RNC_{FtsQ} and 10 μM SecYEG where applicable. Reactions were quenched with 0.75 M KH_2PO_4 (pH 3.3) at different time points, separated by thin layer chromatography (TLC), and quantified by autoradiography.

4.3.11 Translocation assay

Assays for co-translational protein targeting and translocation were carried out as described (Powers and Walter 1997; Shan 2007). Reactions contained 10 μL *in vitro* translation mixtures synthesizing ^{35}S-methionine labeled pPL or pPL signal sequence variants, to which 200 nM Ffh, 333 nM wild-type or mutant SRP RNA, 300 nM FtsY and 0.5 eq/μL of salt washed, trypsin digested microsomal membrane was added to a total volume of 15 μL. Reactions were analyzed by SDS-PAGE followed by autoradiography.

4.4 Acknowledgements

We thank N. Ban and members of the Shan group for helpful comments on the manuscript, C. Richards, L. Cai, T. Zhiyentayev, K. Lee, and R. Zhou for help with RNC labeling and the instrument and software setup, and C.L. Guo, S. Kou, and H. Lester for helpful discussions. This work is supported by NIH grant GM078024 to S.-o.S., an NIH instrument supplement to grant GM45162 to D.C. Rees, and Caltech matching fund 350270 for the single-molecule instruments. S.-o.S. was supported by the Beckman Young Investigator award, the David and Lucile Packard Fellowship in science and engineering, and the Henry Dreyfus teacher-scholar award. T.H. was supported by NSF Physics Frontiers Center program (08222613) and NIH grant GM065367.

4.5 Figures and figure legends

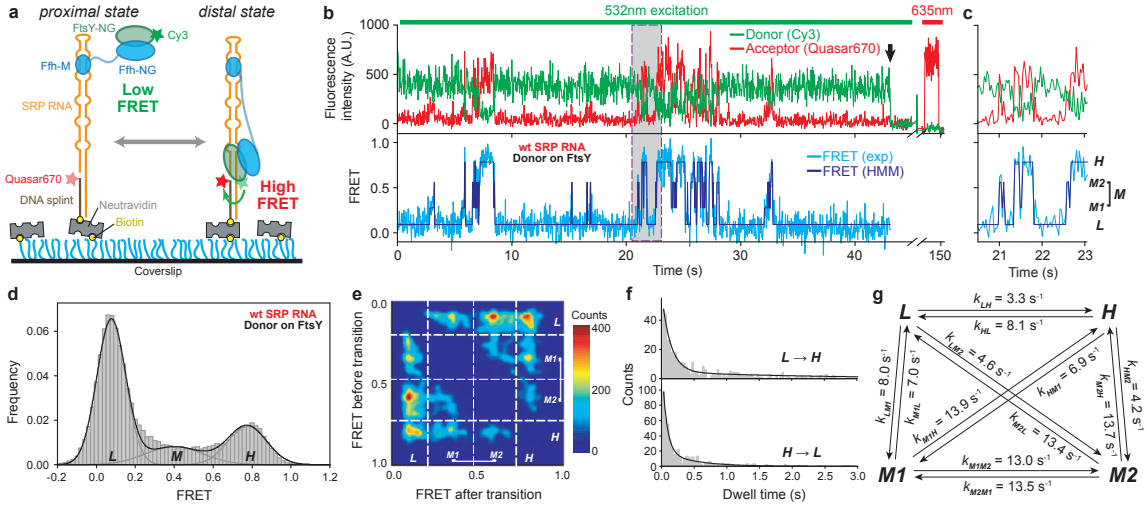

Figure 4.1 | smFRET-TIRF microscopy reveals dynamic movements of the SRP-FtsY complex on the SRP RNA. **a**, smFRET setup for the SRP-FtsY complex. FtsY C345 is labeled with Cy3. The 5'-end of the DNA splint (2 nt from the 3'-end of SRP RNA) is labeled with Quasar670. **b**, Fluorescent signals (upper) and FRET trajectory (lower) of the SRP-FtsY complex in GMPPNP. Hidden Markov Modeling (HMM) of the FRET trajectory is in navy. The arrow denotes the bleaching of Cy3, after which Quasar670 was excited using a 635 nm laser to confirm the presence of the complex. **c**, Magnification of the grey box in **b** to depict the four FRET states resolved by HMM. **d**, smFRET histogram depicting the distribution of molecules in different states. In ***M*** state, the ***M1*** and ***M2*** states are binned together. **e**, Transition density plot (TDP) for the GTPase movements. **f**, Analysis of the transition kinetics between ***L*** and ***H*** states. Exponential fits of the data gave the transition rate constants in **g**.

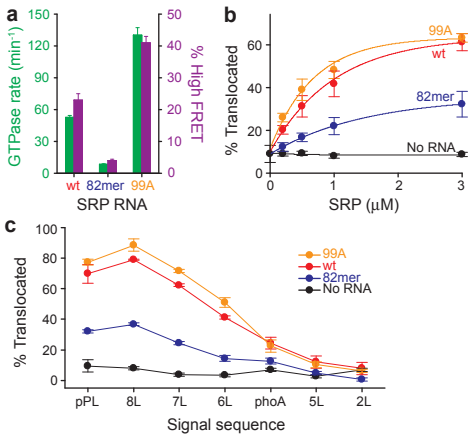

Figure 4.2 | The distal site of SRP RNA is crucial for GTPase activation and protein targeting. **a**, Correlation between GTPase rate constants in the SRP-FtsY complex (green bars) and the frequency of reaching the high FRET state (purple bars) for wild-type (red), 82mer (blue), and 99A SRP RNA (orange). Data points represent mean ± s.d. (n = 5). See Supplementary Figure 4.4a, 4.5, and 4.6 for representative data. **b–c**, Co-translational targeting and translocation of pPL (**b**) and its signal sequence variants (**c**) mediated by the wild-type and mutant SRPs. Color codings are the same as in **a**. Reactions in the absence of SRP RNA are in black. Data points represent mean ± s.d. (n = 3). See Supplementary Figure 4.4c, e for representative data.

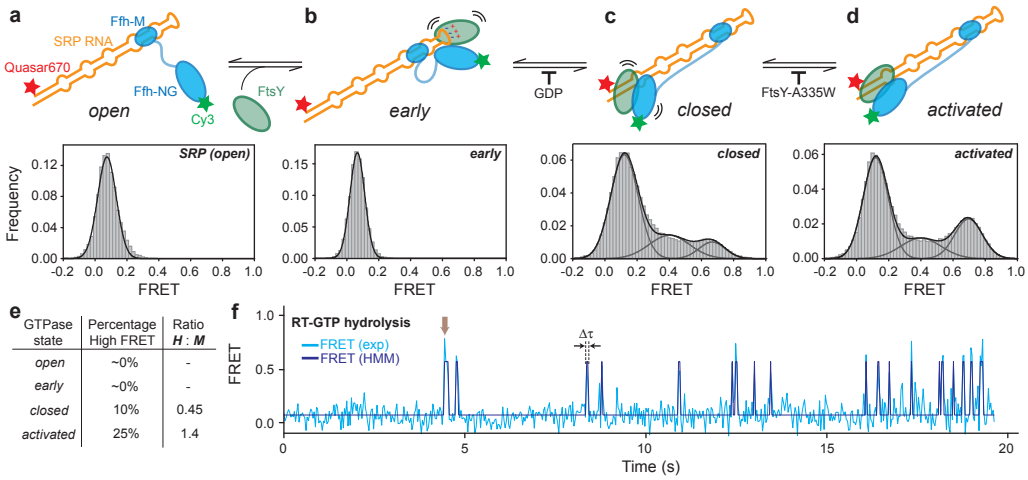

Figure 4.3 | Conformational rearrangements within the SRP-FtsY GTPase complex drive its movement to the RNA distal site. **a–d**, smFRET histograms of free SRP in the open state (**a**) and of the SRP-FtsY complex in the *early* (**b**), *closed* (**c**), and *activated* (**d**) states. Conditions for isolating each conformational state are described in the text and Methods. **e**, Summary of the FRET distributions. **f**, A representative smFRET trajectory of the complex incubated in GTP. The arrow denotes a burst of high FRET that results from GTPase docking at the distal site terminated by rapid GTP hydrolysis driving complex disassembly. Δτ denotes the duration of the high FRET burst.

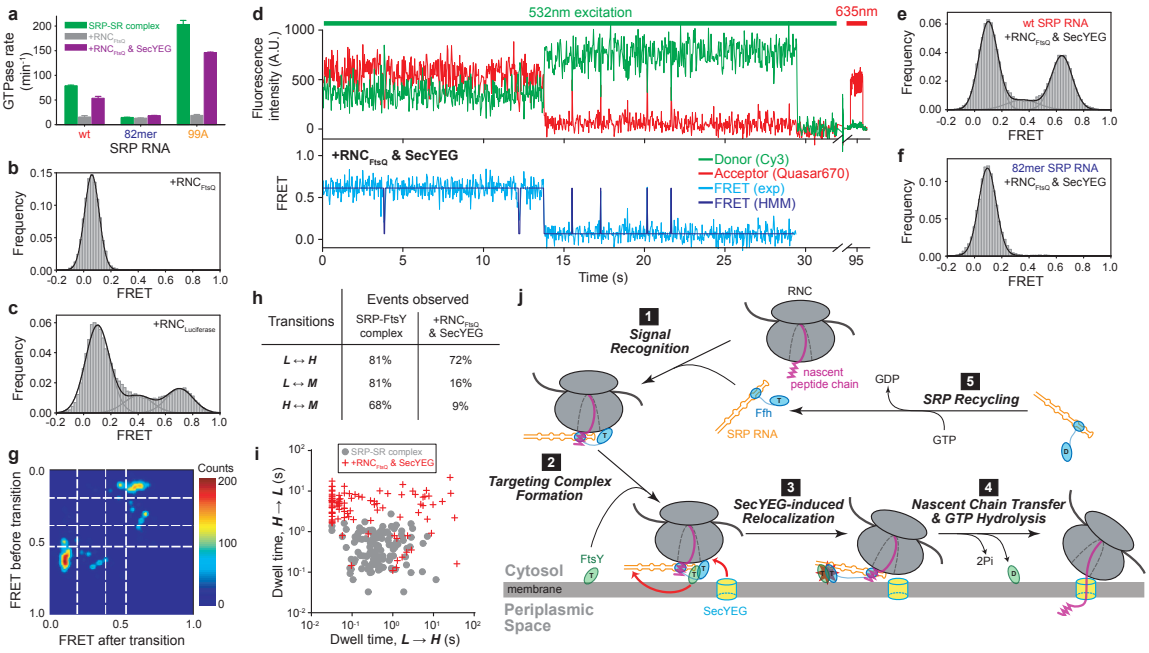

Figure 4.4 | RNC and SecYEG regulate GTPase movements on the SRP RNA. **a**, Effect of RNC_{FtsQ} (grey bars) and SecYEG (purple bars) on the GTPase activity of the SRP-FtsY complex assembled with the wildtype, 82mer, and 99A SRP RNA. Data points represent mean ± s.d. (n = 3). **b–c**, smFRET histograms of the SRP-FtsY complex bound to RNC_{FtsQ} (**b**) or $RNC_{Luciferase}$ (**c**). **d**, Fluorescent signals (upper) and FRET trajectory (lower) of the RNC_{FtsQ}-SRP-FtsY complex in the presence of SecYEG. Color coding is the same as in Figure 4.1b. **e–f**, smFRET histograms of the RNC_{FtsQ}-SRP-FtsY complex in the presence of SecYEG with the wild-type (**e**) or 82mer (**f**) SRP RNA. **g**, TDP of the GTPase movements in the presence of RNC_{FtsQ} and SecYEG. **h**, Summary of the percentage of molecules that exhibit the specified transitions. In the presence of RNC_{FtsQ} and SecYEG, transitions to intermediate FRET states are significantly reduced. **i**, Scatter plot of the transition dwell times of individual molecules in the absence (grey circles) and presence of RNC_{FtsQ} and SecYEG (red crosses). **j**, Model for the role of the SRP RNA-mediated GTPase relocalization in co-translational protein targeting.

4.6 Supplementary figures and legends

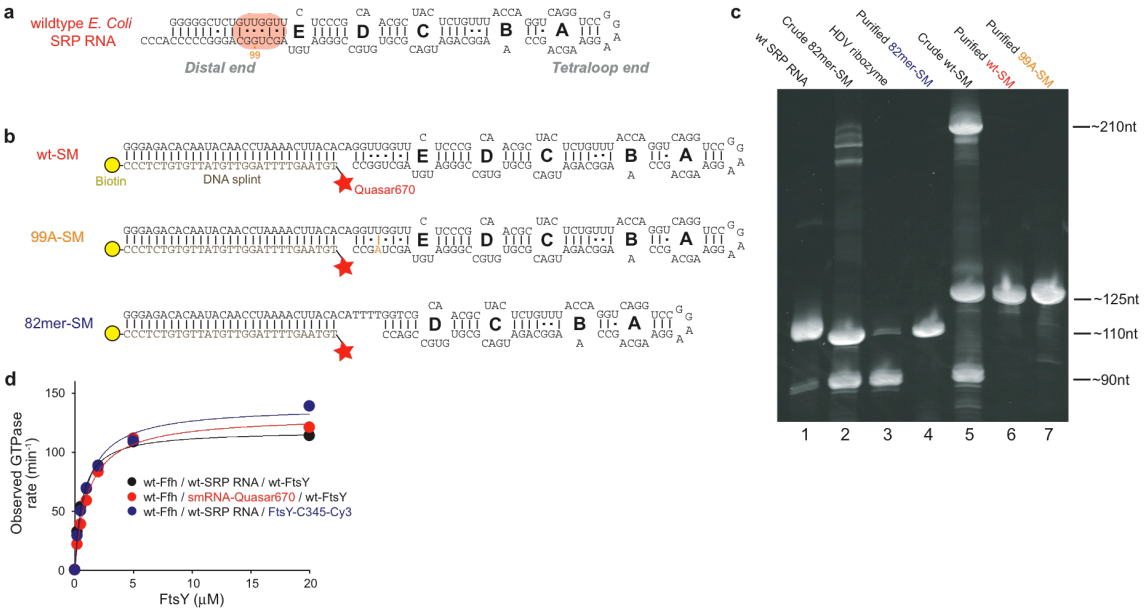

Supplementary Figure 4.1 | SRP RNA constructs used in single-molecule experiments. **a**, Secondary structure of wild-type *E. coli* SRP RNA, which forms an elongated hairpin structure capped by a conserved GGAA tetraloop. Pink region highlights the distal docking site for the SRP-FtsY GTPase complex observed in the crystal structure (PBD code: 2xxa, from Ataide et al., Science, 2011). **b**, Wild-type, 99A, and 82mer smRNA constructs used in this work. **c**, Analytical RNA gel verified the generation and purification of smRNA. smRNAs (lanes 4, 6, 7) were purified from *in vitro* transcription mixtures (lanes 2, 5) by a preparative RNA gel, which removed the HDV ribozyme (90 nt, lane 3) and uncleaved precursor (210 ntd, lane 5). **d**, GTPase reactions for SRPs assembled with DNA-smRNA hybrid and with labeled FtsY.

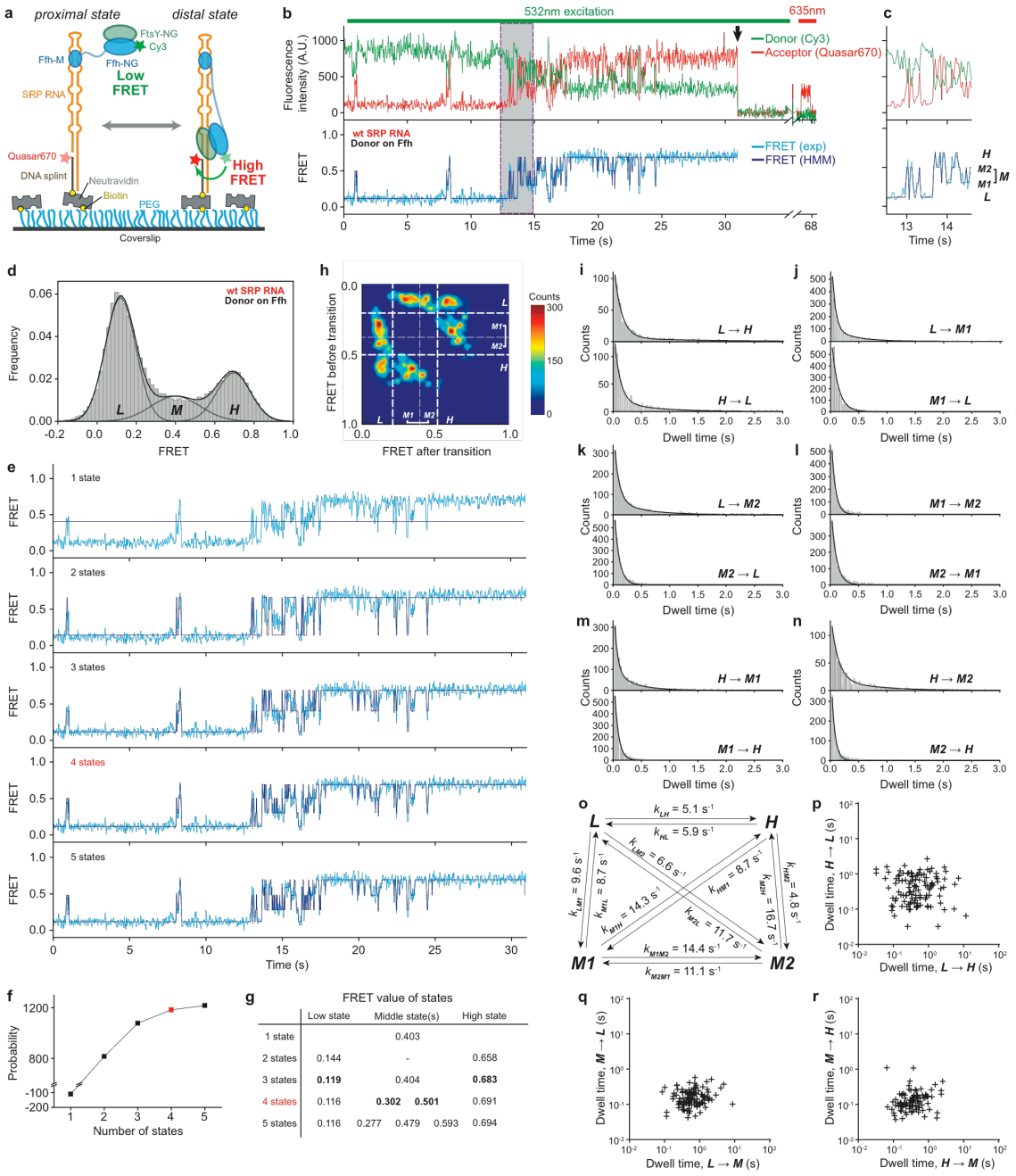

Supplementary Figure 4.2 | smFRET of the SRP-FtsY complex with Cy3-labeled Ffh. **a**, Schematics of the immobilized SRP-FtsY complex on the coverslip with Cy3-labeled Ffh. **b**, Fluorescent signals (upper) and FRET trajectory (lower) of the SRP-FtsY complex. Color coding is the same as in Figure 4.1b. The arrow denotes bleaching of Cy3. **c**, Zoom-in of the grey box in **b** to show the four FRET states resolved by HMM.

d, smFRET histogram. **e**, HMM analysis of a sample FRET trajectory using different numbers of states. As the number of FRET states increases, better fits to experimental data were obtained. **f**, Probability score of each model in the HMM analysis in **e**. The probability maxed out at 4 states, which was chosen as the optimal model to describe experimental data. **g**, The FRET values of each state from the HMM analyses in **e**. Bold indicates the converged FRET values of the identified states. **h**, TDP of the GTPase rearrangement. **i–n**, Analysis of the transition kinetics between states ***L*** and ***H*** (**i**), ***L*** and ***M1*** (**j**), ***L*** and ***M2*** (**k**), ***M1*** and ***M2*** (**l**), ***H*** and ***M1*** (**m**), ***H*** and ***M2*** (**n**). **o**, Summary of transition rates between different FRET states. **p–r**, Scatter plots of the transition dwell times of individual molecules. Each cross represents an individual molecule.

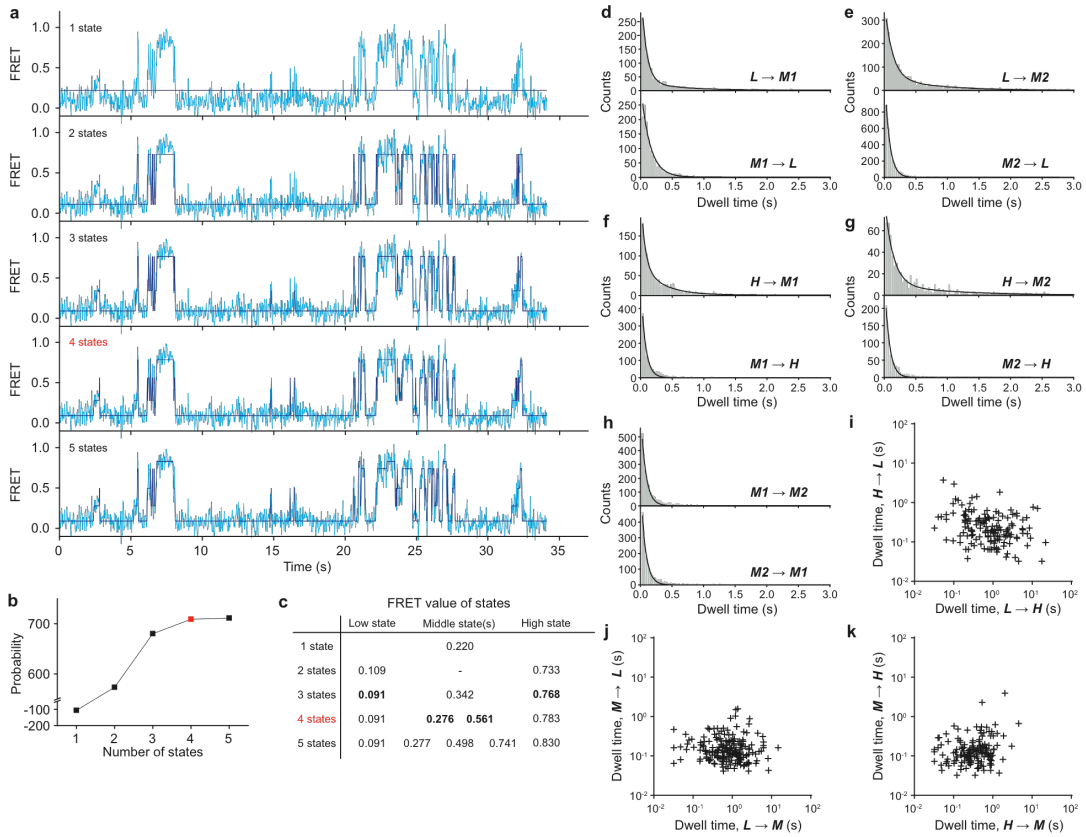

Supplementary Figure 4.3 | smFRET analysis of the SRP-FtsY complex with labeled FtsY. **a**, HMM analysis of the FRET trajectory in Figure 1b using different numbers of FRET states. As the number of FRET states increases, better fits to experimental data were obtained. **b**, Probability score of each model in the HMM analysis in **a**. The probability maxed out at 4 states, which was chosen as the optimal model to describe experimental data. **c**, The FRET values of each state from the HMM analyses in **a**. Bold indicates the converged FRET values of the identified states. **d–h**, Analysis of the transition kinetics between states ***L*** and ***M1*** (**d**), ***L*** and ***M2*** (**e**), ***H*** and ***M1*** (**f**), ***H*** and ***M2*** (**g**), ***M1*** and ***M2*** (**h**). **i–k**, Scatter plots of the transition dwell times of individual molecules. Each cross represents an individual molecule.

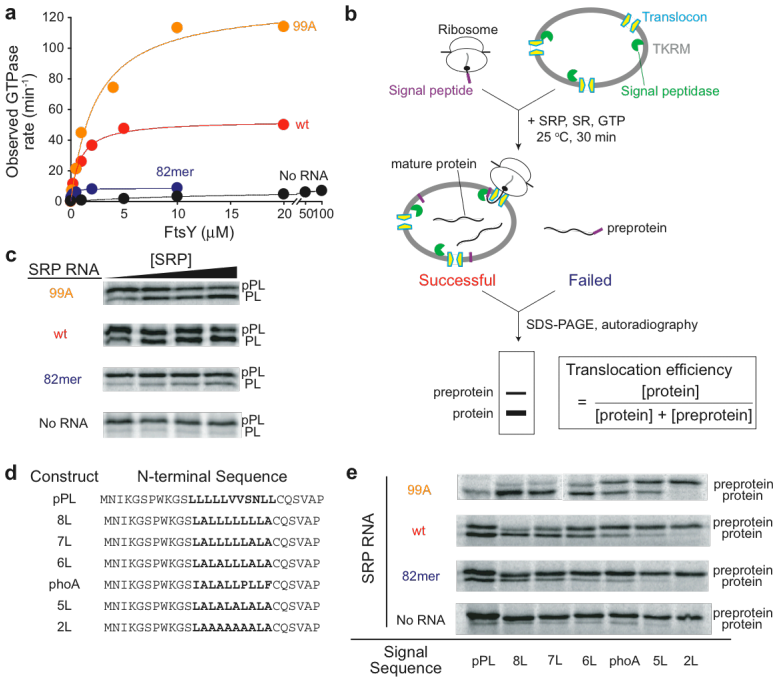

Supplementary Figure 4.4 | Activity of SRP RNA distal-end mutants in GTPase reactions and in co-translational protein targeting and translocation. **a**, Representative data for stimulated GTPase reactions upon assembly of the SRP-FtsY complex with wild-type (red), 82mer (blue), and 99A (orange) SRP RNA. The data in the absence of SRP RNA are in black. Summary of the rate constants, with n = 5, is provided in Figure 4.2a. **b**, Schematics of the co-translational protein targeting and translocation assay. **c & e,** Representative data for co-translational targeting and translocation of pPL (**c**) and pPL signal sequence variants (**e**) by the wild-type and mutant SRPs. Color coding is the same as in **a**. Quantification of the data from three independent experiments is provided in Figure 4.2b and c. **d**, Signal sequence variants of pPL used in this study. Bold highlights the hydrophobic core of the signal sequence.

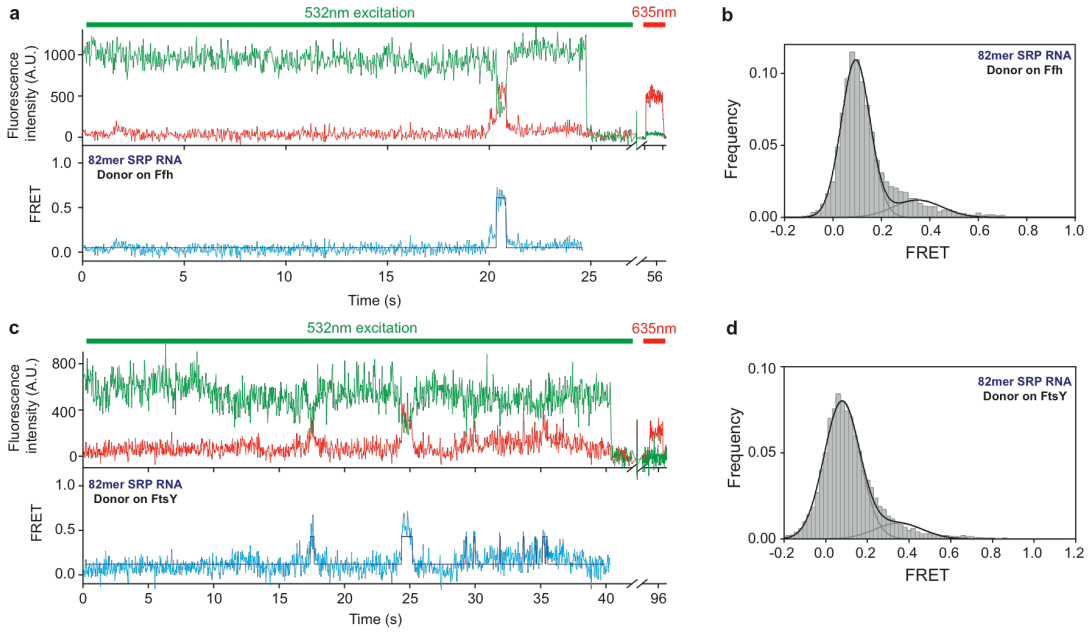

Supplementary Figure 4.5 | smFRET data and analysis for SRP-FtsY complexes assembled with the 82mer SRP RNA. **a & c**, Fluorescent signals (upper) and FRET trajectory (lower) of the SRP(82mer)-FtsY complex with Cy3-labeled Ffh (**a**) or FtsY (**c**). Color coding is the same as in Figure 4.1b. **b & d**, smFRET histograms of the GTPase complex with Cy3-labeled Ffh (**b**) or FtsY (**d**).

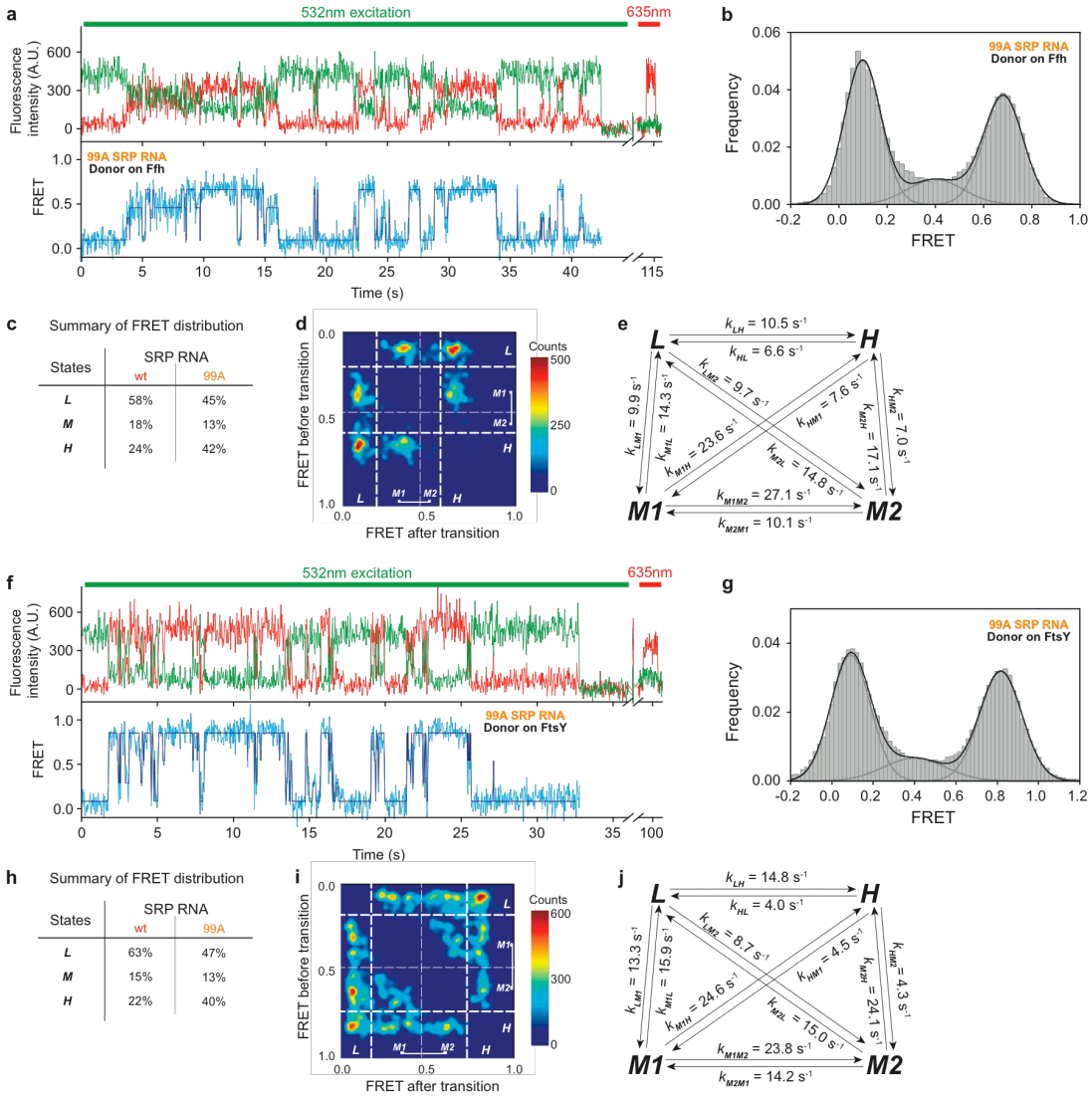

Supplementary Figure 4.6 | smFRET data and analyses for complexes assembled with mutant 99A RNA. **a & f**, Fluorescent signals (upper) and FRET trajectory (lower) of the SRP(99A)-FtsY complex with Cy3-labeled Ffh (**a**) or FtsY (**f**). Color coding is the same as in Figure 4.1b. **b & g**, smFRET histograms of the GTPase complex with Cy3-labeled Ffh (**b**) or FtsY (**g**). **c & h**, Summary of the FRET distributions of SRP(99A)-FtsY and comparison with the wild-type complex for Cy3-labeled Ffh (**c**) or FtsY (**h**). **d & i**, TDP of the SRP(99A)-FtsY complex with Cy3-labeled Ffh (**d**) or FtsY (**i**). **e & j**,

Summary of transition kinetics of the SRP(99A)-FtsY complex with Cy3-labeled Ffh (**e**) or FtsY (**j**).

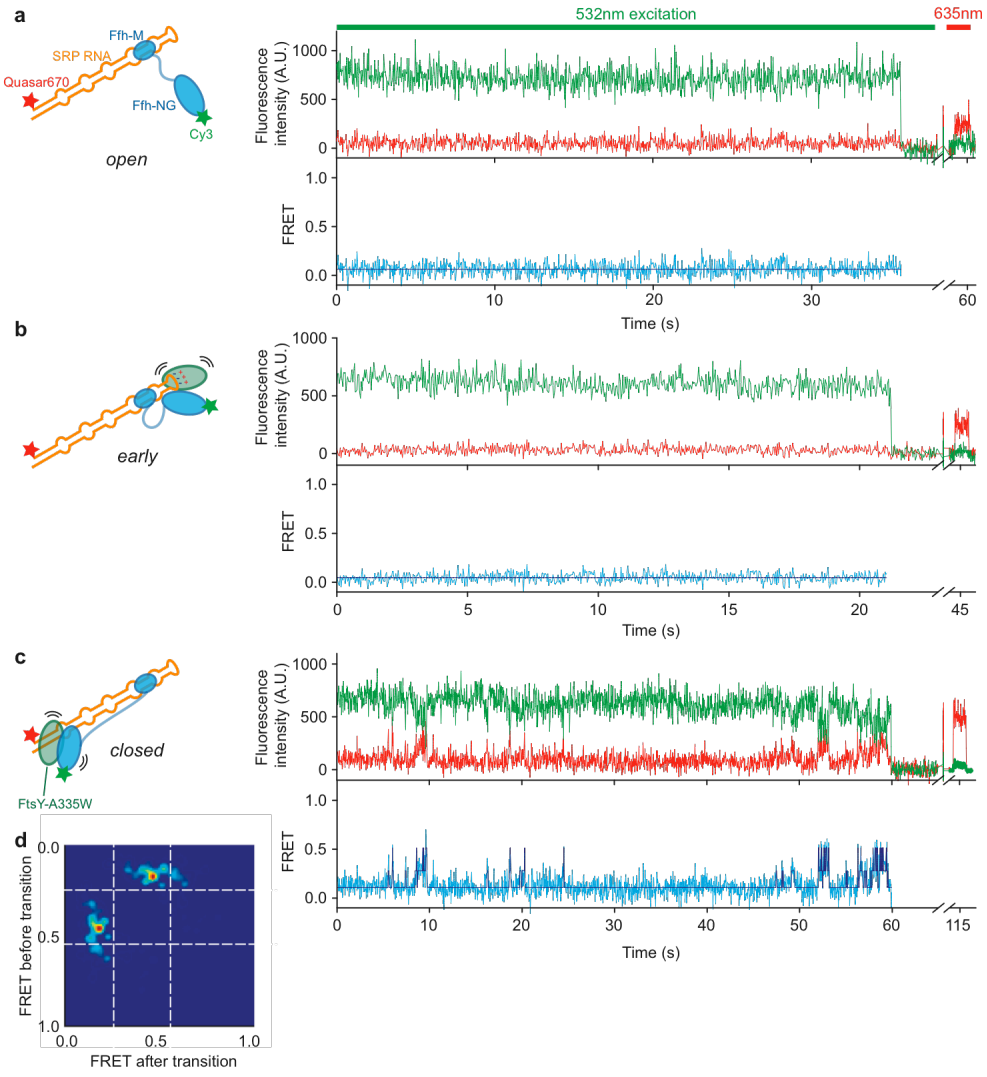

Supplementary Figure 4.7 | smFRET traces of SRP at different stages of its GTPase cycle, including free SRP (**a**) and the SRP-FtsY complex in the *early* (**b**) and *closed* (**c**) states. Ffh was labeled with Cy3. Color coding is the same as in Figure 4.1b. **d**, TDP of the SRP-FtsY complex in the *closed* state.

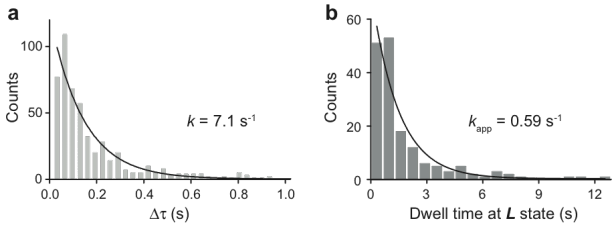

Supplementary Figure 4.8 | Dwell time analysis of real-time GTP hydrolysis. a, Exponential fit of Δτ gave a lower limit for the GTPase rate. **b**, Exponential fit of the low FRET state between high FRET burst clusters.

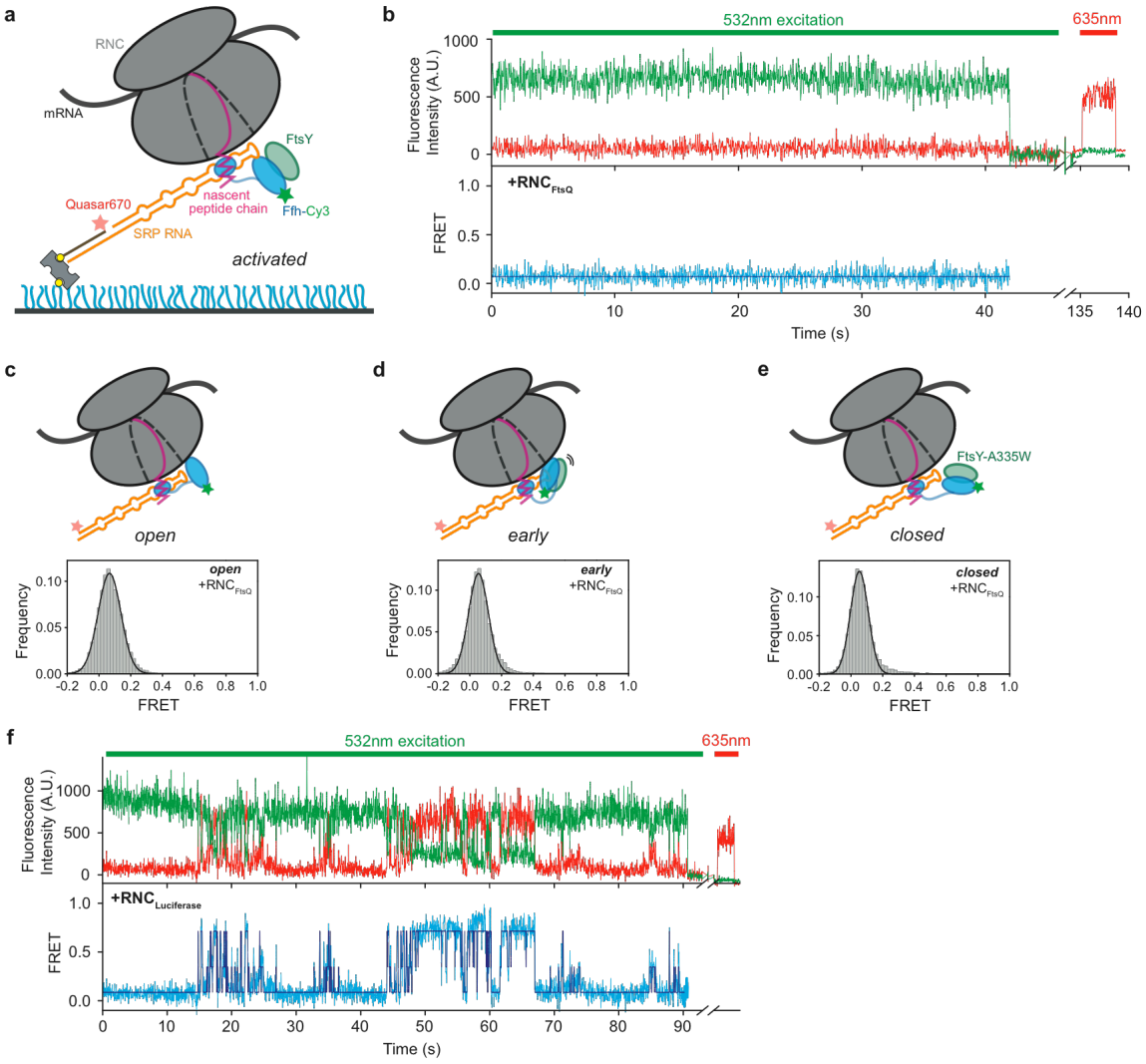

Supplementary Figure 4.9 | RNC carrying a correct SRP substrate abolishes GTPase movement along the SRP RNA. **a**, RNC-bound SRP-FtsY complex on the coverslip surface. **b & f**, Fluorescent signals (upper) and FRET trajectory (lower) of the SRP-FtsY complex bound to RNC_{FtsQ} (**b**) or $RNC_{luciferase}$ (**f**). Color coding is the same as in Figure 4.1b. **c–e**, smFRET histograms of the RNC_{FtsQ}-SRP complex (**c**) and the RNC_{FtsQ}-SRP-FtsY complex in the *early* (**d**) and *closed* (**e**) states.

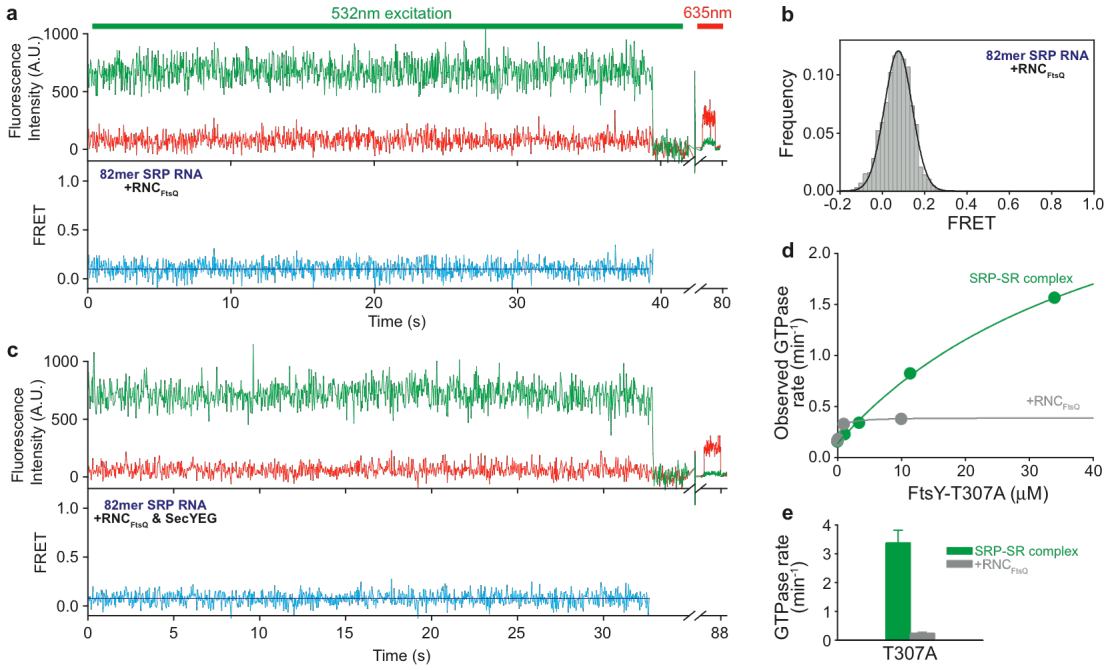

Supplementary Figure 4.10 | RNC's pausing effect is independent of the SRP RNA distal end. **a & c**, Fluorescent (upper) and FRET (lower) trajectory of the RNC_{FtsQ}-SRP(82mer)-FtsY complex in the absence (**a**) and presence (**c**) of SecYEG. Color coding is the same as in Figure 4.1b. **b**, smFRET histogram of the RNC_{FtsQ}-SRP(82mer)-FtsY complex. **d**, Representative data for GTPase assay of mutant FtsY T307A in the absence (green) and presence (grey) of RNC_{FtsQ}. **e**, Summary of the k_{cat} values from (**d**). Data represent mean ± s.d. (n = 3).

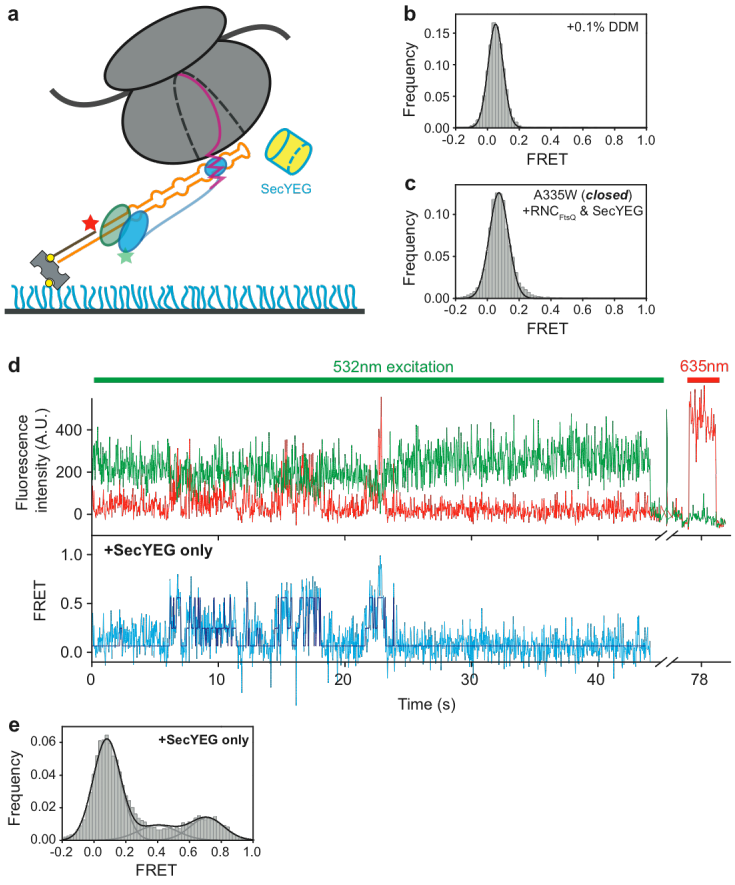

Supplementary Figure 4.11 | SecYEG restores GTPase movement to the SRP RNA distal site. **a**, SecYEG-bound RNC_{FtsQ}-SRP-FtsY complex on the surface of the coverslip. **b**, smFRET histogram of the RNC_{FtsQ}-SRP-FtsY complex in the presence of 0.1% DDM. For comparison, the DDM concentration in reactions containing SecYEG is ≤ 0.07%. **c**, smFRET histogram of the RNC_{FtsQ}-SRP-FtsY(A335W) *closed* complex in the presence of SecYEG. **d & e,** FRET trajectory (**d**) and smFRET histogram (**e**) of the SRP-FtsY complex in the presence of SecYEG but absence of RNC. Cy3-labeled Ffh was used.

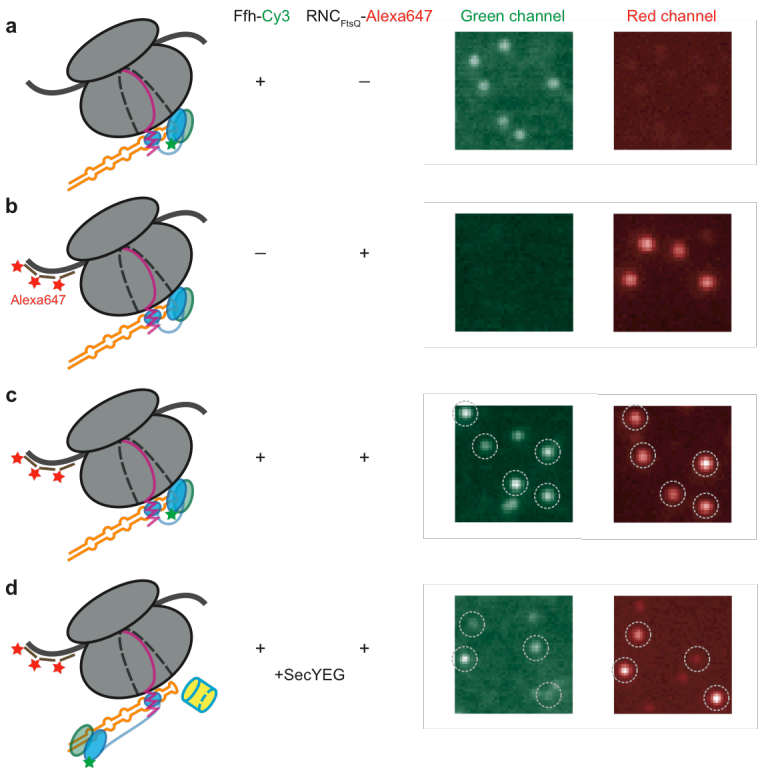

Supplementary Figure 4.12 | Co-localization assay of SRP and RNC. Cy3-labeled SRP (**a**) and Alexa647-labeled RNC_{FtsQ} (**b**) co-localize before (**c**) and after (**d**) incubation with SecYEG.

5

SRP RNA distal end triggers GTP hydrolysis [**]

[**] A modified version of this section will be submitted to *J Am Chem Soc*.

5.1 Abstract

The SRP RNA is a universally conserved and essential component of the signal recognition particle (SRP) that mediates the co-translational targeting of proteins to the correct cellular membrane. During the targeting reaction, two functional ends in the SRP RNA mediate distinct functions. While the RNA tetraloop facilitates initial assembly of two GTPases between the SRP and SRP receptor, this complex subsequently relocalizes ~100 Å to the 5',3'-distal end of the RNA, a conformation crucial for GTPase activation and cargo handover. Here we combined biochemical, single molecule, and NMR studies to investigate the molecular mechanism of this large scale RNA-induced GTPase relocalization and activation. We show that specific nucleotide bases as well as the conformation and dynamics of the internal loop adjacent to the distal site play crucial roles in stable docking of the SRP•SRP receptor GTPase complex. This docking event can be uncoupled from subsequent GTPase activation, which is mediated by conserved bases in the next internal loop. These results, combined with recent structural work, elucidate how the SRP RNA induces GTPase relocalization and activation at the end of the protein targeting reaction.

5.2 Introduction

The signal recognition particle (SRP, Figure 5.1A) is a ribonucleoprotein complex responsible for targeting proteins to their proper membrane destinations (Keenan 2001). SRP recognizes the signal sequence emerging from the ribosomal exit channel (termed ribosome-nascent chain complex or RNC; Figure 5.1A, step 1). The RNC-SRP complex is delivered to the membrane through the interaction between SRP and the SRP receptor (Figure 5.1A, step 2). At the membrane, when the RNC-SRP-SR ternary complex localizes near the SecYEG translocon, RNC dissociates from the SRP-SR complex and is loaded onto the SecYEG (Figure 5.1A, step 3) where the nascent protein is integrated into or translocated across the membrane. The SRP-SR complex then disassembles to start another round of protein targeting (Figure 5.1A, step 4).

In prokaryotic cells, SRP consists of a SRP54 protein (Ffh in bacteria) and a 4.5S SRP RNA (Figure 5.1A, SRP). Ffh contains a methionine-rich M-domain, which binds the SRP RNA and the signal sequence on the translating ribosome. In addition, an NG-domain in Ffh, comprised of a GTP-binding G-domain and a four-helix-bundle N-domain, forms a tight complex with a highly homologous NG-domain in the SRP receptor (called FtsY in bacteria) in the presence of GTP (Egea 2004). GTP hydrolysis at the end of the SRP cycle causes the disassembly of the Ffh-FtsY-NG-domain complex (Peluso 2001). The assembly of the SRP-FtsY-NG-domain complex and their GTPase activation require discrete conformational rearrangements in the SRP (see next paragraph) that are regulated by the RNC and the target membrane, respectively, thus ensuring the spatial and temporal precision of these molecular events during protein targeting (Shen 2012).

In addition to the SRP and SRP-receptor GTPases, the SRP RNA is the only other universally conserved and essential component in the cytosolic SRP system (Figure 5.1B). Extensive previous work showed that the SRP RNA provides an active scaffold that regulates protein-protein interactions and protein conformational rearrangements during the targeting reaction. The bacterial 4.5S SRP RNA adopts a hairpin structure containing five internal loops, capped by a highly conserved GGAA tetraloop (Figure 5.1B). Two internal loops, A and B, mediate binding of the SRP RNA to the Ffh M-domain with picomolar affinity (Batey 2001). The tetraloop of the SRP RNA mediates a transient electrostatic interaction with FtsY during its initial recruitment to the SRP, thus accelerating the assembly of the stable NG-domain complex between Ffh and FtsY 10^2–10^3-fold (Zhang 2008). More recently, crystallographic and single-molecule analyses showed that GTPase activation requires the Ffh-FtsY-NG-domain complex to dock at a distinct site at the 5',3'-distal end of the SRP RNA (Figure 5.1B) (Ataide 2011; Shen 2012). Together with biochemical studies, these data demonstrate a global relocalization of the Ffh-FtsY-NG-complex, from the tetraloop end of the SRP RNA during initial complex assembly to the distal end where the NG-domain complex hydrolyzes GTP (Figure 5.1A, step 3).

The global rearrangement along the SRP RNA is important for multiple reasons. First, it provides temporal regulation of GTP hydrolysis. On the one hand, rapid GTP hydrolysis is desired at the end of the SRP cycle to regenerate free SRP. On the other hand, GTP hydrolysis should be inhibited to minimize pre-mature complex disassembly before the RNC is productively delivered to the Sec translocation machinery. The domain separation on the SRP RNA resolves this issue: the Ffh-FtsY-NG-domain

complex only migrates to the distal end of the RNA and hydrolyzes GTP at the end of the SRP cycle, after encounter with the SecYEG machinery. Second, the global rearrangement of SRP coordinates the protein translocation machinery with the protein targeting machinery. In the RNC-SRP complex, Ffh N-domain binds the L23 protein on the large ribosomal subunit. Strikingly, this site is also where SecYEG binds in the RNC-SecYEG complex (Figure 5.1A). Re-localizing the NG-domain complex to the distal end of the SRP RNA ensures the productive exchange of the targeting and translocation machineries at the L23 binding site and thus efficient co-translational protein targeting.

Despite the biological importance of the GTPase relocalization, its underlying molecular mechanisms remain unclear. First, how the Ffh-FtsY complex interacts specifically with the distal docking site remains obscure, especially given the low degree of sequence conservation at the distal site and the predominantly electrostatic interactions of the NG-domain complex with the distal docking site. Indeed, nonspecific docking of the Ffh-FtsY-NG-domain complex at other sites on the SRP RNA have been observed in single-molecule experiments that represent 'trial and error' searches of the complex for the correct docking site; however, very little is known about what information specifies the correct distal docking site. Second, different crystal structures suggest two different bases, G83 and C86, as potential catalytic moieties that could insert into the GTPase active site (Voigts-Hoffman et al., manuscript submitted). Third, it is unclear whether the GTPase activation step is coupled to, or independent of the GTPase relocalization on the SRP RNA. In this work, we utilized biochemical and single-molecule tools to investigate the molecular mechanism of GTPase docking and activation at the SRP RNA distal end.

We show that specific nucleotide bases as well as the conformation and dynamics of the internal loop adjacent to the distal site play crucial roles in stable docking of the SRP-SRP-receptor GTPase complex. This docking event is independent of subsequent GTPase activation, which is mediated by conserved bases in the next internal loop. These results, combined with recent structural work, elucidate how the SRP RNA induces GTPase relocalization and activation at the end of the protein targeting reaction.

5.3 Results

5.3.1 A proper docking site is required for GTPase activation at the distal end

To provide mechanistic details on how the SRP RNA distal end triggers GTP hydrolysis in the Ffh-FtsY-NG-domain complex, we revisited the 92mer SRP RNA (nucleotides 11-101 of the wild-type SRP RNA), which is the minimal RNA construct that maintains the stimulation of GTP hydrolysis (Ataide 2011). We systematically truncated the individual nucleotide from the 3'-end of the 92mer (Figure 5.2B, 91mer–87mer) and determined the activity of these mutants using a well-established GTPase assay (Figure 5.2A). The k_{cat}/K_m value represents SRP-FtsY complex formation rate constant. The observed GTPase rate constant at saturating FtsY concentrations (k_{cat}) includes both the docking and GTP hydrolysis steps. Deletion of every residue beyond C99 reduced the k_{cat} value of the SRP-FtsY complex to levels in the absence of the SRP RNA (Figure 5.2B), even though single mutations of most of these residues exhibited no significant defect (Figure 5.3 below). These observations suggest that an intact distal docking site is required to stimulate the GTPase activation.

To probe the nucleotide specificity of the interactions between the distal docking site on the SRP RNA and the FtsY-Ffh-NG-domain complex, we mutated the individual nucleotide bases on and surrounding the distal docking site. Several nucleotides stood out in this analysis (Figure 5.3A–D, and summarized in 5.3E): G14, U15, G96, and U98. Mutation of G14 (Figure 5.3A) or G96 (Figure 5.3C) to any other bases lowered the GTPase rate to the level in the absence of SRP RNA. Mutation of U15 (Figure 5.3B) or U98 (Figure 5.3D) also severely impairs GTPase activation, though to a lesser extent than G96 and G14. Besides these four nucleotides, mutation of other residues does not show

defective GTPase stimulation (Figure 5.3E). These results indicate that these four nucleotides mediate highly specific interactions with the Ffh-FtsY-NG-domain complex and are crucial for driving the GTPase docking and activation at the distal site.

An alternative explanation to the observed nucleotide specificity is the base-pair specificity: An appropriate base pair is sufficient to mediate the GTPase interaction, while the property of the bases is not important. To test this hypothesis, we measured the GTPase activity of several base-pair switch mutants, in which the base substitutions at U96, G14, and G86 were combined with mutations at U98, C97, or U15, respectively, that restore the base-pairing interactions at these sites. All the base-pair switched mutants impair the GTPase rate of the SRP-FtsY complex (Figure 5.3F), indicating the specific nucleotide bases, instead of the secondary structure at these sites conferred by the base-pairing interaction, is critical for GTPase activation.

Interestingly, several mutants show higher GTPase activity than wildtype SRP RNA, most notably mutations at G99, U12, and C97 (Figure 5.3E, red). Mutant G99A has been shown to prolong the GTPase docking at the distal end, which correlates with the faster GTP hydrolysis mediated by this mutant RNA (Shen 2012). Based on this observation and the results presented later, we reason that other mutants have similar effects.

5.3.2 Loop E controls the action of the distal-end docking site

Adjacent to the distal-end docking site is the asymmetric loop E (C-UGU in *E. coli*, Figure 5.1B). In the crystal structure, loop E is located on the opposite side of the

distal docking site, and hence does not make direct contact with the GTPase complex (Ataide 2011). However, this asymmetric internal loop is conserved across all species in the SRP RNA. We therefore probed the structure and function of this loop.

Two roles could be envisioned for loop E. It could be crucial for accurately positioning and orienting the distal docking site, optimizing it for docking by the GTPase complex. Alternatively or in addition, loop E could introduce flexibility that enables more efficient search and docking by the GTPase complex. To test these hypotheses, we measured the GTPase activity of several mutant RNAs in which loop E is either replaced by base-pairing residues (Figure 5.4A, ΔE, ΔE+1 and cE) or systematically varied in size (Figure 5.4A, E-1, E+1, E+2). All of the mutations that removed loop E abolished the stimulatory effect of the SRP RNA on GTP hydrolysis (Figure 5.4B, C), indicating an essential role of this loop in GTPase activation. All the mutants that alter the size of loop E reduced the GTPase rate constant to ~ 20% of that of wild-type SRP, only twofold higher than that in the absence of the SRP RNA (Figure 5.4B, upper panel and Figure 5.4C). This indicates that the size of loop E is critical for GTPase docking and activation at the RNA distal site. Finally, when the flexibility of loop E is reduced by replacing the AU pairs that seal the loop with GC pairs, GTPase activation by the SRP RNA is reduced ~ 30% (Figure 5.4B, lower panel). This effect, though small, is nonetheless reproducible and statistically significant. The AU to GC substitution is expected to reduce the flexibility of the loop by 50%. This observation suggests that the flexibility of loop E also makes a real, though modest, contribution to the function of the RNA distal end.

5.3.3 Loop E mutants impair docking at the distal end

To directly test the role of loop E in mediating the docking of the Ffh-FtsY-NG-domain complex at the RNA distal site, we used single-molecule (sm) fluorescence-TIRF microscopy (see Figure 5.5A for experimental setup). We labeled the Ffh protein with a donor (Cy3) dye, and the distal end of the SRP RNA with an acceptor (Quasar670). Successful docking of the GTPase complex at the distal end brings these two dyes into close proximity, resulting in a high efficiency of fluorescence resonance energy transfer (FRET) (cf. Figure 5.5A). In previous work, we showed that wild-type SRP RNA mediates dynamic and reversible movement of the NG-domain complex on the SRP RNA (Figure 5.5B) (Shen 2012). The probability to reach the high FRET state directly correlates with the observed GTPase rate constant, indicating that stable docking is a necessary step during GTPase activation.

With this tool in hand, we measured how the loop E mutants mediate the movement of the Ffh-FtsY-NG-domain complex to the RNA distal end (Figure 5.5C). If loop E assists the stable docking of the GTPase complex at the distal site, mutations in this loop should significantly reduce the number of successful docking events. This was indeed observed. Mutants E-1 and E+1 exhibit a much lower frequency of attaining the high FRET state and a much shorter dwell time in this state compared to wild-type SRP RNA (cf. sample traces in Figure 5.5C and Figure 5.5B). We used Hidden Markov Modeling (HMM)-based statistical analyses to determine the most likely sequence of FRET transitions, the number of distinct FRET states, their FRET values, and their transition frequencies. This information was used to generate FRET histograms for each mutant (Figure 5.5C, right panels). The analysis showed that E-1 and E+1 mutants attain

the high FRET state ~ 10% of the time, while Ecg loop tightening mutant attains ~ 18%. The probability at which each of these mutants attain the high FRET state directly correlates with their corresponding GTPase rate constant, falling on the same linear correlation line generated by wild-type, 99A, and 82mer (Figure 5.5D). This indicates that loop E affects observed GTPase activity by tuning the efficiency of GTPase docking at the RNA distal site.

Although the loop E mutants do not maintain the GTPase complex in the high FRET state as well as wild-type SRP RNA, they allow the GTPase complex to nonspecifically visit intermediate FRET states (Figure 5.5C). However, molecules that reached these intermediate states primarily return to the low FRET state, rather than proceeding to the high FRET state. We reason that these intermediate states represent alternative binding modes of the GTPase complex along the SRP RNA that do not allow stable docking of the GTPase complex and are not conducive to GTPase activation. Further, loop E specifically controls stable docking of the GTPase complex at the distal site.

5.3.4 Conserved bases in Loop D catalyze GTP hydrolysis

Once the GTPase complex docks at the SRP RNA distal site, GTP hydrolysis is activated over 100-fold (Peluso 2001; Shen 2012). In two crystallographic analyses, two distinct nucleotide bases in loop D, C86 or G83, has each been observed to insert into the composite active site formed at the interface between the Ffh-FtsY-NG-domain complex (Figure 5.6A, B). Biochemical studies have demonstrated the importance of these two bases: Deletion or substitution of G83 by any other nucleotides completely abolishes the

stimulatory effect of the SRP RNA on GTP hydrolysis (Voigts-Hoffman et al., manuscript submitted). Similarly, mutations of C86 also exhibit reduced GTPase activity (Ataide 2011), although to a lesser extent than G83.

To distinguish whether these nucleotide bases are responsible for mediating docking of the GTPase complex at the distal site or enhancing GTP hydrolysis after docking, we performed the single-molecule assay with mutants G83A and C86G. This assay allows us to specifically monitor the movement of the GTPase complex to the distal end, regardless of the catalytic function of these nucleotides. Despite defective GTP hydrolysis, neither the G83A nor C86G mutant shows detectable defect in the efficiency of GTPase docking at the distal end (Figure 5.6C). The SRP•FtsY complex assembled with both mutants exhibit long and stable high FRET states, and their frequency of reaching the high FRET state is the same, within experimental error, as that of wild-type SRP RNA (Figure 5.7C). These mutants lie far away from the linear correlation between GTPase activity and the efficiency of attaining high FRET established for the mutants that affect GTPase docking at the distal site (Figure 5.7C), indicating that these mutants uncouple GTP hydrolysis from the movement of the GTPase complex to the RNA distal end. Thus, a guanine at residue 83 or 86 serves as a catalytic base that specifically triggers GTP hydrolysis.

Strikingly, mutation of C87, the nucleotide adjacent to C86, generates higher GTPase activity than wild-type SRP RNA (Figure 5.7A). For example, mutant C87A triggers GTP hydrolysis ~ 2.5-fold faster than wild-type. This suggests that C87 also participates in the docking or activation of the GTPase complex. To distinguish between these possibilities, we tested the C87A mutant using the single-molecule setup. Mutant

C87A displays an even higher efficiency of GTPase docking at the distal end, ~ 45% (Figure 5.7B), than that with wild-type SRP RNA. The data with mutant C87A is consistent with the correlation obtained with other distal site docking mutants (Figure 7C), strongly suggesting that the primary function of this residue is to provide an additional site that assists in the stable docking of the GTPase complex at the RNA distal end.

To further ask whether C87 and the previously identified distal site act independently or cooperatively, we combined the C87A mutation with the G99A or C97U mutation, which also improves docking of the GTPases at the distal docking site (cf. red nucleotides in Figure 5.3E). If the two docking sites are independent of one another, these double mutants should have an additive effect. This was indeed observed (Figure 5.8). Combining either G99A or C97U with C87A generated two "superactive" SRP RNA double mutants that hydrolyze GTP 5.5- and 4.6-fold faster than wild-type SRP RNA, respectively. The observed enhancement in GTPase rate in these double mutants is consistent with an additive effect from the individual mutations. In contrast, combining the two mutations in the previously identified distal docking site, G99A and C97U, did not further enhance GTPase activity compared to the single mutations (Figure 5.8). Together with the single-molecule data, these results strongly suggest that residue C87 provides an auxiliary docking site that further stabilizes the interaction of the GTPase complex at the SRP RNA distal end.

5.4 Discussion

During co-translational protein targeting, a global conformational rearrangement in the SRP has been demonstrated by crystallographic and biochemical studies. In this work, we combined biochemical and biophysical assays to investigate how GTP hydrolysis is triggered at the RNA distal end. We found that the stimulation of the GTP hydrolysis is an independent process than the docking event. These two processes are mediated by different functional domains on the SRP RNA: Loop E and specific bases are responsible for GTPase docking, while G83 is responsible for triggering GTP hydrolysis.

Using mutagenesis screening, we identified several critical bases, including G14, U15, G96, and U98, that are responsible for GTPase docking at the distal end. These bases either directly interact with the GTPase, or control the conformation of the RNA-protein interface, to host the Ffh-FtsY-NG-domain complex. Moreover, loop E also plays an important role in stabilizing the GTPase at the distal-end docking site. Although loop E does not directly interact with the GTPase, it precisely posits the distal-end docking site and thus promotes successful docking. Despite their important functions, the distal-end docking site lacks sequence conservation. We speculate that the docking site and Ffh/FtsY proteins co-evolve. To adapt mutations in the protein, SRP RNA distal end evolves to generate distinct sequences with similar scaffold, to better interact with the Ffh-FtsY-NG-domain complex.

After the initial docking at the distal-end docking site, we identified an auxiliary interaction mediated by C87 base in loop D. Previous chemical probing experiment revealed that two nucleotides in loop D, C87 and G83, are exposed and prone to small

molecule modification. In agreement with this observation, we showed that the C87 mutants trigger GTP hydrolysis better than wild-type SRP RNA, and retain the GTPase complex at the high FRET state for longer time in a base-specific manner. Our results here provide a model to explain the observed behavior. We propose that C87 establishes additional interaction with the GTPase complex, which acts independently of the distal-end docking site. This auxiliary interaction stabilizes the correct GTPase docking, and therefore assists GTP hydrolysis.

Successful docking at the distal end is necessary but not sufficient for efficient GTP hydrolysis. Previous biochemical experiments identified the critical guanine base at position 83, which inserts into the Ffh-FtsY-NG-domain interface and directly triggers GTP hydrolysis. In this study, we utilized single-molecule assay to distinguish the docking step from the GTPase activation step. We found that the docking at the distal end is independent of GTP hydrolysis. The GTPase activation is triggered by a two-step mechanism, where Ffh-FtsY-NG-domain complex first relocalizes to the distal end, followed by G83 insertion and GTP hydrolysis.

What is the biological importance of this RNA-induced GTP hydrolysis? As described before, the SRP RNA provides a molecular ruler that couples GTP hydrolysis with RNC unloading. In the RNC-loading state, two features of the RNC-SRP-FtsY complex prevent GTP hydrolysis and pre-mature complex disassembly. First, the Ffh-FtsY-NG-domain complex localizes at the tetraloop end of the SRP RNA, which is stabilized by the additional interaction between the Ffh-N-domain and the ribosome L23 subunit. This interaction was confirmed by biochemical assay (Saraogi and Shan, unpublished result) and the cryo-EM structure. Second, a recent crystal structure showed

that in the RNC-SRP-FtsY complex, the SRP RNA distal-end docking site and the catalytic nucleotide are facing the ribosome. Therefore, the GTPase complex is physically excluded from the correct docking interaction, and GTP hydrolysis cannot be stimulated.

In the RNC-unloading state, RNC needs to form the interaction with the SecYEG translocon and transfer the nascent chain from Ffh-M-domain to the SecYEG. Moreover, SRP-SR complex needs to hydrolyze the bound GTP and recycle. A quaternary complex was proposed: RNC-SRP-FtsY-SecYEG forms a transient intermediate where this coupled process is initiated. In this complex, SecYEG has been shown to push the Ffh-FtsY-NG-domain complex away from the L23 binding site on the ribosome. However, because the docking site on the RNA distal end is not exposed, the GTPase complex cannot stably reside. Here, we propose that SecYEG also displaces Ffh-M-domain, which in turn dislocates SRP RNA from the original binding mode. The displacement causes the exhibition of the distal-end docking site, and the GTPase complex can then be hosted. This coupled mechanism ensures efficient GTP hydrolysis at the end of the SRP cycle, which promotes RNC-SecYEG interaction and SRP recycling.

5.5 Material and methods

5.5.1 Plasmids

Plasmids for *in vivo* expression of Ffh, full-length FtsY, and SRP RNA have been described in previous studies. Plasmids for SRP RNA mutants were constructed using the QuikChange mutagenesis protocol (Stratagene) following the manufacturer's instructions. The plasmid for *in vitro* transcription of Hammerhead-SRP RNA-HDV was a gift from Adrian Ferre-D'Amare. The hammerhead ribozyme was removed from the 5'-end of the RNA sequence, and the SRP RNA was extended with an overhang sequence to fuse with the DNA splint handle.

5.5.2 Protein and RNA preparations

Ffh, FtsY, and SRP RNA were expressed *in vivo* as described in previous studies. SRP RNAs for smFRET experiments (smRNA) were prepared by *in vitro* transcription using T7 polymerase based on the Megascript protocol (Ambion).

5.5.3 Fluorescence labeling

Single cysteine mutants of Ffh was labeled with Cy3-maleimide (GE Healthcare) using a similar protocol as previous studies. Labeling reaction was carried out with 1:5 protein-to-dye ratio at room temperature for 2 hours. Unconjugated dyes were removed by gel-filtration chromatography using Sephadex G-25 resin (Sigma).

5.5.4 Single-molecule instrument

A home-built objective-type TIRF microscope was used to carry out all the single-molecule experiment. Green (532 nm) and red (635 nm) lasers were introduced in a 100× oil immersed objective and focused on the coverslip where protein complexes were immobilized. Scattering light was removed by a 560 nm and a 660 nm long-pass filters (Chroma) for the green and red lasers, respectively. Cy3 and Quasar670 signals were split by a DV2 Dualview (Photometrics) and focused onto the Ixon 897 camera (Andor). Data were recorded at 30 ms time resolution.

5.5.5 Single-molecule assay and data analysis

All protein samples were ultracentrifuged at 100,000 rpm (Optima TLX, Beckman Coulter) for an hour right before use, to remove aggregates during freeze-thaw cycle. PEGylated slides and coverslips were assembled to a flowing chamber. Neutravidin was applied to the chamber and incubated for 10 minutes before flowing in fluorescent molecules of interest.

SRP complexes were assembled in SRP buffer (50 mM KHEPES, pH 7.5, 150 mM KOAc, 2 mM $Mg(OAc)_2$, 2 mM DTT, 0.01% Nikkol). The samples were diluted to a final concentration of 50 pM in imaging buffer (SRP buffer supplemented with 0.4% glucose and 1% Gloxy in Trolox), flowed into the sample chamber and incubated for 5 minutes before imaging. Movies were recorded at 30 ms intervals until most fluorescent molecules were photobleached. Data were analyzed by home-written scripts in IDL and MATLAB.

5.5.6 GTPase assay

GTPase rate constants were determined using a GTPase assay. In general, reactions contained 100 nM Ffh, 200 nM SRP RNA (wild-type or mutants), and varying concentrations of FtsY were incubated with 100 μM GTP (doped with γ-^{32}P-GTP). Reactions were quenched by 0.75 M KH_2PO_4 (pH 3.3) at different time points, separated by thin layer chromatography (TLC), and quantified by autoradiography.

5.6 Acknowledgements

We thank members of the Shan group for helpful comments on the manuscript. This work is supported by NIH grant GM078024 to S.-o.S., an NIH instrument supplement to grant GM45162 to D.C. Rees, and Caltech matching fund 350270 for the single-molecule instruments. S.-o.S. was supported by the David and Lucile Packard Fellowship in science and engineering, and the Henry Dreyfus teacher-scholar award.

5.7 Figures and figure legends

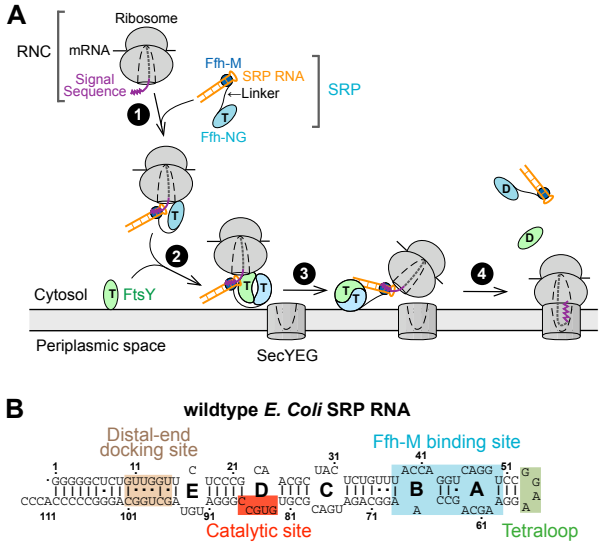

Figure 5.1 General scheme of the function of the SRP RNA during co-translational protein targeting. (A) Working model of co-translational protein targeting by SRP. See main text for introduction. (B) The secondary structure of the *E. Coli* SRP RNA. Four different domains are noted with different colors.

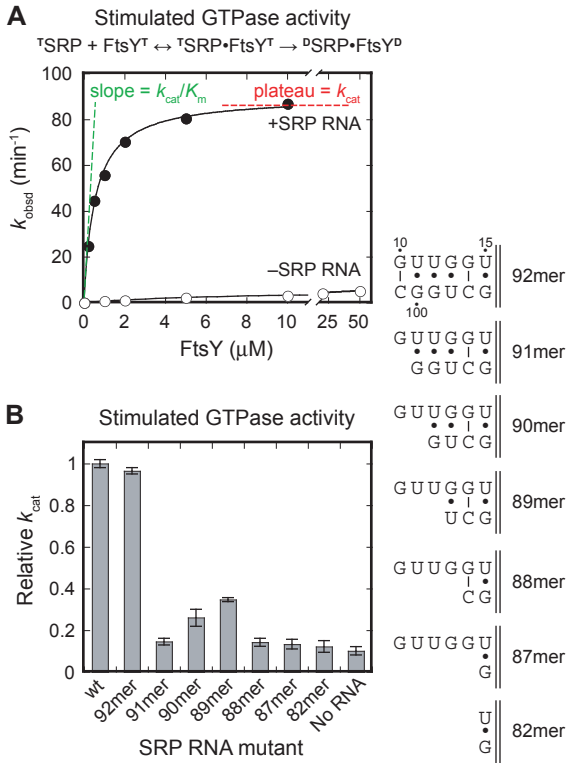

Figure 5.2 An intact SRP RNA distal end is required for efficient GTP hydrolysis. (A) GTPase assay showing the function of the SRP RNA. The k_{cat}/K_m and k_{cat} values are 164 μM^{-1}•min^{-1} and 90 min^{-1} for +SRP RNA curve, 0.69 μM^{-1}•min^{-1} and 8.5 min^{-1} for –SRP RNA curve. (B) Single-nucleotide truncation mutants of 92mer and their GTPase activity relative to wild-type SRP RNA and 82mer.

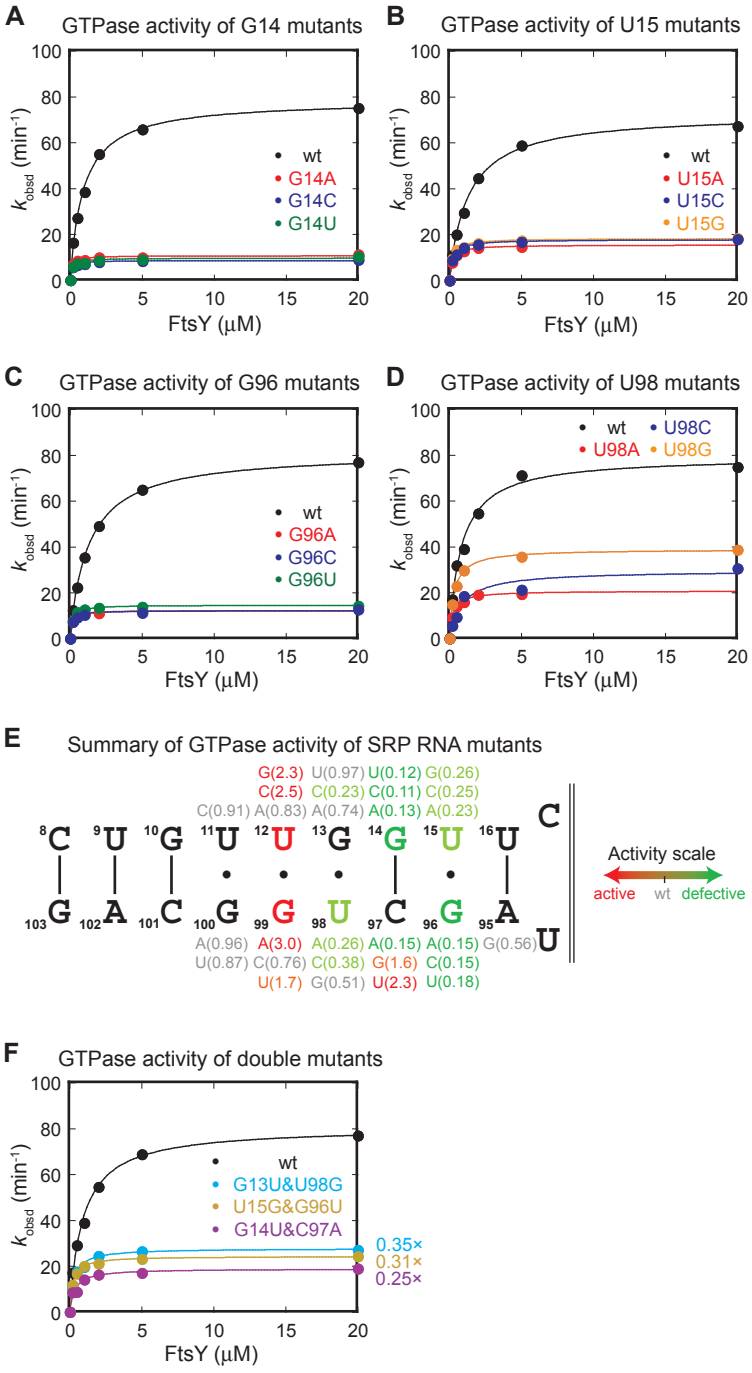

Figure 5.3 Base-specificity of the RNA stimulatory effect. (A-D) Point-mutagenesis of specific SRP RNA distal-end bases and their GTPase activity. Four nucleotides with most defective mutants are shown: G14 (A), U15 (B), G96 (C), and U98 (D). (E)

Summary of the GTPase activity of the point-mutants at the distal-end docking site. (F) GTPase activity of base-pair mutants.

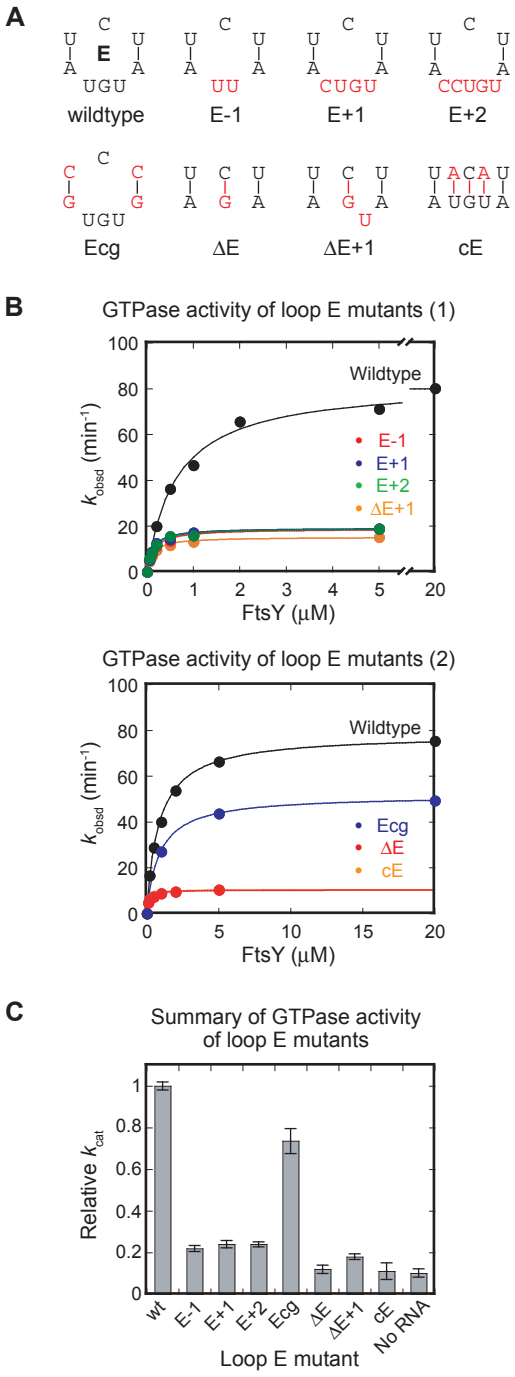

Figure 5.4 Loop E controls the stimulatory activity of the SRP RNA. (A) Design of loop E mutants. E-1, E+1, and E+2 create shrinking and expansion of loop E. Ecg tightens the loop E by replacing the UA pairs with CG pairs. ΔE, ΔE+1, and cE eliminate

loop E. (B) GTPase activity of the loop E mutants in (A). (C) Summary of the relative GTPase rate of the loop E mutants.

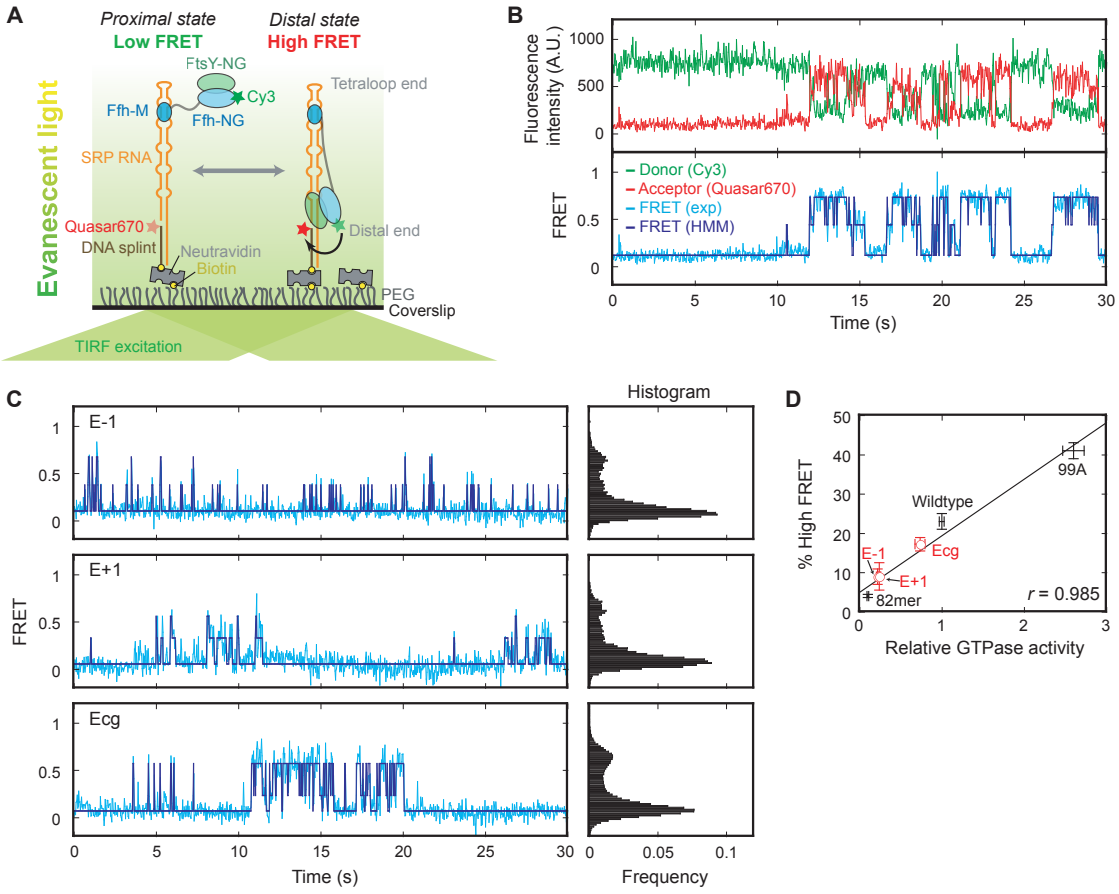

Figure 5.5 Loop E mutants cause defect in the docking of the GTPase complex at the distal end of the SRP RNA. (A) Single-molecule setup for determining the migration of the Ffh-NG/FtsY-NG complex along the SRP RNA scaffold. Ffh C153 is labeled with Cy3. The 3'-end of the SRP RNA is labeled with Quasar670. (B) Fluorescent signals (upper panel) and FRET trajectory (lower panel) of the SRP-FtsY complex in GppNHp. Hidden Markov Modeling (HMM) of the FRET trajectory is shown in navy. (C) Sample FRET trajectories (cyan) and HMM simulation (navy) of E-1, E+1, and Ecg SRP RNA mutants (left panel). The histograms for the FRET traces are shown in the right panel. (D) Correlation between the percentage of high FRET state and the GTPase activity. Standard curve (solid line) is the linear fit of three data points, wild-type SRP RNA, 82mer, and 99A (black crosses). E-1, E+1, and Ecg data points are shown in red cycle.

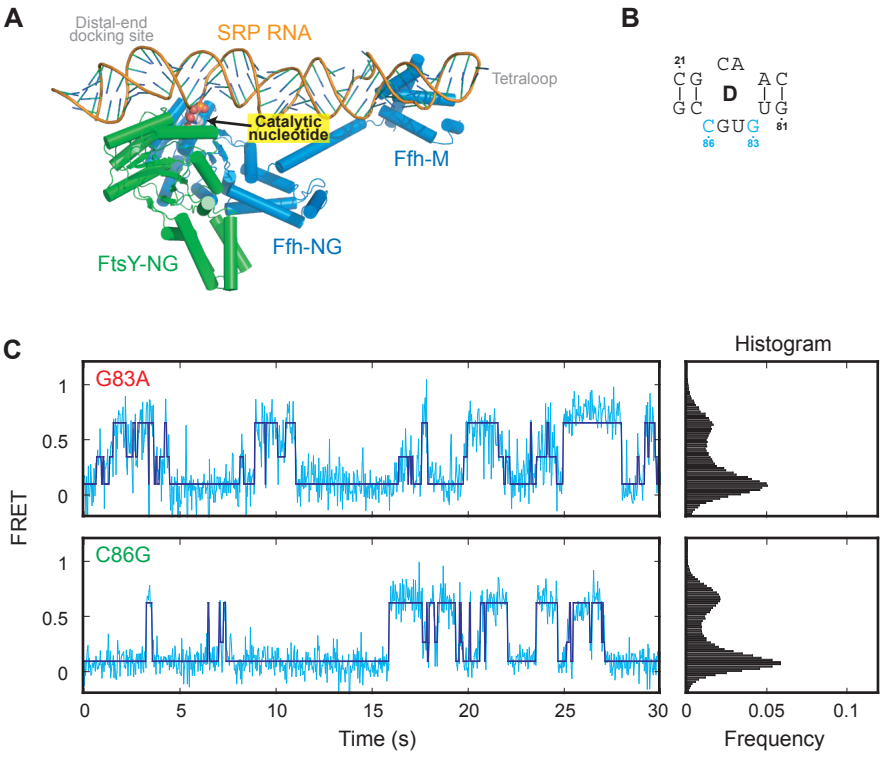

Figure 5.6 Catalytic bases do not contribute to the docking. (A) Crystal structure of the SRP-FtsY complex at the distal state. Shown in yellow is the protruding base that inserts into the Ffh-NG/FtsY-NG interface. (B) Secondary structure of the SRP RNA loop D. (C) Single-molecule traces (left panel) and histograms (right panel) of G83A and C86G mutants.

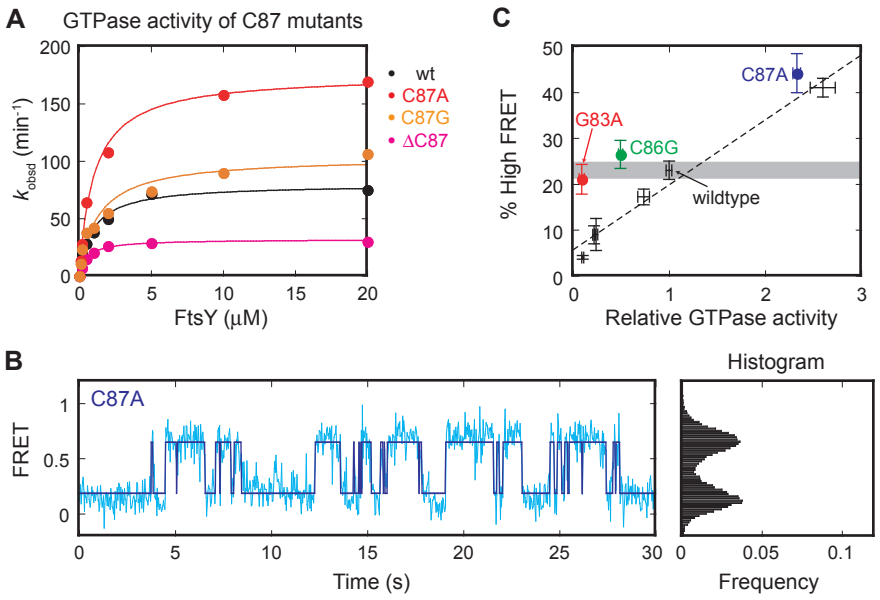

Figure 5.7 Auxiliary docking interaction mediated by C87. (A) GTPase activity of C87 mutants. (B) Single-molecule trace (left panel) and histogram (right panel) of C87A mutant. (C) Correlation between the percentage of high FRET state and the GTPase activity. Standard curve (dashed line) is the linear fit of the six data points in Figure 6D (black crosses). G83A, C86G, and C87A data points are shown in colored cycle.

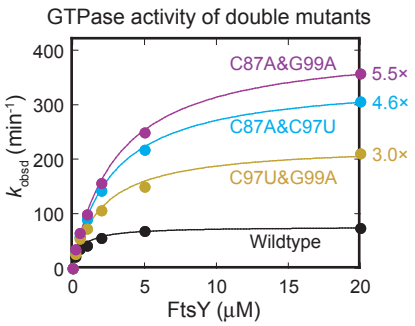

Figure 5.8 C87 acts independently of the distal-end docking site. GTPase activity of the SRP RNA mutants with combined active mutation. C97U and G99A are active mutations at the distal-end docking site. C87A is the active mutation at the auxiliary docking site.

References

Akopian, D., Dalal, K., Shen, K., Duong, F., and Shan, S.O. 2013. SecYEG activates GTPases to drive the completion of cotranslational protein targeting. *J Cell Biol* **200**(4): 397-405.

Alamo, M., Hogan, D.J., Pechmann, S., Albanese, V., Brown, P.O., and Frydman, J. 2011. Defining the specificity of cotranslationally acting chaperones by systematic analysis of mRNAs associated with ribosome-nascent chain complexes. *PLoS Biology* **9**: e1001100.

Aldridge, C., Cain, P., and Robinson, C. 2009. Protein transport in organelles: Protein transport into and across the thylakoid membrane. *FEBS J* **276**: 1177-1186.

Althoff, S., Selinger, D., and Wise, J.A. 1994. Molecular Evolution of SRP Cycle Components–Functional Implications. *Nucleic Acids Research* **22**(11): 1933-1947.

Angelini, S., Boy, D., Schiltz, E., and Koch, H.-G. 2006. Membrane binding of the bacterial signal recognition particle receptor involves two distinct binding modes. *J Cell Biol* **174**: 715-724.

Angelini, S., Deitermann, S., and Koch, H.-G. 2005. FtsY, the bacterial signal recognition particle receptor, interacts functionally and physically with the SecYEG translocon. *EMBO Rep* **6**(5): 476-481.

Ataide, S.F., Schmitz, N., Shen, K., Ke, A., Shan, S.O., Doudna, J.A., and Ban, N. 2011. The crystal structure of the signal recognition particle in complex with its receptor. *Science* **331**(6019): 881-886.

Bahari, L., Parlitz, R., Eitan, A., Stjepanovic, G., Bochkareva, E.S., Sining, I., Bibi, E. 2007. Membrane targeting of ribosomes and their release require distinct and separable functions of FtsY. *J Biol Chem* **282**(44): 32168-32175.

Bals, T., Dünschede, B., Funke, S., Schünemann, D. 2010. Interplay between the cpSRP pathway components, the substrate LHCP and the translocase Alb3: an in vivo and in vitro study. *FEBS Letters* **584**: 4138-4144.

Bange, G., Kummerer, N., Grudnik, P., Lindner, R., Petzold, G., Kressler, D., Hurt, E., Wild, K., and Sinning, I. 2011. Structural basis for the molecular evolution of SRP-GTPase activation by protein. *Nature Struct Molec Biol* **18**: 1376-1380.

Batey, R.T., Rambo, R.P., Lucast, L., Rha, B., and Doudna, J.A. 2000. Crystal structure of the ribonucleoprotein core of the signal recognition particle. *Science* **287**(5456): 1232-1239.

Batey, R.T., Sagar, M.B., and Doudna, J.A. 2001. Structural and energetic analysis of RNA recognition by a universally conserved protein from the signal recognition particle. *Journal of Molecular Biology* **307**(1): 229-246.

Beck, K., Wu, L.-F., Brunner, J., Muller, M. 2000. Discrimination between SRP- and SecA/SecB-dependent substrates involves selective recognition of nascent chains by SRP and trigger factor. *EMBO J* **19**: 134-143.

Becker, T., Bhushan, S., Jarasch, A., Armache, J.P., Funes, S., Jossinet, F., Gumbart, J., Mielke, T., Berninghausen, O., Schulten, K. et al. 2009. Structure of monomeric yeast and mammalian Sec61 complexes interacting with the translating ribosome. *Science* **326**(5958): 1369-1373.

Beckmann, R., Bubeck, D., Grassucci, R., Penczek, P., Verschoor, A., Blobel, G., and Frank, J. 1997. Alignment of conduits for the nascent polypeptide chain in the ribosome-Sec61 complex. *Science* **278**(5346): 2123-2126.

Beckmann, R., Spahn, C.M., Eswar, N., Helmers, J., Penczek, P.A., Sali, A., Frank, J., and Blobel, G. 2001a. Architecture of the protein-conducting channel associated with the translating 80S ribosome. *Cell* **107**(3): 361-372.

Berndt, U., Oellerer, S., Zhang, Y., Johnson, A., and Rospert, S. 2009. A signal-anchor sequence stimulates signal recognition particle binding to ribosomes from inside the exit tunnel. *Proc Natl Acad Sci* **106**: 1398-1403.

Bernstein, H.D., Poritz, M. A., Strub, K., Hoben, P. J., Brenner, S., and Walter, P. 1989. Model for signal sequence recognition from amino-acid sequence of 54K subunit of signal recognition particle. *Nature* **340**: 482-486.

Bernstein, H.D., Zopf, D., Freymann, D. M., and Walter, P. 1993. Functional substitution of the signal recognition particle 54-kDa subunit by its *Escherichia coli* homolog. *Proc Natl Acad Sci U S A* **90**: 5229-5234.

Bornemann, T., Jockel, J., Rodnina, M.V., and Wintermeyer, W. 2008. Signal sequence-independent membrane targeting of ribosomes containing short nascent peptides within the exit tunnel. *Nat Struct Mol Biol* **15**: 494-499.

Bourne, H.R., Sanders, D. A., McCormick, F. 1990. The GTPase superfamily: a conserved switch for diverse cell functions. *Nature* **348**: 125-128.

Bradshaw, N., and Walter, P. 2007. The Signal Recognition Particle (SRP) RNA links conformational changes in the SRP to protein targeting. *Mol Biol Cell* **18**(7): 2728-2734.

Bradshaw, N., Neher, S.B., Booth, D.S., and Walter, P. 2009. Signal Sequences Activate the Catalytic Switch of SRP RNA. *Science* **323**(5910): 127-130.

Braig, D., Mircheva, M., Sachelaru, I., van der Sluis, E.O., Sturn, L., Beckmann, R., and Koch, H.G. 2011. Signal sequence-independent SRP-SR complex formation at the membrane suggests an alternative targeting pathway within the SRP cycle. *Mol Biol Cell* **22**: 2309-2323.

Buskiewicz, I., Deuerling, E., Gu, S.Q., Jockel, J., Rodnina, M.V., Bukau, B., Wintermeyer, W. 2004. Trigger factor binds to ribosome-signal-recognition particle (SRP) complexes and is excluded by binding of the SRP receptor. *Proc Natl Acad Sci U S A* **101**: 7902-7906.

Buskiewicz, I., Jockel, J., Rodnina, M.V., and Wintermeyer, W. 2009. Conformation of the signal recognition particle in ribosomal targeting complexes. *RNA* **15**: 44-54.

Buskiewicz, I., Kubarenko, A., Peske, F., Rodnina, M.V., and Wintermeyer, W. 2005a. Domain rearrangement of SRP protein Ffh upon binding 4.5S RNA and the SRP receptor FtsY. *RNA* **11**: 947-957.

Buskiewicz, I., Peske, F., Wieden, H.J., Gryczynski, I., Rodnina, M.V., and Wintermeyer, W. 2005b. Conformations of the signal recognition particle protein Ffh from Escherichia coli as determined by FRET. *J Mol Biol* **351**(2): 417-430.

Cannon, K.S., Or, E., Clemons, W. M., Jr., Shibata, Y., and Rapoport, T.A. 2005. Disulfide bridge formation between SecY and a translocating polypeptide localizes the translocation pore to the center of SecY. *J Cell Biol* **169**: 219-225.

Chandrasekar, S., Chartron, S., Ampornpan, P., and Shan, S. 2008. Crystal structure of the chloroplast signal recognition particle (SRP) receptor: domain arrangement modulates SRP-receptor interaction. *J Mol Biol* **375**: 425-436.

Chappie, J.S., Acharya, S., Leonard, M., Schmid, S.L., and Dyda, F. 2010. G domain dimerization controls dynamin's assembly-stimulated GTPase activity. *Nature* **465**: 435-440.

Chen, M., Xie, K., Yuan, J., Yi, L., Facey, S.J., Pradel, N., Wu, L.F., Kuhn, A., and Dalbey, R.E. 2005. Involvement of SecDF and YidC in the membrane insertion of M13 procoat mutants. *Biochemistry* **44**: 10741-10749.

Cheng, Z., Jiang, Y., Mandon, E.C., Gilmore, R. 2005. Identification of cytoplasmic residues of Sec61p involved in ribosome binding and cotranslational translocation. *J Cell Biol* **168**: 67-77.

Ciufo, L.F., and Brown, J.D. 2000. Nuclear export of yeast signal recognition particle lacking Srp54p via the Xpo1p/Crm1p, NES-dependent pathway. *Curr Biol* **10**: 1256-1264.

Cline, K., Henry, R., Li, C., and Yuan, J. 2002. Multiple pathways for protein transport into or across the thylakoid membrane. *EMBO J* **12**: 4105-4114.

Connolly, T., Rapiejko, P.J., and Gilmore, R. 1991. Requirement of GTP hydrolysis for dissociation of the signal recognition particle from its receptor. *Science* **252**(5010): 1171-1173.

Cross, B.C.S., Sinning, I., Luirink, J., and High, S. 2009. Delivering proteins for export from the cytosol. *Nature Rev Mol Cell Biol* **10**: 255-264.

Dalal, K. and Duong, F. 2010. Reconstitution of the SecY translocon in nanodiscs. *Methods Mol Biol* **619**: 145-156.

Dalbey, R.E., Wang, P., and Kuhn, A. 2011. Assembly of bacterial inner membrane proteins. *Annu Rev Biochem* **80**: 161-187.

de Gier, J.W., and Luirink, J. 2003. The ribosome and YidC. New insights into the biogenesis of Escherichia coli inner membrane proteins. *EMBO Rep* **4**: 939-943.

de Leeuw, E., te Kaat, K., Moser, C., Memestrina, G., Demel, R., de Kruijff, B., Oudegam B., Luirink, J., and Sinning, I. 2000. Anionic phospholipids are involved in membrane association of FtsY and stimulate its GTPase activity. *EMBO J* **19**: 531-541.

de Plessis, D.J., Nouwen, N., Diriessen, A.J. 2011. The Sec translocase. *Biochim Biophys Acta* **1808**: 851-865.

de Vruje, T., de Swart, R.L., Dowhan, W., Tommassen, J., de Kruijff, B. 1988. Phosphotidylglycerol is involved in protein translocation across Escherichia coli inner membranes. *Nature* **334**: 173-175.

Delille, J., Peterson, E. C., Johnson, T., Morre, M., Kight, A., and Henry, R. 2000. A novel precursor recognition element facilitates posttranslational binding to the signal recognition particle in chloroplasts. *Proc Natl Acad Sci U S A* **97**: 1926-1931.

Deshaies, R.J., Koch, B.D., Werner-Washburne, M., Craig, E.A., and Schekman, R. 1988. A subfamily of stress proteins facilitates translocation of secretory and mitochondrial precursor polypeptides. *Nature* **332**: 800-805.

Doyle, S.M., and Wickner, S. 2008. Hsp104 and ClpB: protein disaggregating machines. *Trends in Biochemical Sciences* **34**: 40-48.

Driessen, A.J., and Nouwen, N. 2008. Protein translocation across the bacterial cytoplasmic membrane. *Annu Rev Biochem* **77**: 643-667.

Dunschede, B., Bals, T., Funke, S., Schunemann, D. 2011. Interaction studies between the chloroplast signal recognition particle subunit cpSRP43 and the full-length translocase Alb3 reveal a membrane-embedded binding region in Alb3. *J Biol Chem* **PMID: 21832051**.

Duong, F. 2003. Binding, activation and dissociation of the dimeric SecA ATPase at the dimeric SecYEG translocase. *EMBO Journal* **22**(17): 4375-4384.

Egea, P.F., Napetschnig, J., Walter, P., and Stroud, R.M. 2008. Structures of SRP54 and SRP19, the two proteins that organize the ribonucleic core of the signal recognition particle. *PloS ONE* **3**: e3528.

Egea, P.F., Shan, S.O., Napetschnig, J., Savage, D.F., Walter, P., and Stroud, R.M. 2004. Substrate twinning activates the signal recognition particle and its receptor. *Nature* **427**(6971): 215-221.

Eisner, G., Moser, M. Schafer, U., Beck, K., Muller, M. 2006. Alternative recruitment of signal recognition particle and trigger factor to the signal sequence of a growing nascent polypeptide. *J Biol Chem* **281**: 7172-7179.

Eitan, A., and Bibi, E. 2004. The core Escherichia coli signal recognition particle receptor contains only the N and G domains of FtsY. *J Bacteriol* **186**: 2492-2494.

Erez, E., Stjepanovic, G., Zelazny, A.M., Brugger, B., Sinning, I., and Bibi, E. 2010. Genetic evidence for functional interaction of the Escherichia coli signal recognition particle receptor with acidic lipids in vivo. *J Biol Chem* **285**: 40508-40514.

Estrozi, L.F., Boehringer, D., Shan, S., Ban, N., and Schaffitzel, C. 2011. Cryo-EM structure of the E. coli translating ribosome in complex with SRP and its receptor. *Nat Struct Mol Biol* **18**: 88-90.

Facey, S.J., Neugebauer, S.A., Krauss, S., and Kuhn, A. 2007. The mechanosensitive channel protein MscL is targeted by the SRP to the novel YidC membrane insertion pathway of Escherichia coli. *J Mol Biol* **365**: 995-1004.

Falk, S., and Sinning, I. 2010a. cpSRP43 is a novel chaperone specific for light-harvesting chlorophyll a,b-binding proteins. *J Biol Chem* **285**: 21655-21661.

Falk, S., Ravaud, S., Koch, J., and Sinning, I. 2010b. The C-terminus of the Alb3 membrane insertase recruits cpSRP43 to the thylakoid membrane. *J Biol Chem* **285**: 5954-5962.

Fedyukina, D.V., Cavagnero, S. 2011. Protein folding at the exit tunnel. *Ann Rev Biophys* **40**: 337-359.

Ferre-D'Amare, A.R. and Doudna, J.A. 1996. Use of cis- and trans-ribozymes to remove 5' and 3' heterogeneities from milligrams of in vitro transcribed RNA. *Nucleic Acids Res* **24**(5): 977-978.

Fersht, A.R., and Kaethner, M.M. 1976. Enzyme hyperspecificity. Rejection of threonine by the valyl-tRNA synthetase by misacylation and hydrolytic editing. *Biochemistry* **15**: 3342-3346.

Flanagan, J.J., Chen, J.C., Miao, Y., Shao, Y., Lin, J., Bock, P.E., and Johnson, A.E. 2003. Signal recognition particle binds to ribosome-bound signal sequences with fluorescence-detected subnanomolar affinity that does not diminish as the nascent chain lengthens. *J Biol Chem* **278**(20): 18628-18637.

Focia, P.J., Gawronski-Salerno, J., Coon, J.S.t., and Freymann, D.M. 2006. Structure of a GDP:AlF4 complex of the SRP GTPases Ffh and FtsY, and identification of a peripheral nucleotide interaction site. *J Mol Biol* **360**(3): 631-643.

Focia, P.J., Shepotinovskaya, I.V., Seidler, J.A., and Freymann, D.M. 2004. Heterodimeric GTPase core of the SRP targeting complex. *Science* **303**(5656): 373-377.

Franklin, K.E., and Hoffman, N. E. 1993. Characterization of a chloroplast homologue of the 54-kDa subunit of the signal recognition particle. *J Biol Chem* **268**: 22175-22180.

Fraunfeld, J., Gumbart, J., Sluis, E.O., Funes, S., Gartmann, M., Beatrix, B., Mielke, T., Berninghausen, O., Becker, T., Schulten, K., and Beckmann, R. 2011. Cryo-EM structure of the ribosome-SecYE complex in the membrane environment. *Nature Struct Molec Biol* **18**: 614-621.

Freymann, D.M., Keenan, R.J., Stroud, R.M., and Walter, P. 1997. Structure of the conserved GTPase domain of the signal recognition particle. *Nature* **385**(6614): 361-364.

Freymann, D.M., Keenan, R. J., Stroud, R.M., and Walter, P. 1999. Functional changes in the structure of the SRP GTPase on binding GDP and Mg2+GDP. *Nat Struct Biol* **6**: 793-801.

Frobel, J., Rose, P., and Muller, M. 2012. Twin-arginine-dependent translocation of folded proteins. *Philos Trans R Soc Lond B Biol Sci* **367**: 1029-1046.

Funke, S., Knechten, T., Ollesch, J., and Schunemann, D. 2005. A unique sequence motif in the 54-kDa subunit of the chloroplast signal recognition particle mediates binding to the 43-kDa subunit. *J Biol Chem* **280**: 8912-8917.

Gasper, R., Meyer, S., Gotthardt, K., Sirajuddin, M., and Wittinghofer, A. 2009. It takes two to tango: regulation of G proteins by dimerization. *Nat Rev Mol Cell Biol* **10**(6): 423-429.

Gawronski-Salerno, J., Coon Y. J. S., Focia, P. J., and Freymann, D. M. 2006. X-ray structure of the T. Aquaticus Ftsy:GDP complex suggests functional roles for the C-terminal helix of the SRP GTPases. *Proteins* **66**: 984-995.

Gawronski-Salerno, J. and Freymann, D.M. 2007. Structure of the GMPPNP-stabilized NG domain complex of the SRP GTPases Ffh and FtsY. *J Struct Biol* **158**(1): 122-128.

Gierasch, L.M. 1989. Signal sequences. *Biochemistry* **28**: 923-930.

Gilman, A.G. 1987. G proteins: transducers of receptor-generated signals. *Annu Rev Biochem* **56**: 615-649.

Gilmore, R., Blobel, G., and Walter, P. 1982a. Protein translocation across the endoplasmic reticulum. I. Detection in the microsomal membrane of a receptor for the signal recognition particle. *J Cell Biol* **95**(2 Pt 1): 463-469.

Gilmore, R., Walter, P., and Blobel, G. 1982b. Protein translocation across the endoplasmic reticulum. II. Isolation and characterization of the signal recognition particle receptor. *J Cell Biol* **95**(2 Pt 1): 470-477.

Gold, V.A.M., Robson, A., Bao, H., Romantsov, T., Duong, F., Collinson, I. 2010. The action of cardiolipin on the bacterial translocon. *Proc Natl Acad Sci* **in press**.

Goldshmidt, H., Sheiner, L., Butikofer, P., Roditi, I., Uliel, S., Gunzel, M., Engstler, M., and Michaeli, S. 2008. Role of protein translocation pathways across the endoplasmic reticulum in Trypanosoma brucei. *J Biol Chem* **283**: 32085-32098.

Grosshans, H., Deinert, K., Hurt, E., and Simos, G. 2001. Biogenesis of the signal recognition particle (SRP) involves import of SRP proteins into the nucleolus, assembly with the SRP-RNA, and Xpo1p-mediated export. *J Cell Biol* **153**: 745-762.

Gu, S.Q., Peske, F., Wieden, H.J., Rodnina, M.V., and Wintermeyer, W. 2003. The signal recognition particle binds to protein L23 at the peptide exit of the Escherichia coli ribosome. *RNA* **9**(5): 566-573.

Ha, T., Enderle, T., Ogletree, D.F., Chemla, D.S., Selvin, P.R., and Weiss, S. 1996. Probing the interaction between two single molecules: Fluorescence resonance energy transfer between a single donor and a single acceptor. *Proceedings of the National Academy of Sciences of the United States of America* **93**(13): 6264-6268.

Hainzl, T., Huang, S., and Sauer-Eriksson, A.E. 2002. Structure of the SRP19-RNA complex and implication for signal recognition particle assembly. *Nature* **417**: 767-771.

Hainzl, T., Huang, S., Merilainen, G., Brannstrom, K., and Sauer-Eriksson, A.E. 2011. Structural basis of signal sequence recognition by the signal recognition particle. *Nature Struct Molec Biol* **18**: 389-391.

Halic, M., Becker, T., Pool, M.R., Spahn, C.M., Grassucci, R.A., Frank, J., and Beckmann, R. 2004. Structure of the signal recognition particle interacting with the elongation-arrested ribosome. *Nature* **427**(6977): 808-814.

Halic, M., Blau, M., Becker, T., Mielke, T., Pool, M.R., Wild, K., Sinning, I., and Beckmann, R. 2006. Following the signal sequence from ribosomal tunnel exit to signal recognition particle. *Nature* **444**(7118): 507-511.

Halic, M., Gartmann, M., Schlenker, O., Mielke, T., Pool, M.R., Sinning, I., and Beckmann, R. 2006. Signal recognition particle receptor exposes the ribosomal translocon binding site. *Science* **312**: 745-747.

Hegde, R.S., and Keenan, R.J. 2011. Tail-anchored membrane protein insertion into the endoplasmic reticulum. *Nat Rev Mol Cell Biol* **12**: 787-798.

Heinrich, S.U., Mothes, W., Brunner, H., and Rapoport, T.A. 2000. The Sec61p complex mediates the integration of a membrane protein by allowing lipid partitioning of the transmembrane domain. *Cell* **102**: 233-244.

Helmers, J., Schmidt, D., Glavy, J.S., Blobel, G., and Schwartz, T. 2003. The b-subunit of the protein-conducting channel of the endoplasmic reticulum functions as the guanine nucleotide exchange factor for the b-subunit of the signal recognition particle receptor. *J Biol Chem* **278**: 23686-23690.

Hendrick, J.P., Wickner, W. 1991. SecA protein needs both acidic phospholipids and SecY/E protein for functional high affinity binding to the Escherichia coli plasma membrane. *J Biol Chem* **266**: 24596-24600.

Hermkes, R., Funke, S., Richter, C., Kuhlmann, J., and Schunemann, D. 2006. The a-helix of the second chromodomain of the 43 kDa subunit of the chloroplast signal recognition particle facilitates binding to the 54 kDa subunit. *FEBS Lett* **580**: 2107-3111.

Hoskins, A.A., Gelles, J., and Moore, M.J. 2011. New insights into the spliceosome by single molecule fluorescence microscopy. *Curr Opin Chem Biol* **15**(6): 864-870.

Huber, D., Boyd, D., Xia, Y., Olma, M.H., Gerstein, M., and Beckwith, J. 2005. Use of thioredoxin as a reporter to identify a subset of Escherichia coli signal sequences that promote signal recognition particle-dependent translocation. *J Bacteriol* **187**: 2983-2991.

Huber, D., Rajagopalan, N., Preissler, S., Rocco, M.A., Merz, F., Kramer, G., Bukau, B. 2011. SecA interacts with ribosomes in order to facilitate posttranslational translocation in bacteria. *Mol Cell* **41**: 343-353.

Iakhiaeva, E., Bhuiyan, S.H., Yin, J., and Zwieb, C. 2006. Protein SRP68 of human signal recognition particle: identification of the RNA and SRP72 binding domains. *Protein Sci* **15**: 1290-1302.

Iakhiaeva, E., Hinck, C.S., Hinck, A.P., and Zwieb, C. 2009. Characterization of the SRP68/72 interface of human signal recognition particle by systematic site-directed mutagenesis. *Protein Sci* **18**: 2183-2195.

Iakhiaeva, E., Iakhiaev, A., and Zwieb, C. 2010. Identification of amino acid residues in protein SRP72 required for binding to a kinked 5e motif of the human signal recognition particle RNA. *BMC Mol Biol* **11**.

Iakhiaeva, E., Wower, J., Wower, I.K., and Zwieb, C. 2008. The 5e motif of eukaryotic signal recognition particle RNA contains a conserved adenosine for the binding of SRP72. *RNA* **14**: 1143-1153.

Iakhiaeva, E., Yin, J., and Zwieb, C. 2005. Identification of an RNA-binding domain in human SRP72. *J Mol Biol* **345**: 659-666.

Iwahara, J. and Clore, G.M. 2006. Detecting transient intermediates in macromolecular binding by paramagnetic NMR. *Nature* **440**(7088): 1227-1230.

Jacobson, M.R., and Pederson, T. 1998. Localization of signal recognition particle RNA in the nucleolus of mammalian cells. *Proc Natl Acad Sci U S A* **95**: 7981-7986.

Jagath, J.R., Matassova, N.B., De Leeuw, E., Warnecke, J.M., Lentzen, G., Rodnina, M.V., Luirink, J., and Wintermeyer, W. 2001. Important role of the tetraloop region of 4.5S RNA in SRP binding to its receptor FtsY. *RNA* **7**(2): 293-301.

Janda, C.Y., Li, J., Oubridge, C., Hernandez, H., Robinson, C.V., and Nagai, K. 2010. Recognition of a signal peptide by the signal recognition particle. *Nature* **465**(7297): 507-510.

Jaru-Ampornpan, P., Chandrasekar, S., and Shan, S. 2007. Efficient interaction between two GTPases allows the chloroplast SRP pathway to bypass the requirement for an SRP RNA. *Mol Biol Cell* **18**(7): 2636-2645.

Jaru-Ampornpan, P., Nguyen, T.X., and Shan, S.O. 2009. A distinct mechanism to achieve efficient signal recognition particle (SRP)-SRP receptor interaction by the chloroplast SRP pathway. *Mol Biol Cell* **20**(17): 3965-3973.

Jaru-Ampornpan, P., Shen, K., Lam, V.Q., Ali, M., Doniach, S., Jia, T.Z., and Shan, S. 2010. ATP-independent reversal of a membrane protein aggregate by a chloroplast SRP subunit. *Nature Struct Molec Biol* **17**: 696-702.

Jiang, Y., Cheng, Z., Mandon, E.C., and Gilmore, R. 2003. An interaction between the SRP receptor and the translocon is critical during cotranslational protein translocation. *J Cell Biol* **180**: 1149-1161.

Johnson, A.E., and van Waes, M.A. 1999. The translocon: A dynamic gateway at the ER membrane. *Annu Rev Cell Dev Biol* **18**: 799-842.

Jonas-Straube, E., Hutin, C., Hoffman, N.E., and Schunemann, D. 2001. Functional analysis of the protein-interacting domains of chloroplast SRP43. *J Biol Chem* **276**: 24654-24660.

Jones, J.D., McKnight, C.J., and Gierasch, L.M. 1990. Biophysical studies of signal peptides: implications for signal sequence functions and the involvement of lipid in protein export. *J Bioenerg Biomembr* **22**: 213-232.

Jungnickel, B., and Rapoport, T. A. 1995. A posttargeting signal sequence recognition event in the endoplasmic reticulum membrane. *Cell* **82**: 261-270.

Kaiser, C.A., Preuss, D., Grisafi, P., and Botstein, D. 1987. Many random sequences functionally replace the secretion signal sequence of yeast invertase. *Science* **235**: 312-317.

Kathir, K.M., Rajalingam, D., Sivaraja, V., Kight, A., Goforth, R.L., Yu, C., Henry, R., and Kumar, T.K.S. 2008. Assembly of chloroplast signal recognition particle involves structural rearrangement in cpSRP43. *J Mol Biol* **381**: 49-60.

Keenan, R.J., Freymann, D.M., Stroud, R.M., and Walter, P. 2001. The signal recognition particle. *Annual Review of Biochemistry* **70**: 755-775.

Keenan, R.J., Freymann, D.M., Walter, P., and Stroud, R.M. 1998. Crystal structure of the signal sequence binding subunit of the signal recognition particle. *Cell* **94**(2): 181-191.

Klimyuk, V.I., Persello-Cartieaux, F., Havaux, M., Contard-David, P., Schuenemann, D., Meiherhoff, K., Gouet, P., Jones, J.D.G., Hoffman, N.E., and Nussaume, L. 1999. A chromodomain protein encoded by the Arabidopsis CAO gene is a plant-specific component of the chloroplast signal recognition particle pathway that is involved in LHCP targeting. *Plant Cell* **11**: 87-99.

Knoops, K., Schoehn, G., and Schaffitzel, C. 2011. Cryo-electron microscopy of ribosomal complexes in cotranslational folding, targeting, and translocation. *Wiley Interdiscip Rev RNA* **DOI: 10.1002/wrna.119**.

Kol, S., Nouwen, N., Driessen, A.J. 2008. Mechanisms of YidC-mediated insertion and assembly of multimeric membrane protein complexes. *J Biol Chem* **283**: 31269-31273.

Kramer, G., Boehringer, D., Ban, N., Bukau, B. 2009. The ribosome as a platform for co-translational processing, folding and targeting of newly synthesized proteins. *Nat Struct Mol Biol* **16**: 589-597.

Krieg, U.C., Walter, P., and Johnson, A.E. 1986. Photocrosslinking of the signal sequence of nascent preprolactin to the 54-kilodalton polypeptide of the signal recognition particle. *Proc Natl Acad Sci U S A* **83**: 8604-8608.

Kuhn, P., Weiche, B., Sturm, L., Sommer, E., Drepper, F., Warscheid, B., Sourjik, V., and Koch, H.G. 2011. The bacterial SRP receptor, SecA and the ribosome use overlapping binding sites on the SecY translocon. *Traffic* **12**: 563-578.

Kundel, T.A., and Bebenek, K. 2000. DNA replication fidelity. *Ann Rev Biochem* **69**: 497-529.

Kurzchalia, T.V., Wiedmann, M., Girshovich, A.S., Bochkareva, E.S., Bielka, H., and Rapoport, T.A. 1986. The signal sequence of nascent preprolactin interacts with the 54K polypeptide of the signal recognition particle. *Nature* **320**: 634-636.

Kusters, R., Dowhan, W., de Kruijff, B. 1991. Negatively charged phospholipids restore prePhoE translocation across phosphatidylglycerol-depleted Escherichia coli inner membranes. *J Biol Chem* **266**: 8659-8662.

Lakkaraju, A.K.K., Mary, C., Scherrer, A., Johnson, A.E., and Strub, K. 2008. SRP keeps polypeptides translocation-competent by slowing translation to match limiting ER-targeting sites. *Cell* **133**: 440-451.

Lam, V.Q., Akopian, D., Rome, M., Shen, Y., Henningsen, D., and Shan, S. 2010. Lipid activation of the SRP receptor provides spatial coordination of protein targeting. *J Cell Biol* **190**: 623-635.

Lee, H.C., Bernstein, H.D. 2002. Trigger factor retards protein export in Escherichia coli. *J Biol Chem* **277**: 43527-43535.

Leipe, D.D., Wolf, Y.I., Koonin, E.V., and Aravid, L. 2002. Classificaiton and evolution of P-loop GTPases and related ATPases. *J Mol Biol* **317**: 41-72.

Leung, E., and Brown, J.D. 2010. Biogenesis of the signal recognition particle. *Biochem Soc Trans* **38**: 1093-1098.

Lewis, N.E., Marty, N.J., Kathir, K.M., Rajalingam, D., Kight, A.D., Daily, A., Kumar, T.K.S., Henry, R.L., Goforth, R.L. 2010. A dynamic cpSRP43-Albino3 interaction mediates translocase regulation of cpSRP targeting components. *J Biol Chem* **285**: 34220-34230.

Li, X., Henry, R., Yuan, J., Cline, K., and Hoffman, N. 1995. A chloroplast homologue of the signal recognition particle subunit SRP54 is involved in the posttranslational integration of a protein into thylakoid membranes. *Proc Natl Acad Sci U S A* **92**: 3789-3793.

Liao, S., Lin, J., Do, H., and Johnson, A. E. 1997. Both luminal and cytosolic gating of the aqueous ER translocon pore are regulated from inside the ribosome during membrane protein integration. *Cell* **90**: 31-41.

Lill, R., Dowhan, W., Wickner, W. 1990. The ATPase activity of SecA is regulated by acidic phospholipids, SecY, and the leader and mature domains of precursor proteins. *Cell* **60**: 271-280.

Lohman, T.M. and Bjornson, K.P. 1996. Mechanisms of helicase-catalyzed DNA unwinding. *Annu Rev Biochem* **65**: 169-214.

Low, H.H. and Lowe, J. 2006. A bacterial dynamin-like protein. *Nature* **444**(7120): 766-769.

Luirink, J., Hagen-Jongman, C. M. ten, Weijden, C., Oudega, B., High, S. Dobberstein, B., and Kusters, R. 1994. An alternative protein targeting pathway in *Escherichia coli*: studies on the role of FtsY. *EMBO J* **13**: 2289-2296.

Luirink, J., Samuelsson, T., and de Gier, J.W. 2001. YidC/Oxa1p/Alb3: evolutionarily conserved mediators of membrane protein assembly. *FEBS Lett* **501**: 1-5.

Mainprize, I.L., Beniac, D.R., Falkovskala, E., Cleverley, R.M., Gierasch, L.M., Ottensmeyer, F.P., and Andrews, D.W. 2006. The structure of Escherichia coli signal recognition particle revealed by scanning transmission electron microscopy. *Mol Biol Cell* **17**: 5063-5074.

Maity, T.S., and Weeks, K.M. 2007. A threefold RNA-protein interface in the signal recognition particle gates native complex assembly. *J Mol Biol* **369**: 512-524.

Maity, T.S., Fried, H.M., and Weeks, K.M. 2008. Anti-cooperative assembly of the SRP19 and SRP68/72 components of the signal recognition particle. *Biochem J* **415**: 429-437.

Maity, T.S., Leonard, C.W., Rose, M.A., Fried, H.M., and Weeks, K.M. 2006. Compartmentalization directs assembly of the signal recognition particle. *Biochemistry* **45**: 14955-14964.

Mariappan, M., Li, X., Stefanovic, S., Sharma, A., Mateja, A., Keenan, R., and Hegde, R.S. 2010. A ribosome-associating factor chaperones tail-anchored membrane proteins. *Nature* **466**: 1120-1124.

Marty, N., Rajalingam, D., Kight, A.D., Lewis, N., Fologea, D., Kumar, T.K.S., Henry, R., Goforth, R.L. 2009. The membrane binding motif of chloroplast signal recognition particle receptor (cpFtsY) regulates GTPase activity. *J Biol Chem* **284**: 14891-14903.

Mary, C., Scherrer, A., Huck, L., Lakkaraju, A.K., Thomas, Y., Johnson, A.E., and Strub, K. 2010. Residues in SRP9/14 essential for elongation arrest activity of the signal recognition particle define a positively charged functional domain on one side of the protein. *RNA* **16**: 969-979.

McKinney, S.A., Joo, C., and Ha, T. 2006. Analysis of single-molecule FRET trajectories using hidden Markov modeling. *Biophys J* **91**(5): 1941-1951.

Menetret, J.F., Neuhof, A., Morgan, D.G., Plath, K., Radermacher, M., Rapoport, T.A., and Akey, C.W. 2000. The structure of ribosome-channel complexes engaged in protein translocation. *Mol Cell* **6**(5): 1219-1232.

Menetret, J.F., Schaletzky, J., Clemons, W.M. Jr, Osborne, A.R., Skanland, S.S., Denison, C., Gygi, S.P., Kirkpatrick, D.S., Park, E., Ludtke, S.J., Rapoport, T.A., Akey, C.W. 2007. Ribosome binding of a single copy of the SecY complex: implications for protein translocation. *Mol Cell* **28**: 1083-1092.

Menichelli, E., Isel, C., Oubridge, C., and Nagai, K. 2007. Protein-induced conformational changes of RNA during the assembly of human signal recognition particle. *J Mol Biol* **367**: 187-203.

Meyer, S., Bohme, S., Kruger, A., Steinhoff, H.J., Klare, J.P., and Wittinghofer, A. 2009. Kissing G domains of MnmE monitored by X-ray crystallography and pulse electron paramagnetic resonance spectroscopy. *PLoS Biol* **7**(10): e1000212.

Miller, J.D., Tajima, S., Lauffer, L., and Walter, P. 1995. The β subunit of the signal recognition particle receptor is a transmembrane GTPase that anchors the a subunit, a peripheral membrane GTPase, to the endoplasmic reticulum. *J Cell Biol* **128**: 273-282.

Mircheva, M., Boy, D., Weiche, B., Hucke, F., Graumann, P., Koch, H.-G. 2009. Predominant membrane localization is an essential feature of the bacterial signal recognition particle receptor. *BMC Biology* **7**.

Mitra, K., Schaffitzel, C., Shaikh, T., Tanna, F., Jenni, S., Brooks, C.L., Ban, N., and Frank, J. 2005. Structure of the E. coli protein conducting channel bound to a translating ribosome. *Nature* **438**: 318-324.

Moazed, D. and Noller, H.F. 1989. Interaction of tRNA with 23S rRNA in the ribosomal A, P, and E sites. *Cell* **57**(4): 585-597.

Montoya, G., Svensson, C., Luirink, J., and Sinning, I. 1997. Crystal structure of the NG domain from the signal-recognition particle receptor FtsY. *Nature* **385**(6614): 365-368.

Mothes, W., Jungnickel, B., Brunner, J., and Rapoport, T.A. 1998. Signal sequence recognition in cotranslational translocation by protein components of the endoplasmic reticulum membrane. *Journal of Cell Biology* **142**(2): 355-364.

Muller, L., de Escauriaza, M.D., Lajoie, P., Theis, M., Jung, M., Muller, A., Burgard, C., Greiner, M., Snapp, E.L., Dudek, J., and Zimmermann, R. 2010. Evolutionary gain of function for the ER membrane protein Sec62 from yeast to humans. *Mol Biol Cell* **21**: 691-703.

Murray, N.E. 2000. Type I restriction systems: sophisticated molecular machines (a legacy of Bertani and Weigle). *Microbiol Mol Biol Rev* **64**(2): 412-434.

Natale, P., Bruser, T., Driessen, A.J. 2008. Sec- and Tat-mediated protein secretion across the bacterial cytoplasmic membrane–distinct translocases and mechanisms. *Biochim Biophys Acta* **1778**: 1735-1756.

Neher, S.B., Bradshaw, N., Floor, S.N., Gross, J.D., and Walter, P. 2008. SRP RNA controls a conformational switch regulating the SRP-SRP receptor interaction. *Nature Structural & Molecular Biology* **15**(9): 916-923.

Nevo-Dinur, K., Nussbaum-Shochat, A., Ben-Yehuba, S., and Amster-Choder, O. 2011. Translation-independent localization of mRNA in E. coli. *Science* **331**: 1081-1084.

Nilsson, R., and van Wikj, K.L. 2002. Transient interaction of cpSRP54 with elongating nascent chains of the chloroplast-encoded D1 protein; 'cpSRP54 caught in the act'. *FEBS Lett* **524**: 127-133.

Ogg, S.C., and Walter, P. 1995. SRP samples nascent chains for the presence of signal sequences by interacting with ribosomes at a discrete step during translation elongation. *Cell* **81**: 1075-1084.

Oubridge, C., Kuglstatter, A., Jovine, L., and Nagai, K. 2002. Crystal structure of SRP19 in complex with the S domain of SRP RNA and its implication for the assembly of the signal recognition particle. *Molecular Cell* **9**: 1251-1261.

Ouyang, M., Li, X., Ma, J., Chi, W., Xiao, J., Zou, M., Chen, F., Lu, C., and Zhang, L. 2011. LTD is a protein required for sorting light-harvesting chlorophyll-binding proteins to the chloroplast SRP. *Nat Commun* **2**.

Padmanabhan, W., and Freymann, D. M. 2001. The conformation of bound GMPPNP suggests a mechanism for gating the active site of the SRP GTPase site. *Structure* **9**: 859-863.

Parlitz, R., Eitan, A., Stjepanovic, G., Bahari, L., Bange, G., Bibi, E., and Sinning, I. 2007. Escherichia coli signal recognition particle receptor FtsY contains an essential and autonomous membrane-binding amphipathic helix. *J Biol Chem* **282**(44): 32176-32184.

Payan, L.A., and Cline, K. 1991. A stromal protein factor maintains the solubility and insertion competence of an imported thylakoid membrane protein. *J Cell Biol* **112**: 603-613.

Peluso, P., Herschlag, D., Nock, S., Freymann, D.M., Johnson, A.E., and Walter, P. 2000. Role of 4.5S RNA in assembly of the bacterial signal recognition particle with its receptor. *Science* **288**(5471): 1640-1643.

Peluso, P., Shan, S.O., Nock, S., Herschlag, D., and Walter, P. 2001. Role of SRP RNA in the GTPase cycles of Ffh and FtsY. *Biochemistry* **40**(50): 15224-15233.

Peterson, J.H., Szabady, R.L., and Bernstein, H.D. 2006. An unusual signal peptide extension inhibits the binding of bacterial presecretory proteins to the signal recognition particle, trigger factor, and the SecYEG complex. *J Biol Chem* **281**: 9038-9048.

Peterson, J.H., Woolhead, C.A., and Bernstein, H.D. 2003. Basic amino acids in a distinct subset of signal peptides promote interaction with the signal recognition particle. *J Biol Chem* **278**: 46155-46162.

Plath, K., Mothes, W., Wikinson, B.M., Sterling, C.J., and Rapoport, T.A. 1998. Signal sequence recognition in post-translational protein transport across the yeast ER membrane. *Cell* **94**: 795-807.

Pool, M.R. 2005. Signal recognition particles in chloroplasts, bacteria, yeast and mammals. *Mole Membr Biol* **22**: 3–15.

Pool, M.R. 2009. A trans-membrane segment inside the ribosome exit tunnel triggers RAMP4 recruitment to the Sec61p translocase. *J Cell Biol* **185**: 889-902.

Pool, M.R., Stumm, J., Fulga, T.A., Sinning, I., and Dobberstein, B. 2002. Distinct modes of signal recognition particle interaction with the ribosome. *Science* **297**(5585): 1345-1348.

Pop, O.I., Soprova, Z., Koningstein, G., Scheffers, D.J., van Ulsen, P., Wickstrom, D., de Gier, J.W., Luirink, J. 2009. YidC is required for the assembly of the MscL homopentameric pore. *FEBS Lett* **276**: 4891-4899.

Poritz, M.A., Strub, K., and Walter, P. 1988. Human SRP RNA and E. coli. 4.5S RNA contain a highly homologous structural domain. *Cell* **55**: 4-6.

Powers, T., and Walter, P. 1997. Co-translational protein targeting catalyzed by the Escherichia coli signal recognition particle and its receptor. *EMBO J* **16**: 4880-4886.

Prilusky, J., and Bibi, E. 2009. Studying membrane proteins through the eyes of the genetic code revealed a strong uracil bias in their coding mRNAs. *Proc Natl Acad Sci U S A* **106**: 6662-6666.

Rapaport, T.A., Jungnickel, B., and Kutay, U. 1996. Protein transport across the eukaryotic endoplasmic reticulum and bacterial inner membranes. *Annu Rev Biochem* **65**: 271-303.

Ravaud, S., Stjepanovic, G., Wild, K., and Sinning, I. 2008. The crystal structure of the periplasmic domain of the Escherichia coli membrane protein insertase YidC. *J Biol Chem* **283**: 9350-9358.

Reed, J.E., Cline, K., Stephens, L.C., Bacot, K.O., Viitanen, P.V. 1990. Early events in the importn/assembly pathway of an integral thylakoid protein. *Eur J Biochem* **194**: 33-42.

Reyes, C.L., Rutenber, E., Walter, P., and Stroud, R.M. 2007. X-ray structures of the signal recognition particle receptor reveal targeting cycle intermediates. *PloS ONE* **2**: e607.

Richter, C.V., Bals, T., and Schunemann, D. 2010. Component interactions, regulation and mechanisms of chloroplast signal recognition particle-dependent protein transport. *Eur J Cell Biol* **89**: 965-973.

Richter, C.V., Trager, C., and Schunemann, D. 2008. Evolutionary substitution of two amino acids in chloroplast SRP54 of higher plants cause its inability to bind SRP RNA. *FEBS Lett* **582**(21-22): 3223-3229.

Ridder, A.N.J.A., Kuhn, A., Killian, J.A., de Kruijff, B. 2001. Anionic lipids stimulate Sec-independent insertion of a membrane protein lacking charged amino acid side chains. *EMBO Rep* **2**: 403-408.

Rinke-Appel, J., Osswald, M., Von Knoblauch, K., Mueller, F., Brimacombe, R., Sergiev, P., Avdeeva, O., Bogdanov, A., and Dontsova, O. 2002. Crosslinking of 4.5S RNA to the Escherichia coli ribosome in the presence or absence of the protein Ffh. *RNA-A Publication of the RNA Society* **8**(5): 612-625.

Rodnina, M.V., and Wintermeyer, W. 2001. Ribosome fidelity: tRNA discrimination, proofreading and induced fit. *TIBS* **26**: 124-130.

Römisch, K., Webb, J., Herz, J., Prehn, S., Frank, R. et al. 1989. Homology of the 54K protein of signal recognition particle, docking protein, and two E. coli proteins with putative GTP-binding domains. *Nature* **340**: 478-482.

Rosenblad, M.A., Gorodkin, J., Knudsen, B., Zwieb, C., and Samuelsson, T. 2003. SRPDB: Signal Recognition Particle Database. *Nuc Acids Res* **31**: 363-364.

Rosendal, K.R., Wild, K., Montoya, G., and Sinning, I. 2003. Crystal structure of the complete core of archaeal signal recognition particle and implications for interdomain communication. *Proc Natl Acad Sci U S A* **100**(25): 14701-14706.

Roy, R., Hohng, S., and Ha, T. 2008. A practical guide to single-molecule FRET. *Nat Methods* **5**(6): 507-516.

Rubio, A., Jiang, X., Pogliano, K. 2005. Localization of translocation complex components in Bacillus subtilis: enrichment of the signal recognition particle receptor at early sporulation septa. *J Bacteriol* **187**: 5000-5002.

Saraogi, I., Zhang, D., Chandrasekaran, S., and Shan, S. 2011. Site-specific fluorescent labeling of nascent proteins on the translating ribosome. *J Am Chem Soc* **133**: 14936-14939.

Sauer-Eriksson, A.E., and Hainzl, T. 2003. S-domain assembly of the signal recognition particle. *Curr Opin Struct Biol* **13**: 64-70.

Schaffitzel, C. and Ban, N. 2007. Generation of ribosome nascent chain complexes for structural and functional studies. *Journal of Structural Biology* **158**(3): 463-471.

Schaffitzel, C., Oswald, M., Berger, I., Ishikawa, T., Abrahams, J.P., Koerten, H.K., Koning, R.I., and Ban, N. 2006. Structure of the E-coli signal recognition particle bound to a translating ribosome. *Nature* **444**(7118): 503-506.

Schreiber, G. and Fersht, A.R. 1996. Rapid, electrostatically assisted association of proteins. *Nat Struct Biol* **3**(5): 427-431.

Schunemann, D., Amin, P., and Hoffman, N.E. 1999. Functional divergence of the plastid and cytosolic forms of the 54-kDa subunit of signal recognition particle. *Biochem Biophys Res Commun* **254**(1): 253-258.

Schunemann, D. 2004. Structure and function of the chloroplast signal recognition particle. *Curr Genetics* **44**: 295-304.

Schunemann, D., Gupta, S., Persello-Cartieaux, F., Klimyuk, V. I., Jones, J. D. G., Nussaume, L., and Hoffman, N. E. 1998. A novel signal recognition particle targets light-harvesting proteins to the thylakoid membranes. *Proc Natl Acad Sci U S A* **95**: 10312-10316.

Schwartz, T., and Blobel, G. 2003. Structural basis for the function of the b-subunit of the eukaryotic signal recognition particle receptor. *Cell* **112**: 793-803.

Selinger, D., Liao, X., and Wise, J.A. 1993. Functional interchangeability of the structurally similar tetranucleotide loops GAAA and UUCG in fission yeast signal recognition particle RNA. *Proc Natl Acad Sci U S A* **90**(12): 5409-5413.

Semlow, D.R., and Staley, J.P. 2012. Staying on message: ensuring fidelity in pre-mRNA splicing. *TIBS* **37**: 263-273.

Shan, S., and Walter, P. 2003. Induced Nucleotide Specificity in a GTPase. *Proc Natl Acad Sci USA* **100**: 4480-4485.

Shan, S., Chandrasekar, S., and Walter, P. 2007. Conformational changes in the GTPase modules of SRP and its receptor drive initiation of protein translocation. *J Cell Biol* **178**: 611-620.

Shan, S., Schmid, S.L., and Zhang, X. 2009. Signal recognition particle (SRP) and SRP receptor: a new paradigm for multi-state regulatory GTPases. *Biochemistry* **48**: 6696-6704.

Shan, S., Stroud, R., and Walter, P. 2004. Mechanism of association and reciprocal activation of two GTPases. *PLoS Biology* **2**(10): e320.

Shan, S.O. and Walter, P. 2003. Induced nucleotide specificity in a GTPase. *Proceedings of the National Academy of Sciences of the United States of America* **100**(8): 4480-4485.

Shao, S., and Hegde, R.S. 2011. Membrane protein insertion at the endoplasmic reticulum. *Ann Rev Cell Dev Biol* **27**: 25-56.

Shen, K., Arslan, S., Akopian, D., Ha, T., and Shan, S.O. 2012. Activated GTPase movement on an RNA scaffold drives co-translational protein targeting. *Nature* **492**(7428): 271-275.

Shen, K. and Shan, S.O. 2010. Transient tether between the SRP RNA and SRP receptor ensures efficient cargo delivery during cotranslational protein targeting. *Proc Natl Acad Sci U S A* **107**(17): 7698-7703.

Shen, K., Zhang, X., and Shan, S.O. 2011. Synergistic actions between the SRP RNA and translating ribosome allow efficient delivery of the correct cargos during cotranslational protein targeting. *RNA* **17**(5): 892-902.

Shepotinovskaya, I.V., and Freymann, D. M. 2001. Conformational change of the N-domain on formation of the complex between the GTPase domains of *Thermus aquaticus* Ffh and FtsY. *Biochemica et Biophysica Acta* **1597**: 107-114.

Siegel, V., and Walter, P. 1985. Elongation arrest is not a prerequisite for secretory protein translocation across the microsomal membrane. *J Cell Biol* **100**: 1913-1921.

Siegel, V., and Walter, P. 1988a. Each of the activities of Signal Recognition Particle (SRP) is contained within a distinct domain: Analysis of biochemical mutants of SRP. *Cell* **52**: 39-49.

Siegel, V. and Walter, P. 1988b. The affinity of signal recognition particle for presecretory proteins is dependent on nascent chain length. *EMBO J* **7**(6): 1769-1775.

Simon, S.M. and Blobel, G. 1991. A protein-conducting channel in the endoplasmic reticulum. *Cell* **65**(3): 371-380.

Siu, F.Y., Spanggord, R.J., and Doudna, J.A. 2007. SRP RNA provides the physiologically essential GTPase activation function in cotranslational protein targeting. *RNA* **13**(2): 240-250.

Sivaraja, V., Kumar, T.K.S., Leena, P.S.T., Chang, A., Vidya, C., Goforth, R.L., Rajalingam, D., Arvind, K., Ye., J.L., Chou, J., Henry, R., and Yu, C. 2005. Three dimensional solution structures of the chromodomains of cpSRP43. *J Biol Chem* **280**: 41465-41471.

Spanggord, R.J., Siu, F., Ke, A.L., and Doudna, J.A. 2005. RNA-mediated interaction between the peptide-binding and GTPase domains of the signal recognition particle. *Nature Struct Mol Biol* **12**(12): 1116-1122.

Stengel, K.F., Holdermann, I., Cain, P., Robinson, C., Wild, K., and Sinning, I. 2008. Structural basis for specific substrate recognition by the chloroplast signal recognition particle protein cpSRP43. *Science* **321**: 253-256.

Stengel, K.F., Holdermann, I., Wild, K., and Sinning, I. 2007. The structure of the chloroplast signal recognition particle (SRP) receptor reveals mechanistic details of SRP GTPase activation and a conserved membrane targeting site. *FEBS Lett* **581**: 5671-5676.

Stiegler, N., Dalbey, R.E., Kuhn, A. 2011. M13 procoat protein insertion into YidC and SecYEG proteoliposomes and liposomes. *J Mol Biol* **406**: 362-370.

Stjepanovic, G., Kapp, K., Bange, G., Graf, C., Parlitz, R., Wild, K., Mayer, M.P., and Sinning, I. 2011. Lipids trigger a conformational switch that regulates signal recognition particle (SRP0-mediated protein targeting. *J Biol Chem* **286**: 23489-23497.

Swain, J.F., and Gierasch, L.M. 2001. Signal peptides bind and aggregate RNA: an alternative explanation for GTPase inhibition in the signal recognition particle. *J Biol Chem* **276**: 12222-12227.

Tajima, S., Lauffer, L., Rath, V. L., and Walter, P. 1986. The signal recognition particle receptor is a complex that contains two distinct polypeptide chains. *J Cell Biol* **103**: 1167-1178.

Tang, C., Iwahara, J., and Clore, G.M. 2006. Visualization of transient encounter complexes in protein-protein association. *Nature* **444**(7117): 383-386.

Terzi, L., Pool, M.R., Dobberstein, B., and Strub, K. 2004. Signal Recognition Particle Alu Domain Occupies a Defined Site at the Ribosomal Subunit Interface upon Signal Sequence Recognition. *Biochemistry* **43**: 107-117.

Tu, C.-J., Schuenemann, D., and Hoffman, N. E. 1999. Chloroplast FtsY, Chloroplast Signal Recognition Particle, and GTP are required to reconstitute the soluble phase of light-harvesting chlorophyll protein transport into thylakoid membranes. *J Biol Chem* **274**: 27219-27224.

Tu, C.J., Peterson, E. C., Henry, R., and Hoffman, N. E. 2000. The L18 domain of light-harvesting chlorophyll proteins binds to chloroplast signal recognition particle 43. *J Biol Chem* **275**: 13187-13190.

Ullers, R.S., Houben, E.N., Raine, A., ten Hagen-Jongman, C.M., Ehrenberg, M., Brunner, J., Oudega, B., Harms, N., and Luirink, J. 2003. Interplay of signal recognition particle and trigger factor at L23 near the nascent chain exit site on the Escherichia coli ribosome. *J Cell Biol* **161**(4): 679-684.

Uptain, S.M., Kane, C.M., and Chamberlin, M.J. 1997. Basic mechanisms of transcript elongation and its regulation. *Ann Rev Biochem* **66**: 117-172.

Van den Berg, B., Clemons, W.M., Jr., Collinson, I., Modis, Y., Hartmann, E., Harrison, S.C., and Rapoport, T.A. 2004. X-ray structure of a protein-conducting channel. *Nature* **427**(6969): 36-44.

van der Laan, M., Bechtluft, P., Kol, S., Nouwen, N., and Driessen, A.J. 2004. F1F0 ATP Synthase subunit c is a substrate of the novel YidC pathway for membrane protein biogenesis. *J Cell Biol* **165**: 213-222.

van der Sluis, E.O., Nouwen, N., and Driessen, A.J. 2002. SecY-SecY and SecY-SecG contacts revealed by site-specific crosslinking. *FEBS Lett* **527**(1-3): 159-165.

Volkov, A.N., Worrall, J.A., Holtzmann, E., and Ubbink, M. 2006. Solution structure and dynamics of the complex between cytochrome c and cytochrome c peroxidase determined by paramagnetic NMR. *Proc Natl Acad Sci U S A* **103**(50): 18945-18950.

von Heijne, G. 1985. Signal sequences: The limits of variation. *J Mol Biol* **184**: 99-105.

von Hippel, P.H. and Berg, O.G. 1989. Facilitated target location in biological systems. *J Biol Chem* **264**(2): 675-678.

Walter, P., and Blobel, G. 1980. Purification of a membrane-associated protein complex required for protein translocation across the endoplasmic reticulum. *Proc Natl Acad Sci U S A* **77**: 7112-7116.

Walter, P. and Blobel, G. 1981. Translocation of proteins across the endoplasmic reticulum. II. Signal recognition protein (SRP) mediates the selective binding to microsomal membranes of in-vitro-assembled polysomes synthesizing secretory protein. *J Cell Biol* **91**(2 Pt 2): 551-556.

Walter, P., Gilmore, R., and Blobel, G. 1984. Protein translocation across the endoplasmic reticulum. *Cell* **38**(1): 5-8.

Walter, P., Ibrahimi, I., and Blobel, G. 1981. Translocation of proteins across the endoplasmic reticulum. I. Signal recognition protein (SRP) binds to in-vitro-assembled polysomes synthesizing secretory protein. *J Cell Biol* **91**(2 Pt 1): 545-550.

Walter, P. and Johnson, A.E. 1994. Signal sequence recognition and protein targeting to the endoplasmic-reticulum membrane. *Ann Rev Cell Biol* **10**: 87-119.

Wang, P., and Dalbey, R.E. 2011. Inserting membrane proteins: the YidC/Oxa1/Alb3 machinery in bacteria, mitochondria, and chloroplasts. *Biochim Biophys Acta* **1808**: 866-875.

Wang, Z., Jones, J., Rizo, J., and Gierasch, L.M. 1993. Membrane-bound conformation of a signal peptide: A transferred nuclear Overhauser effect analysis. *Biochemistry* **32**: 13991-13999.

Weiche, B., Burk, J., Angelini, S., Schiltz, E., Thumfart, J.O., Koch, H.-G. 2008. A cleavable N-terminal membrane anchor is involved in membrane binding of the Escherichia coli SRP receptor. *J Mol Biol* **377**: 761-773.

Wild, K., Sinning, I., and Cusack, S. 2001. Crystal structure of an early protein-RNA assembly complex of the signal recognition particle. *Science* **294**: 598-601.

Wittke, S., Dunnwald, M., Albertsen, M., and Johnsson, N. 2002. Recognition of a subset of signal sequences by Ssh1p, a Sec61p-related protein in the membrane of endoplasmic reticulum of yeast Saccharomyces cerevisiae. *Mol Biol Cell* **13**: 2223-2232.

Xie, K., and Dalbey, R.E. 2008. Inserting proteins into the bacterial cytoplasmic membrane using the Sec and YidC translocases. *Nat Rev Microbiol* **6**: 234-244.

Yi, L., Celebi, N., Chen, M., Dalbey, R.E. 2004. Sec/SRP requirements and energetics of membrane insertion of subunits a, b, and c of the *Escherichia coli* F1F0 ATP synthase. *J Biol Chem* **279**: 39260-39267.

Yin, J., Iakhiaeva, E., Menichelli, E., and Zwieb, C. 2007. Identification of the RNA binding regions of SRP68/72 and SRP72 by systematic mutagenesis of human SRP RNA. *RNA Biol* **4**: 154-159.

Yodh, J.G., Schlierf, M., and Ha, T. 2010. Insight into helicase mechanism and function revealed through single-molecule approaches. *Q Rev Biophys* **43**(2): 185-217.

Yuan, R. 1981. Structure and mechanism of multifunctional restriction endonucleases. *Annu Rev Biochem* **50**: 285-319.

Zhang, X., Kung, S., and Shan, S.O. 2008. Demonstration of a multistep mechanism for assembly of the SRP-SRP receptor complex: Implications for the catalytic role of SRP RNA. *J Mol Biol* **381**(3): 581-593.

Zhang, X., Lam, V.Q., Mou, Y., Kimura, T., Chung, J., Chandrasekar, S., Winkler, J.R., Mayo, S.L., and Shan, S.O. 2011. Direct visualization reveals dynamics of a transient intermediate during protein assembly. *Proc Natl Acad Sci U S A* **108**(16): 6450-6455.

Zhang, X., Rashid, R., Wang, K., and Shan, S.O. 2010. Sequential checkpoints govern substrate selection during cotranslational protein targeting. *Science* **328**(5979): 757-760.

Zhang, X., Schaffitzel, C., Ban, N., and Shan, S.O. 2009. Multiple conformational switches in a GTPase complex control co-translational protein targeting. *Proc Natl Acad Sci U S A* **106**(6): 1754-1759.

Zhang, Y., Berndt, U., Golz, H., Tais, A., Oellerer, S., Wolfle, T., Fitzke, E., and Rospert, S. 2012. NAC functions as a modulator of SRP during the early steps of protein targeting to the ER. *Mol Biol Cell* **PMID: 22740632**.

Zheng, N. and Gierasch, L.M. 1996. Signal sequences: the same yet different. *Cell* **86**(6): 849-852.

Zhou, H.X. 1993. Brownian dynamics study of the influences of electrostatic interaction and diffusion on protein-protein association kinetics. *Biophys J* **64**(6): 1711-1726.

Zopf, D., Bernstein, H.D., Johnson, A.E., and Walter, P. 1990. The methionine-rich domain of the 54 kd protein subunit of the signal recognition particle contains an RNA binding site and can be crosslinked to a signal sequence. *EMBO J* **9**(13): 4511-4517.